12-2016

Characterization of Vesicular Monoamine Transporter 2 and its role in Parkinson's Disease Pathogenesis using Drosophila

Antonio Joel Tito Jr.

Sheng Zhang

TMC LIBRARY
Health Sciences Resource Center

CHARACTERIZATION OF *VESICULAR MONOAMINE TRANSPORTER 2* AND ITS ROLE IN PARKINSON'S DISEASE PATHOGENESIS USING *DROSOPHILA*

By

Antonio Joel Tito Jr., M.S.

APPROVED:

_____
Sheng Zhang, Ph.D.

_____
Hugo Bellen, Ph.D.

_____
Richard Behringer, Ph.D.

_____
Kartik Venkatachalam, Ph.D.

_____
Momiao Xiong, Ph.D.

_____
Nick Justice, Ph.D.

_____
Andrew Bean, Ph.D.

APPROVED:

_____
Dean, UTHealth

Graduate School of Biomedical Sciences at Houston

CHARACTERIZATION OF *VESICULAR MONOAMINE TRANSPORTER 2* AND ITS ROLE IN PARKINSON'S DISEASE PATHOGENESIS USING *DROSOPHILA*

A

DISSERTATION

Presented to the Faculty of

The University of Texas

Health Science Center at Houston

And

The University of Texas

M.D. Anderson Cancer Center

Graduate School of Biomedical Sciences

In partial fulfillment of the requirements

For the degree of

DOCTOR OF PHILOSOPHY

By **Antonio Joel Tito Jr., M.S.**

Houston, Texas

December, 2016

II

DEDICATION

I dedicate this dissertation to God, my father, Jorge Tito-Izquierdo, Ph.D. P.E., my mother, Elizabeth Tito, my brothers, Juan Pablo Tito and Jorge Francisco Tito for their patience and devotion to growing in faith, wisdom, knowledge, and love.

"The aim of natural science is not simply to accept the statements of others, but to investigate the causes that are at work in nature."

By St. Albertus Magnus, *Doctor Universalis* of the Church

ACKNOWLEDGEMENTS

Characterization of Drosophila homologue of vmat2 and its role in a genetic model of Parkinson's disease

Antonio J. Tito Jr., M.Sc.

Supervisory Professor: Sheng Zhang, Ph.D.

Parkinson's disease (PD) is a progressive neurodegenerative disorder caused by the selective loss of the dopaminergic neurons (DN) in the *substantia nigra pars compacta* region of the brain. PD is also the most common neurodegenerative disorder and the second most common movement disorder. PD patients exhibit the cardinal symptoms, including tremor of the extremities, rigidity, slowness of movement, and postural instability, after 70-80% of DN degenerate. It is, therefore, imperative to elucidate the underlying mechanisms involved in the selective degeneration of DN. Although increasing numbers of PD genes have been identified, why these largely widely expressed genes induce selective loss of DN is still not known. Notably, dopamine (DA) itself is a chemically labile molecule and can become oxidized to toxic byproducts while induce the accumulation of harmful molecules such as Reactive Oxygen Species (ROS). Accordingly, DA toxicity has long been suspected to play a role in selective neuronal loss in PD. Vesicular monoamine transporter (VMAT) is essential for proper vesicular storage of monoamines such as DA and their regulated release. Increasing evidence have linked VMAT dysfunction with Parkinson's disease. In this study, we reexamine the gain- and loss-of-function phenotypes of the sole VMAT homolog in *Drosophila*. Our results suggest that the C-terminal sequences in the two encoded VMAT isoforms not only determine their differential subcellular localizations, but also their activities in content release. In particular, VMAT2 orthologue potentially poses a unique, previously unexplored activity in promoting DA release. On the other hand, by examining DA distribution in wildtype and *VMAT* mutant animals, we find that there exists intrinsic difference in the dynamics of intracellular DA handling among DN clustered in different brain regions. Furthermore, loss of VMAT causes severe loss of total DA levels and a redistribution of DA in *Drosophila* brain. Lastly, removal of both VMAT and another PD gene *parkin,* which is also conserved in *Drosophila,* results in the selective loss of DN, primarily in the protocerebral anterior medial (PAM) clusters of the brain. Our results suggest a potential involvement of cytoplasmic DA in selective degeneration of DN and also implicating a role of differential intracellular DA handling in the regional specificity of neuronal loss in PD.

TABLE OF CONTENTS

LIST OF FIGURES

Chapter 4

LIST OF ABBREVIATIONS AND ACRONYMS

PD   Parkinson's disease

DA   Dopamine

TH   Tyrosine Hydroxylase

Ddc   Dopamine Decarboxylase

L-Dopa   L-dihydroxyphenylanaline

SNPC   *Substantia nigra pars compacta*

VTA   Ventral Tegmental Area

SNCA   Synuclein Alpha (commonly known as Alpha Synuclein)

LLRK2   Park8

GBA   Glucocerebrosidase

Parkin   Parkin RBR E3 Ubiquitin Protein Ligase (Park2)

Pink1   PTEN induced putative kinase 1

DJ-1   Park7

ROS   Reactive Oxygen Species

ATP   Adenosine triphosphate

AR-PD   Autosomal Recessive Juvenile form of PD

IBR   In-Between-Ring Domain

Drosophila   Used instead of *Drosophila melanogaster*

LOF   Loss-of-Function

ADHD   Attention Deficit Hyperactive Disorder

DAQ	DA *o*-quinone
NM	Neuromelanin
MAO	Monoamine Oxidase
MPTP	1-methyl-4-phenyl-1,2,3,6-tetrahydropyridine
BH4	Tetrahydrobiopterin
CHO	Chinese hamster ovary
COMT	Catechol-O-methyltransferase
CSF	Cerebrospinal fluid
DAT	Plasma membrane dopamine transporter
DDC	Dopamine decarboxylase
DOPAC	3,4-dihydroxyphenylacetic acid
HPLC-EC	high-performance liquid chromatography with electrochemical detection
5-HT	Serotonin
LDCV	Large dense-core vesicles
SDS-PAGE	Sodium dodecyl sulfate polyacrylamide gel electrophoresis
SNP	Single nucleotide polymorphism
GFP	Green Fluorescent Protein
SG	Salivary Gland

LIST OF APPENDICES

1   LITERATURE REVIEW AND INTRODUCTION

1.1   <u>Pathological Hallmark and PD symptoms</u>

Parkinson's disease (PD) is the most common movement disorder and the second most common neurodegenerative disease (Pringsheim *et al.*, 2014). PD patients exhibit the four cardinal symptoms, including resting tremor of the extremities, cogwheel rigidity, bradykinesia, and postural instability; all of which are highly debilitating to the patients and contribute to high incidence of falls (Rodriguez-Oroz *et al.*, 2009). The hallmark of PD is characterized by a gradual loss of dopamine (DA) neurons in the *Substantia nigra* ("black substance") *pars compacta* (SNPc)*,* which is a relatively small region of the mesencephalon that controls movement.

A common pathological feature of PD brains is the presence of proteineous aggregates, called 'Lewy bodies,' containing ubiquitinated proteins and Alpha-synuclein. PD symptoms manifest following a loss of 30-40% of DA neurons (Ehringer and Hornykiewicz, 1960; Gibb and Lees, 1991; Greenfield and Bosanquet, 1953; Hornykiewicz, 1998). Currently, there are no curative or preventive treatments against this dreadful disease.

The first pathological observations were obtained from post-mortem brain samples of a tuberculosis patient admitted to Charcot's Neurology Ward at 'la Salpetriere' for unilateral parkinsonian tremor. Blocq and Marinesco discovered an encapsulated tumor in the SNPc and concluded that the symptoms were caused by the midbrain lesion (Hostiuc *et al.*, 2016). Edouard Brissaud hypothesized that the

pathogenesis came from a major dysfunction in pigmented neurons. Later, Constantin Tretiakoff conclusively linked idiopathic and post-encephalitic Parkinsonism, with the degenerative phenotype in the SNPc (Crocker and Sehgal, 2010).

DA neurons were later identified as the specific type of cells that are targeted for degeneration. One puzzling observation concerning PD is the regional specificity of the disease pathology: despite the prominent loss of DA neurons in the SNPc, those in ventral tegmental area (VTA) are largely spared (Blesa and Przedborski, 2014).

1.2 Clinical Manifestations of the Disease

PD-like symptoms were first described in 175 AD by physician Galen as "shaking palsy." One of the unique features of PD is the gradual appearance of cardinal symptoms that bear a remarkable similarity to other *motor* dysfunctions, including resting tremors and festination. A snapshot of the PD symptoms was elegantly depicted Dr. Parkinson's observation of a patient: "Involuntary tremulous motion, with lessened muscular power, in parts not in action and even when supported; with a propensity to bend the trunk forward, and to pass from a walking to a running pace: the senses and intellects being uninjured" (Auluck *et al.*, 2002).

Dr. Jean-Martin Charcot coined the term PD to group all the cardinal symptoms associated with the disease. Charcot also differentiated bradykinesia, which is characterized by a "considerable time lapse between thought and action," from symptoms of rigidity, stiffness, and tremor of the extremities (Goetz, 1986).

1.3   PD Prevalence

PD is the most common movement disorder and the second most common neurodegenerative disease. A meta-study determined that the prevalence of PD varies across age, sex, and geographical boundaries.

The study demonstrated that the age of onset for most individuals with PD is around 60 years of age. It is estimated that the disease affects 1 out of 1,000 people between the ages of 55 and 64. Disease prevalence increases with age, as 1 out of 233 individuals are afflicted between the ages of 60 to 74, while an alarming rate of 1 out of 50 people older than 80 years of age develop the disease. Interestingly, men have a 3.5 greater risk than women (Pringsheim *et al.*, 2014).

Results from these studies, however, produced large margins of errors, which could have been contributed by the under-representation of PD patients.

1.4   A Bio-Molecular Snapshot of PD Treatments

George Cotzias first demonstrated that DA precursor L-dopa, which can pass the blood brain barrier, is effective in relieving the symptoms of PD patients. For his groundbreaking finding, Cotzias received the 1969 Lasker DeBakey Clinical Medical Research Award "For his demonstration of the effectiveness of large daily dosages of L-DOPA in the treatment of Parkinson's disease". Patients unresponsive to treatment with L-Dopa were originally co-administered with drugs that facilitate sustained release of DA to the synaptic cleft and prevent the degradation of DA by enzymes, such MAO and COMT inhibitors, thus reducing the incidence of dyskinesia and akinesia events (Barbeau *et al.*, 1972).

Unfortunately, many of available therapies only treat symptoms associated with PD, while others lead to unexpected consequences. Many of the PD symptoms are linked to the rapid conversion of DA to highly reactive, intermediary products. Co-administration of L-Dopa with a MAO inhibitor, for instance, contribute to adverse reactions, including uncontrolled movements and mental abnormalities (Yahr, 1978). There are two MAO isoenzymes, including MAO-A and MAO-B. MAO-A is localized primarily to mitochondrial membranes in DA neurons and serotonergic neurons. The close proximity of MAO-A to the mitochondria suppresses the accumulation of oxidative species generated by cellular respiration while MAO-B is expressed in the cytosol of serotonergic and histaminergic neurons and in astrocytes (Myohanen *et al.*, 2010; Sejourne *et al.*, 2011). The high turnover rate of DA and wide expression of MAO in the brain, makes it difficult for L-Dopa to generate a sustained response on the target neurons of the striatum.

However, MAO catalyzes the oxidative deamination of the amine group of DA to 3,4-dihydroxyphenylacetaldehyde, producing toxic ammonia and hydrogen peroxide in the process (Segura-Aguilar and Lind, 1989).

Some of L-Dopa replacement strategies include replacing L-Dopa with more stable biosimilar compounds and co-administering DA receptor agonists (Schwab *et al.*, 1951). These drugs improve the quality of life of patients at advanced stages (Brooks *et al.*, 1995; Rinne *et al.*, 1997). Patients showing dyskinesia during the characteristic "off" state of L-Dopa, also benefit from methods that significantly improve drug absorbance into the bloodstream (Goetz *et al.*, 1989).

Yet, all of these treatments only ameliorate the symptoms and/or reduce the adverse effects of L-Dopa. Therefore, it is of utmost importance to develop treatments, aimed at preventing the cellular death of DA neurons, rather than just focusing on ameliorating the symptoms of PD.

1.5   Familial Cases and Cellular Pathways Implicated in PD

The vast majority of PD cases are of unknown etiology and idiopathic in nature. Over the past 15 years, a growing number of PD-associated genes have been identified from newly discovered hereditary PD cases (Corti *et al.*, 2011; Martin *et al.*, 2011). Although they contribute to a small portion of diagnosed PD cases, many of these mutations cause a wide variety of cellular dysfunctions that lead to disease pathogenesis.

Mutations in these PD genes can include point mutations and deletions, or even duplication and triplication events, which include loss of function and gain of toxicity mutations, such as those in the *SNCA* gene that codes for alpha-synuclein.   In particular, mutations in *SNCA* contribute to rare cases of autosomal-dominant disease, which is characterized by an induction in the levels of aggregates in the diseased brain (Polymeropoulos *et al.*, 1997).

Alpha-synuclein containing aggregates are also present in the Lewy body formations of patients with sporadic PD, suggesting there are common elements in both familial and idiopathic PD cases (Singleton *et al.*, 2003). The most common mutations in patients with autosomal dominant PD are found in the LLRK2 (Park8) gene

(Paisan-Ruiz *et al.*, 2004). Notably, a missense mutation (*PARK8* - G2019S) occurs in 30 to 40% of PD patients of North African descent (Gilks *et al.*, 2005; Lesage *et al.*, 2006).

Another genetic risk factor includes heterozygous mutations in the *glucocerebrosidase* gene (*GBA*), present in 4% of patients. Homozygous mutations of the *GBA* gene causes Gaucher's disease, a recessive lysosomal storage disorder (Neumann *et al.*, 2009).

Finally, autosomal recessive mutations in *Park2* and *Pink1* are the leading cause of early onset PD, followed by recessive mutations in *DJ-1* (Hardy, 2010). These genes code for important molecular players of the ubiquitin proteasome system, mitophagy, and anti-ROS protective mechanisms (Bonifati *et al.*, 2003; Hague *et al.*, 2003; Kitada *et al.*, 1998; Valente *et al.*, 2004).

Functional characterization of these genes implicate multiple cellular pathways in PD pathogenesis, including protein misfolding, mitochondria dysfunction, excessive reactive oxygen species (ROS), defective vesicular trafficking and others (Corti *et al.*, 2011; Martin *et al.*, 2011). Summaries of these mutations and associated functions are provided in Figure 1.1. These genetic risk factors increase the vulnerability of DA neurons to the damaging effects incurred by a continuous exposure to harmful toxicants in the environment (Nall *et al.*, 2016).

However, given that almost all the PD genes are widely expressed, and since the implicated cellular pathways are ubiquitous and systematic, it again raise the intriguing question on how these nonspecific pathogenic factors induce a relatively selective loss of DA neurons in the brain (Blesa and Przedborski, 2014).

PD Causes	Transmission	Function
Sporadic (~ 85%)		
LRRK2	**Dominant**	kinase
a-Synuclein	**Dominant**	Unknown
Ubiquitin C-Terminal Hydrolase-L1 (UCHL-1)	**Dominant**	Ubiquitin ligase
parkin	*recessive*	E3 ubiquitin ligase
PINK1	*recessive*	kinase
DJ-1	*recessive*	Anti-oxidative
glucocerebrosidase (GBA)	*recessive*	Metabolic enzyme
ATP13A2	*recessive*	ATPase transporter

Figure 1.1 Inheritance of gene mutations that contribute to the early onset PD.

The *LRRK2, alpha-Synuclein* and *UCHL1* genes harbor dominant mutations, while the *parkin, pink1, dj-1,* and *glucocerebrosidase* (GBA) genes harbor recessive mutations. The functions linked to each gene are outlined on the right column.

1.6   **Parkin**

Parkin is one of the best-studied PD genes and its loss of function has been linked to early onset, autosomal recessive juvenile form of PD (AR-PD) (Kitada *et al.*, 1998; Lucking *et al.*, 2000). *Parkin* encodes an E3 ubiquitin ligase and is broadly expressed in the brain and other tissues at different stages of development and adulthood (Kitada *et al.*, 1998).

Functionally, Parkin has been linked to the ubiquitin-proteasome system (UPS) and autophagy pathways, especially autophagy-mediated clearance of mitochondria (mitophagy) (Corti *et al.*, 2011; Erion *et al.*, 2012; Exner *et al.*, 2012; Scarffe *et al.*, 2014; Trempe and Fon, 2013; Winklhofer, 2014).

Mitochondrial dysfunction is one of the earliest and most prominent cellular defects observed in *parkin* mutants of different cell and animal models, including those in *Drosophila* and rodents. However, *parkin* mutant animals do not show an apparent loss of DA neurons, suggesting additional pathogenic factors playing a role in the initiation and acceleration of the degeneration process of DA neurons.

These pathogenic events are normally manifested over decades in PD patients harboring similar genetic lesions, thus, it is possible for these secondary hits to build up in DA neurons as the person ages (Berg *et al.*, 2015; Blesa and Przedborski, 2014; Chege and McColl, 2014; Dawson, 2000; Guo, 2012; Matsui *et al.*, 2014). Therefore, it will be critical to examine age-dependent dysregulated pathways that are specifically affected in DA neurons.

Figure 1.2 Parkin is conserved in *Drosophila*

(A) Black boxes show amino acids of identical nature between *Drosophila* and human sequences. Green boxes indicate amino acids with similar biochemical properties. (B) Cartoon representation of amino acid sequences of human and *Drosophila* Parkin indicates greatest similarity in the functional domains Ubl, Ring1, IBR, and Ring2.

1.7 Mitochondrial Dysfunction as a Shared Feature of PD models

Recent identification of dysfunctional mechanisms have shed light to the etiology of DA neurons degeneration in PD patients (Shulman *et al.*, 2011). Pathogenic mechanisms are associated with a significant reduction in the capacity to turnover depolarized mitochondria by mitophagy, a dysregulated metabolism of alpha-synuclein, and an exacerbated inflammatory response (Shulman *et al.*, 2011).

Mitochondrial dysfunction has emerged as a major subcellular defect in most of the animal models of PD. As an example, in *Drosophila*, mutations in *parkin* and *pink1* contribute to severe mitochondrial abnormalities due to a defective fission process (Greene *et al.*, 2003; Lesage *et al.*, 2006; Pesah *et al.*, 2004; Yang *et al.*, 2006). Additional studies have shown that Parkin and Pink1 function in overlapping cellular pathways. For example, *Parkin* overexpression can partially rescue the *pink1* mutant phenotypes and enhance the process of mitophagy (Clark *et al.*, 2006). Together, they implicate an important role of mitochondria in the etiology of PD. Similar phenotypes are also reported in several mammalian PD models.

Interestingly, mitochondrial dysfunction was first observed in people exposed to high levels of toxic pesticides, including MPTP (1-methyl-4-phenyl-1,2,3,6-tetrahydropyridine) and Rotenone (Langston and Ballard, 1983), which contribute to the disruption of complex I (Betarbet *et al.*, 2000). Further pathological studies on post-mortem samples from PD brains, showed a higher incidence of LOF mutations in the mtDNA polymerase POLG and mtDNA helicase, Twinkle, resulting in a defective mtDNA replication machinery (Baloh *et al.*, 2007; Bender *et al.*, 2006; Wanrooij *et al.*, 2004).

Notably, phenotypes of dysfunctional mitochondria have also been observed in several unrelated neuronal disorders, such as Alzheimer's and Huntington's, which largely spare the DA neurons in the brain (Johri and Beal, 2012). Although it is still not clear why in PD, DA neurons in the *substantia nigra* are primarily affected, mitochondria defect *alone* cannot account for the relatively selective degeneration of

DA neurons in PD. Additional factors that are *innate to* DA neurons most likely contribute to disease pathogenesis.

1.8   DA, an Unstable and Potentially Toxic Neuromodulator

DA neurons are defined by the ability to synthesize and utilize DA, a neuro-modulator that is derived from the precursor L-Tyrosine. DA is primarily responsible for modulatory functions such as motor planning, motivation, sleep, and appetitive memory consolidation (Bromberg-Martin *et al.*, 2010; Dayan and Balleine, 2002; Wise, 2004). DA also plays important roles in goal-oriented and reward seeking behaviors among others (Nieoullon, 2002).

Dysfunction of the DA system has been linked to addiction and a diverse spectrum of diseases such as ADHD, PD, and schizophrenia (Carlsson, 1972; Creese *et al.*, 1976; Eisenberg *et al.*, 1988; Freis, 1954; Ritz *et al.*, 1988; Song *et al.*, 2012). Notably, DA is a chemically labile molecule, since it contains a benzene group with two hydroxyl molecules, in addition to its amine side-chain (Fig. 1.3B). *Importantly*, this unique chemical motif converts DA into a highly reactive molecule in basic conditions.

DA-induced cellular toxicity has long been suspected to play roles in PD pathogenesis, although little evidence is available, *in vivo*. When DA is exposed to free oxygen in the PH-neutral cytosol, it can spontaneously oxidize into toxic by-products. Auto-oxidation of DA results in the formation of DA Quinones (DAQ), along with the simultaneous production of toxic reactive oxidative species (ROS), such as hydrogen peroxide and superoxide anion.

Both superoxide anion, DA *o*-quinone, and DA *o*-semiquinone are neurotoxic. DA-*o*-quinone metabolites are quickly stabilized via glutathione mediated synthesis of 5-*S*-glutathionyl-DA (Bisaglia *et al.*, 2007). Yet, the amine group of DA *o*-quinone can convert into leuco-Aminochrome (commonly known as Aminochrome).

In addition, DAQ can also serve as catalysts for the subsequent polymerization and condensation with freely floating amino acids and proteins (Bisaglia *et al.*, 2010). Aminochrome can rearrange into 5,6-dihydroxyindole, which can impart significant damage to the mitochondria, induce the formation of rigid protofibrils, disrupt the recycling of misfolded proteins, increase oxidative stress, and induce an inflammatory response (Bisaglia *et al.*, 2007).

Interestingly, Aminochrome inactivates DA transporter, tyrosine hydroxylase, and alpha- and Beta- tubulin, principal components of the cytoskeleton (Whitehead et al., 2001). Interfering with the function of the cytoskeleton is deleterious since neurons use the microtubules to transport the autophagy vacuoles to the lysosome. Mechanisms that halt the production of Aminochrome will, consequently, prevent the synthesis of 5,6-dihydroxyindole and other toxic by-products (Bisaglia *et al.*, 2007).

Neurons employ protective mechanisms that contribute to the formation of Neuromelanin (NM), consisting of a conglomerate of pigmented molecules linked to peptides, lipids, heavy metals, and toxic chemicals. NM contributes to the accumulation of iron inside the eumelanin and pheomelanin polymers. Further, upon inflammation, activated microglia disrupts the surface layer of pheomelanin (Bush *et al.*, 2006) (McGeer *et al.*, 1988); (Banati *et al.*, 1998). Neuromelanin releases toxic

chemicals after breaking open. Iron is a strong catalyst in the oxidation of DA to DA *o-quinone* (Wakamatsu *et al.*, 2012).

Injection of NM into the *SNPC* of rats resulted in the activation of microglia surrounding dying DA neurons (Zhang *et al.*, 2011). In response to inflammation, the MAO enzyme is activated, producing hydrogen peroxide. H_2O_2 attacks the pheomelanin layer of the NM, releasing its inner contents (Sulzer *et al.*, 2000).

Other chemicals detected inside NM that predispose people to PD have included pesticides, such as paraquat and MPTP, as well as drugs, like Chlorpromazine and Haloperidol (Lindquist *et al.*, 1988), and heavy metals, including Mercury, Lead, Cobalt and Cadmium (Coon *et al.*, 2006).
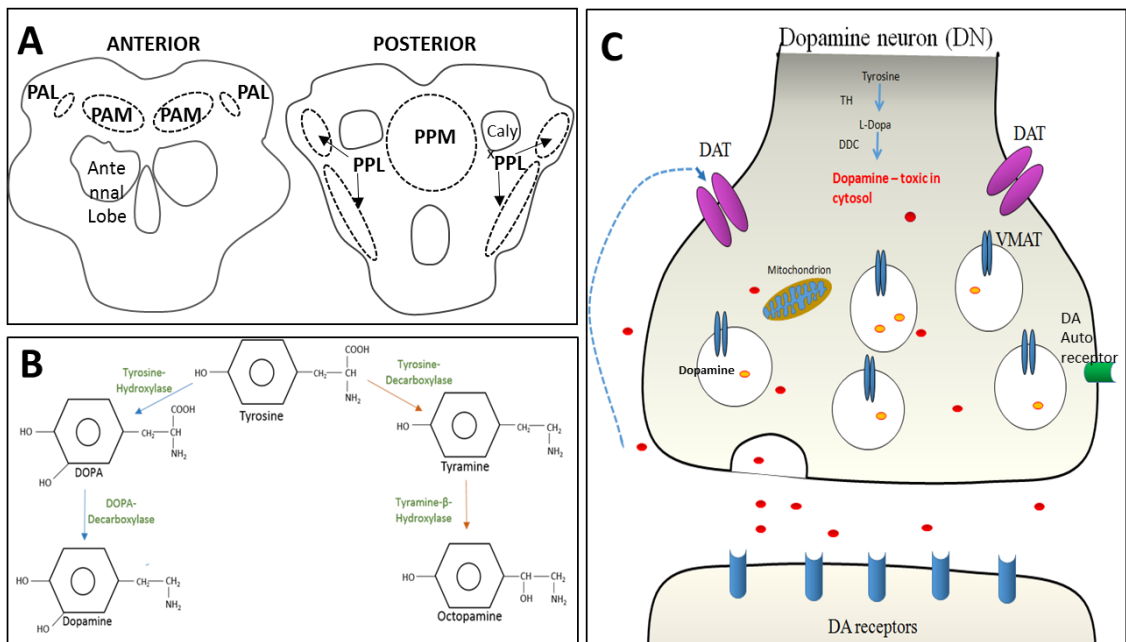
Figure 1.3 DA system and distribution of DN in adult *Drosophila* brain.

(A) *DA neuron clusters in adult fly brain*, including the protocerebral anterior medial (PAM) and protocerebral anterior lateral (PAL) clusters in the anterior view; and the protocerebral posterior lateral (PPL) and the protocerebral posterior medial (PPM) in the posterior views of the brain. (B) *DA and octopamine synthesis pathway*. DA is synthesized from precursor tyrosine by Tyrosine hydroxylase (TH) to DOPA, an intermediary molecule, which undergoes decarboxylation into DA by DA decarboxylase (DdC). Octopamine is synthesized from precursor tyrosine by Tyrosine decarboxylase 2 (Tdc2) to Tyramine, an intermediary molecule, which undergoes hydroxylation by Tyramine B-Hydroxylase to Octopamine. (C) *Intracellular handling of DA*. Synaptic DA is sequestered inside acidic synaptic vesicles by Vesicular Monoamine Transporter (VMAT), released to the synaptic cleft, and recycled back into the cytosol by DA Transporter (DAT).

1.9   DAT and VMAT: Transporters Essential for DA Function and Stability

Like all other neurotransmitters, DA is normally sequestered inside synaptic vesicles (SVs), whose acidic environment (normally at PH ~5.5) protonates and stabilizes the DA molecules in DA neurons (Guillot and Miller, 2009). The precursor for DA is the amino acid, L-tyrosine.

The rate-limiting tyrosine hydrolase (TH) catalyzes the hydroxylation of tyrosine to L-dihydroxyphenylanaline (L-Dopa). Immediately after, DA decarboxylase (DDC), which is also known as aromatic amino acid decarboxylase (AADC), decarboxylates L-Dopa into DA and generates CO_2 in the process.

These anabolic reactions take place inside a complex of proteins that is localized at the periphery of the vesicular membrane and is physically linked to vesicular monoamine transporter 2 (VMAT2), which acts for vesicular package of DA (Cartier *et al.*, 2010) (Miller *et al.*, 1999). VMAT2 is a neuron-specific 12-transmembrane (TM)-domain protein spanning the vesicular membrane (Liu and Edwards, 1997; Moriyama and Futai, 1990; Torres *et al.*, 2003).

Synthesizing DA at the periphery of the vesicular membrane prevents the accumulation of metabolites from DA oxidation in the cytoplasm (Linert *et al.*, 1996). VMAT is also responsible for packaging other monoamines, such as serotonin and octopamine, into synaptic vesicles for storage and regulated release (Torres *et al.*, 2003; Yamamoto and Seto, 2014). Therefore, VMAT is an important regulator of monoamine

biology and function (Torres *et al.*, 2003), and VMAT expression can serve as a marker for monoamine (DA, catecholamine, serotonin, histamine, and octopamine) producing neurons in the brain proper.

During synaptic DA release, SVs migrate to the synaptic cleft where they fuse with the plasma membrane and release their contents extracellularly to modulate neuronal response. Dopamine active transporter (DAT) is another 12-transmembrane domain protein that localizes around the active sites of the plasma membrane, and is responsible for the re-uptake of released extracellular dopamine back into the neuron, thereby terminating its action (Figure 1C) (Torres *et al.*, 2003).

Thus, not only does VMAT2 mediate vesicular packaging of DA, but also protects DA from basic conditions and oxidative agents in the cytosol. Through their concerted effort, the two monoamine transporters (VMAT2 and DAT), regulate the proper storage and transmission of DA.

1.10   **VMAT2 and PD**

As discussed, VMAT2 plays a due role in protecting DA inside acidic vesicles and facilitating its regulated release to the synaptic cleft. Consistent with its protective role, increasing evidence have implicated a potential causative effect of compromised VMAT2 function to PD pathogenesis (Lohr and Miller, 2014).

In particular, mice with reduced expression of VMAT2 develop progressive degeneration of nigrostriatal DA neurons and increased vulnerability to DA neuron toxin MPTP (Caudle *et al.*, 2007; Takahashi *et al.*, 1997; Taylor *et al.*, 2014; Taylor *et al.*, 2011).

Moreover, in a study that directly evaluated VMAT2 activity from samples of post-mortem brains, the efficiency of VMAT2 on vesicular uptake of DA from idiopathic PD patients is profoundly reduced, as compared to those from healthy controls. Such reduction in VMAT2 activity was not observed in brains from monkeys treated with the DA neuron toxicant, MPTP (Pifl *et al.*, 2014), which serves as an acute model of PD. Additionally, A loss-of-function VMAT2 mutation is linked to a familial infantile form of PD (Rilstone *et al.*, 2013).

Treating mice with MPTP also depletes striatal DA and causes PD-like symptoms in the *SNPc* of humans and non-human primates, causing a substantial reduction in expression of VMAT, TH and DAT. Concomitantly, MPTP significantly reduces the levels of striatal DA and its metabolites, namely DOPAC and HVA, but does not induce the activity of MAO and COMT.

Nevertheless, the vesicular uptake of dopamine and binding of the VMAT2-selective label [(3)-H$^+$]-dihydrotetrabenazine was significantly reduced in DA storage vesicles obtained from the striatum of six autopsied brain tissues of PD patients (Xu *et al.*, 2015). Conversely, overexpression of VMAT2 protects DA neurons from the toxic effect of MPTP in adult neurons of *Drosophila* and mice (Inamdar *et al.*, 2013; Lawal *et al.*, 2010; Lohr *et al.*, 2014).

1.11   VMAT Structure and Function

VMAT possesses twelve trans-membrane domains, with both terminal tails ending in the cytoplasm. The catalytic sites for VMAT-mediated serotonin transport, Asp 431 and Asp 404, were identified in the transmembrane segments X and XI,

through mutagenic analysis. Replacing Asp 431 with either Glu or Ser, or Asp 404 with either Ser or Cys, inhibits serotonin transport. However, mutating the proteins, does not impair the ability of the transporter to recognize the ligand, as measured by the high affinity ligand [3H] reserpine, nor does it hinder coupling to the Delta micro H+ gradient. These results suggest that ligand binding activity is independent from transport site (Steiner-Mordoch *et al.*, 1996).

VMAT is a vesicular ATPase, which hydrolyses ATP to ADP and inorganic phosphate, generating an H^+ gradient that acidifies the vesicles. As an antiporter, VMAT2 exchanges one monoamine molecule for two H+ protons (Bischof *et al.*, 2013).

1.12 VMAT Expression Pattern, Subcellular Localization and Heterologous Systems of Investigation

Mammalian genomes have two independent *vmat* genes encoding two homologous VMAT proteins, VMAT-1 and VMAT-2 (Peter *et al.*, 1995). Both genes were cloned from the human adrenal glands, as well as in the chromaffin granules of the rat and bovine. The mRNA of VMAT-1 is primarily expressed in peripheral neuroendocrine tissues such as adrenal medulla glands, whereas VMAT-2 is mainly expressed in the central nervous system.

In the rat brain, the region with the highest expression of the transporters is the solitary tract nuclei. The transporters are also expressed in the parotid gland, submandibular, sublingual and salivary glands of Wistar rats (Tomassoni *et al.*, 2015). During the embryonic development of the rat, VMAT2 localizes to neuronal tissues,

while VMAT1 is present in the thymus and in cells of the endocrine system, including the adrenal glands, medulla, pituitary gland, and testis.

The central, peripheral and enteric nervous system only express VMAT2, suggesting a role for VMAT2 in mediating the transport of psychopharmacologic and neurotoxic agents (Hansson *et al.*, 1998).

In the central nervous system, the monoamine transporters are localized to both small synaptic vesicles and large dense core vesicles. Some of the first studies describing the subcellular localization of VMAT2 and VMAT1 were performed on adrenal glands and chromaffin cells. At the subcellular level, VMAT2 is localized to LDCVs that are distanced from the synaptic cleft, but is also found on small synaptic vesicles in axon terminals. The DCVs are found near organelles involved in vesicular membrane recycling, such as near the tuberous vesicles of the smooth endoplasmic reticulum (Nirenberg *et al.*, 1995).

Furthermore, heterologous systems are used to assess the subcellular localization of VMATs and determine the effects of loss of function mutations in the *vmat* gene. These have included the use of chromaffin granule from bovine adrenal glands and *Xenopus laevis* oocytes. For instance, the *X. laevis* oocytes have been employed to express mutated versions of synthetic mRNA of the rat VMAT2. These results demonstrated that mutations that change the localization of VMAT2 to the plasma membrane do not alter its ability to transport DA (Whitley *et al.*, 2004).

1.13   Substrates of VMAT

The substrate specificity of psychoactive molecules was originally determined using digitonin-permeabilized fibroblastic (CV-1) cells. Expression of VMAT2 in CV-1 cells induced the uptake of catecholamines, including DA, 5-HT, and histamine. Interestingly, histamine showed a 30-fold higher affinity for VMAT2 than VMAT1. The other catecholamines showed a 3-fold higher affinity for VMAT2 than for VMAT1 (Erickson *et al.*, 1996). In *C. elegans*, cat-1 knock-outs are deficient of DA controlled behaviors and VMAT immunostaining (Duerr *et al.*, 1999).

The enzymatic pathways regulating DA homeostasis are also highly conserved in *Drosophila,* including DA synthesis (TH and DDC), packaging (VMAT), reuptake (DAT), and signaling (DA receptors 1 and 2).

A study examining the effects of factors modulating histamine biosynthesis determined that VMAT2 has a specific affinity to histamine in the gastric corpus. In this study, it was found that treating rats with the H^+-K^+ ATPase inhibitor, omeprazole, increased the mRNA expression of VMAT2 in the gastric corpus. Omeprazole also increases the transport of histamine from enterochromaffin-like (ECL) secretory vesicles, suggesting that VMAT2 mediates histamine storage upon an induction in Histamine biosynthesis (Dimaline and Struthers, 1996).

1.14 VMAT-mediated Transport of Monoamine Analogs and their Effects

Monoamine transporters such as VMAT also have the ability to transport various cytotoxic compounds such as ethidium, rhodamine, doxorubicin, tetrabenazine, verapamil (a calcium channel blocker), ketanserin, and reserpine. The last three compounds are competitive inhibitors of VMAT1 and VMAT2, while tetrabenazine only binds to and inhibits VMAT2. Tetrabenazine also induces PD like symptoms in Huntington's disease patients who are prescribed with the drug to treat chorea. Mechanistically, tetrabenazine contributes to a depletion of striatal DA in rodents, induces tremulous jaw movements (TMJ), reduces locomotion, and induces mastication in rodents (Podurgiel *et al.*, 2013; Podurgiel *et al.*, 2016).

Tetrabenazine also induces depressive symptoms in humans by depleting dopamine levels in the striatum. Rats administered with tetrabenazine showed an increased preference for aversive food choices. This suggests that the drug confers major effects on decision making since it reduces the intake of pleasant food by rats (Nunes *et al.*, 2013).

In fact, a study showed that rats administered with tetrabenazine, via IP injection, had less preference for decisions requiring effort. This negative effect was reversed with the co-administration of anti-depressants, which reduced the preference for effortless behaviors (Nunes *et al.*, 2013). The direct link between the effects of tetrabenazine induced VMAT inhibition and PD-like symptoms in rodents are

reaffirmed by another study that also demonstrated similar PD like symptoms after reserpine injection to mice (de Freitas *et al.*, 2016).

1.15   <u>VMAT Inhibitors</u>

IP injection of Reserpine to rats increases the quantity, size, and volume of granules in the stomach and significantly reduces the number of secretory vesicles. Blocking VMAT2 function in rats with a high-dose administration of METH also redistributes VMAT-2 from vesicle-enriched synaptosomes to the soma. This suggests that sustained release of monoamines to the synaptic cleft are mediated by VMAT2. These results also suggest that the disruption of VMAT2 function prevents the release of vesicular contents, and induces formation of granules and vacuoles. The latter structures serve as repositories for monoamines and prevent the accumulation of reactive metabolites (Riddle *et al.*, 2002; Zhao *et al.*, 1999).

Psychoactive agents that selectively inhibit VMAT2, including amphetamine and phenylethylamine, induce psychosis. "Drug-induced psychosis" is prevalent in *Vmat2* heterozygous mutant Zebrafish as anxiety like behaviors, which are demonstrated through frequent movement between dark and light zones (Wang *et al.*, 2016). To the contrary, VMAT2 agonists, including Phencyclidine (PCP) and Pramipexole, which are also used to treat restless leg syndrome, induces sedative and anti-schizophrenic effects (Crosby *et al.*, 2002; Rehavi *et al.*, 2002; Torres *et al.*, 2003).

1.16   **VMAT Regulation**

VMAT activity is regulated by the N-glycosylation sites of the luminal loop, as well as the phosphorylation sites of the cytoplasmic domains. The N-glycosylation sites mediate the formation of trafficking complexes that regulate VMAT2 localization in large dense core vesicles.

These results were obtained from PC12 cell lines over-expressing VMAT2. Further, induction of VMAT2 expression in PKA-deficient cells, or in wild-type cells co-administered with a PKA inhibitor, increased trafficking of VMAT2 to synaptic-like micro-vesicles (Yao *et al.*, 2004).   Co-expression of the PKA catalytic subunit with VMAT2 redistributed the transporter to large dense core vesicles.   Additionally, injection of Reserpine into the rat striatum changes the localization of VMAT2 from the dorsal to the caudal sub-region of the striatum (Naudon *et al.*, 1996).

1.17   **VMAT Loss of Function**

VMAT2 knockout mice show aberrant neurotransmission of monoamines, resulting in starvation and early death. *VMAT* knockout pups survive only up to 2 weeks following subcutaneous administration of amphetamine. Histological analysis of their cerebral cortex show an increased incidence of cell death, a phenotype complemented by the inhibition of MAO-A enzyme (Fon *et al.*, 1997; Wang *et al.*, 1997).

Mice that only express five percent of wild-type Vmat2 levels, by contrast, develop to adulthood but show weak age-dependent motor loss phenotypes. These

vmat2 hypomorph mice also exhibit a more selective loss of nigrostriatal neurodegeneration, along with the associated motor dysfunction phenotypes (Caudle *et al.*, 2007; Mooslehner *et al.*, 2001).

1.18 *Drosophila melanogaster* as an Excellent Model to Study VMAT Regulation and Model PD

Drosophila, a genetic versatile system, is the ideal *in vivo* model to <u>study the function and regulation of VMAT and its role in PD</u>. The model organism *Drosophila* has long been valued for its elegant genetic tools, short reproductive times, and highly conserved molecular and cellular pathways.

The fruit fly has been successfully employed to dissect basic signaling pathways, the patterning mechanisms of multicellular organisms, as well as mechanisms underlying neuronal development, functions, and diseases (Nagarkar-Jaiswal et al., 2015b; Wangler et al., 2015). Historically, due to its high fecundity, ease of handling, and shorter generation time, *Drosophila* has been the ideal model system for many fruitful genome-wide saturation screens, which have contributed to the discovery of evolutionarily conserved signaling pathways from Wnt/wingless, Hedgehog, to Notch (Nagarkar-Jaiswal et al., 2015b; Wangler et al., 2015).

With over a century of genetic manipulations, *Drosophila* biologists have established a large arsenal of experimental tools such as targeted gene engineering, MiMIC-based genome tagging, FRT/FLP-based mosaic analysis, and the UAS/Gal4 binary expression system, among others. The latter technology has been implemented

in generating fly lines indispensable for anatomical and functional dissection of neuronal circuitry in the brain (Brand and Perrimon, 1993; Jenett *et al.*, 2012).

These versatile tools allow investigators to control the exact location and timing of gene expression throughout development. *Drosophila* has been employed extensively to study the regulation and function of DA and model related neurological disorders. Flies also present robust neuronal-based behavioral responses which can faithfully mimic some of the PD symptoms (Waddell, 2010; Wangler *et al.*, 2015; Yamamoto and Seto, 2014).

As a classical genetic model organism, the fruit fly is also emerging as an excellent model for the study of DA neuron loss in PD patients, for the following reasons: First, the fly has a well-characterized DA neural system with easily identifiable DA neurons in its CNS. Compared to about 20,000 DA neurons in the mice brains (Bjorklund and Dunnett, 2007), there are only 280 DA neurons in the protocerebrum of the adult *Drosophila* brain (Budnik and White, 1988; Mao and Davis, 2009).

Resembling mammalian DA neuron distribution, the DA neurons in fly brains are also distributed in clusters in a relatively stereotypical pattern (Figure 1.3A) with distinct projection patterns that modulate discrete brain functions, including locomotion, motivation, sleep, arousal, as well as learning, and memory (Bjorklund and Dunnett, 2007; Mao and Davis, 2009; Waddell, 2010). Equally important, both the enzymatic pathways regulating DA homeostasis are highly conserved in *Drosophila,* including DA synthesis (dTH and dDDC), vesicular packaging (dVMAT), reuptake (dDAT), and signaling (DA receptors 1 and 2) (Figure 1.3C) (Yamamoto and Seto, 2014).

Similarly to mammals, DA is synthesized from the precursor amino acid Tyrosine, through the sequential catalytic activities of the rate-limiting enzyme TH and DDC (Figure 1.3B). In *Drosophila,* as is the case with other neurotransmitters, DA is normally sequestered inside synaptic vesicles (SVs) and dense core vesicles for proper storage and regulated release.

Drosophila VMAT homolog (dVMAT) on the vesicular membrane pumps and sequesters cytosolic dopamine into the SVs. Upon stimulation, SVs fuse with the plasma membrane to release their inner contents. There is only a single d*vmat* gene that expresses two splice isoforms, dVMAT-A (hereby known as dVMAT2) and dVMAT-B. The two VMAT proteins differ only at their very C-termini, which primarily modulates the dynamics of intracellular trafficking of the corresponding proteins (Chang *et al.*, 2006; Greer *et al.*, 2005; Grygoruk *et al.*, 2014; Grygoruk *et al.*, 2010; Romero-Calderon *et al.*, 2008).

dVMAT-A is expressed in all the DA, octopamine and 5-HT neurons in the brain and optic lobes where it is responsible for the vesicular packaging of these monoamines (Chang *et al.*, 2006; Chen *et al.*, 2013; Greer *et al.*, 2005; Simon *et al.*, 2009). By contrast, dVMAT-B shows a more restricted expression pattern. It is expressed in a layer of glial cells in the eye and is involved in the packaging and recycling of histamine, the primary neurotransmitter in fly photoreceptor cells (Romero-Calderon *et al.*, 2008).

Finally, multiple PD genes exist in the fly genome, such as Parkin, Pink1 and LRRK2. In fact, the PD-related mitochondrial defects were first reported by studying

parkin mutants in the fly (Guo, 2012). Fly lines carrying mutations for all of these genes have been generated, and all the reported homozygous mutants are viable as adults (Guo, 2012). Together, given the high degree of conservation of DA system and PD-related genes, as well as its abundance of experimental tools, *Drosophila* is an ideal in vivo model system to study the regulation and function of VMAT, and to evaluate its role in PD pathogenesis.

1.19   Challenges in PD Studies and Rationale for this Study

Currently there is no effective preventative or therapeutic methods to treat PD. Despite extensive studies in different model organisms, the pathogenic mechanisms underlying PD are still unclear. In PD studies, several important questions should be addressed. First is on the selective death of DA neurons.

Almost all the PD-associated genes are broadly expressed in the brain and other tissues, and the cellular pathways implicated in the disease, such as mitochondria dysfunction and defective protein turnover and aggregate formation, are mostly systematic and not restricted simply to DA neurons. But why DA neurons are particularly vulnerable and degenerate in PD brains?

Additionally, why DA neurons in the substantial nigra region are selectively affected whereas those in the VTA are mostly spared in PD? Lastly, the most important phenotype of PD, the selective destruction of DA neurons, is barely recapitulated in most of the established genetic PD models, such as Parkin, Pink1 and DJ-1 knockout or αSyn overexpression in mice or *Drosophila*.

Does this suggest that additional pathogenic factors are required to unmask or initiate/accelerate the pathogenic events controlled by these PD genes in these model systems that normally entertain much shorter lifespans than humans, considering that it takes decades before the considerable loss of DA neurons and the manifestation of the symptoms in PD patients?

As discussed, a growing body of evidence is implicating DA toxicity and dysfunctional VMAT as an important and potentially specific contributor of PD pathogenesis. Despite the long-recognized roles of VMAT in regulating DA function and its subcellular sequestration, there are limited *systematic* investigations on its role in the degeneration of dopamine neurons in the context of animal PD models.

The *objectives* of this dissertation are to apply the *Drosophila* model system to investigate the function and regulation of VMAT, to examine the effect of its depletion in the survival of DA neurons in a whole animal model, and to further test whether its disruption can potentiate *selective* degeneration of DA neurons in a sensitized *parkin* mutant background, which by itself does not manifest overt loss of DA neurons.

I expect that outcome of the study should establish a platform for future functional study of this important regulator of dopamine activity and protection, and clarify its role in PD pathogenesis, thereby providing clues for potential therapeutic and intervention avenues. My studies have been grouped into three related topics:

Aim1: Establish platform to study DA neuron organization and VMAT function in *Drosophila*

To facilitate future analysis of VMAT function and DA neurons in an intact brain tissue, I have developed a more efficient method to dissect and analyze adult *Drosophila* brains (Chapter 2).

I have also established new tools to study dVMAT, including an endogenous Gal4-trap and GFP-tagging lines for the dVMAT gene. I have subsequently carried out a detailed analysis of DA neurons in adult brains and demonstrated that in the Protocerebral Anterior Medial (PAM) cluster of *Drosophila* brain, where the majority of DA neurons reside, octopamine neurons also exist (Chapter 3).

Aim2: Functional characterization of VMAT in *Drosophila*

As a first step for the future functional study of VMAT in *Drosophila,* I have characterized the overexpression phenotypes of dVMAT isoforms (Chapter 4).

I have also established a heterologous system to study the subcellular localization patterns of dVMAT isoforms. I have further examined the phenotypes of new dVMAT mutant alleles (Chapter 4).

Aim3: Test the "two-hit" PD hypothesis: evaluate whether dysregulation VMAT will specifically accelerate the loss of DA neurons in *parkin* mutant animals.

I have tested in the sensitized *parkin* mutant background, a well-characterized PD models, whether dysregulation of VMAT can induce *selective* degeneration of DA neurons (Chapter 4).

2   A ONE-STEP DISSECTION OF ADULT BRAINS

2.1   Introduction

The relatively small size of the fruit fly makes it permissive to perform whole-mount preparations of the adult fly brain, which can be examined with a regular compound or confocal microscope. This feature enables detailed anatomic and functional analyses of single neurons and neuronal circuitries, thus providing a better understanding of their functionality at the cellular and subcellular levels.

With recent advances in cell labeling and imaging technologies, the fruit fly's brain has become especially powerful in fine mapping of neuronal circuitry and in dissecting the molecular and cellular basis of higher brain functions such as learning, memory, and circadian rhythm (Aso *et al.*, 2014; Nern *et al.*, 2015; Reiter *et al.*, 2001; Waddell, 2016; Wangler *et al.*, 2015; Wolff *et al.*, 2015; Yamagata *et al.*, 2015).

However, the rather miniature size of the brain also makes it technically challenging to isolate an intact brain from the protective head case. Various effective dissection methods have been described in detail, which involve careful and step-wise removal of the head case and the associated tissues, including the eyes, trachea, and fat from the brain proper (Sweeney *et al.*, 2011; Wu and Luo, 2006).

These microsurgical dissection methods often place rather stringent demands on the quality of the dissection forceps, requiring forceps with fine well-aligned tips that can be easily damaged. Moreover, the dissected brains can be easily lost during the subsequent staining and washing processes since they are separated from the rest

of the body. Their small sizes and transparency makes it difficult to see in the processing buffer. Here, we describe a relatively simple and easy-to-learn, one-step dissection protocol that keeps the dissected brains attached to the torso. The dissection process clears away most of the brain-associated tissues, such as the eye, and reduces the demand for good quality dissection forceps.

Additionally, when imaging the brain under the fluorescent compound microscope or confocal microscope, the side of the brain that is away from the fluorescent light source often produces a weaker signal and less clear images due to the thickness of the whole-mount brain. Here, we also describe a simple mounting method that allows easy flipping of the brain samples, enabling convenient imaging of both sides of the brain with similar signal intensity and quality.

As a proof-of-concept for the application of this method, we further examined the presence of DA neurons in the brains of w^{1118} flies; a genotype that is often used as the parental line for generating transgenic flies and the wildtype control in many *Drosophila* studies.

2.2   Results

TH controls the rate-limiting step in DA synthesis and is the enzyme specific for DN. Using immunofluorescent staining with anti-TH antibody on whole-mount adult brains, we analyzed the presence and distribution of DN in the protocerebrum from w^{1118} flies (Figure 2.2).

Figure 2.1 illustrates the main procedures for adult brain dissection. Figures 2.2 and 2.3 are representative images of 3-day-old w^{1118} adult fly brains, which were co-stained with an antibody against tyrosine hydroxylase (TH, colored in red in Figure 2.2 and white in Figure 2.3), in addition to the DNA dye DAPI that labels all the cell nuclei, and an antibody against Elav protein, which is a marker for all differentiated neurons in the fly (colored in green). Taken together, IF staining with these markers revealed the overall structure of the brain.

We grouped the DN into different clusters largely following the early designation (Mao and Davis, 2009) (Fig. 1.3a).   Figures 2.2A-D and 2.3 A and C show the anterior view of a brain, whereas Figures 2.2 E-H and 2.3 B and D show the posterior view of the same brain after flipping the cover slips that hold the brain samples, which display a similar level of signal intensity between two sides of the brain for all the three imaged channels.

The panels in figure 2.3 show anterior and posterior views of the same brain in high-magnification, revealing the different clusters of DN on both sides of the brain. The DN were grouped into different clusters following the early designation (Mao and Davis, 2009), although here we use the name Paired Posterior Medial (PAM); Paired

Posterior Medial (PPM) to include the PPM1, PPM2, and PPM3 clusters at the anterior side of the brain; and the name Paired Posterior Lateral (PPL) to cover the PPL1 and PPL2 clusters from the posterior side of the brain, as depicted in Figures 2.3A (Anterior view) and 2.3B (Posterior view). The white dashed lines highlight the prominent PAM and Paired Anterior Lateral (PAL) clusters in the anterior side of the brain (Figure 2.3A) as well as the PPL and the PPM clusters in the posterior side of the brain (Figure 2.3C).

Figure 2.4A and 2.4B show quantification results for DN clusters in w^{1118} flies. We counted DN slice by slice and also from 3-D reconstructed images, which should prevent the generation of imprecise results. We estimate that the 3-day-old w^{1118} flies have an average of 27 DA neurons in the PPM clusters of the whole brain, 16 DN in the PPL cluster per hemisphere, 5 DN in PAL cluster per hemisphere (Figure 2.4A), and 97 DN in each of the PAM clusters (Figure 2.4B).

Figure 2.4C is a representative 3-D reconstruction of DA neurons in the PAL and PAM clusters, projected from high-magnification images. It is apparent that compared to other clusters such as the PAL, DA neurons in the PAM cluster have relatively smaller cell sizes and weaker TH staining signal.
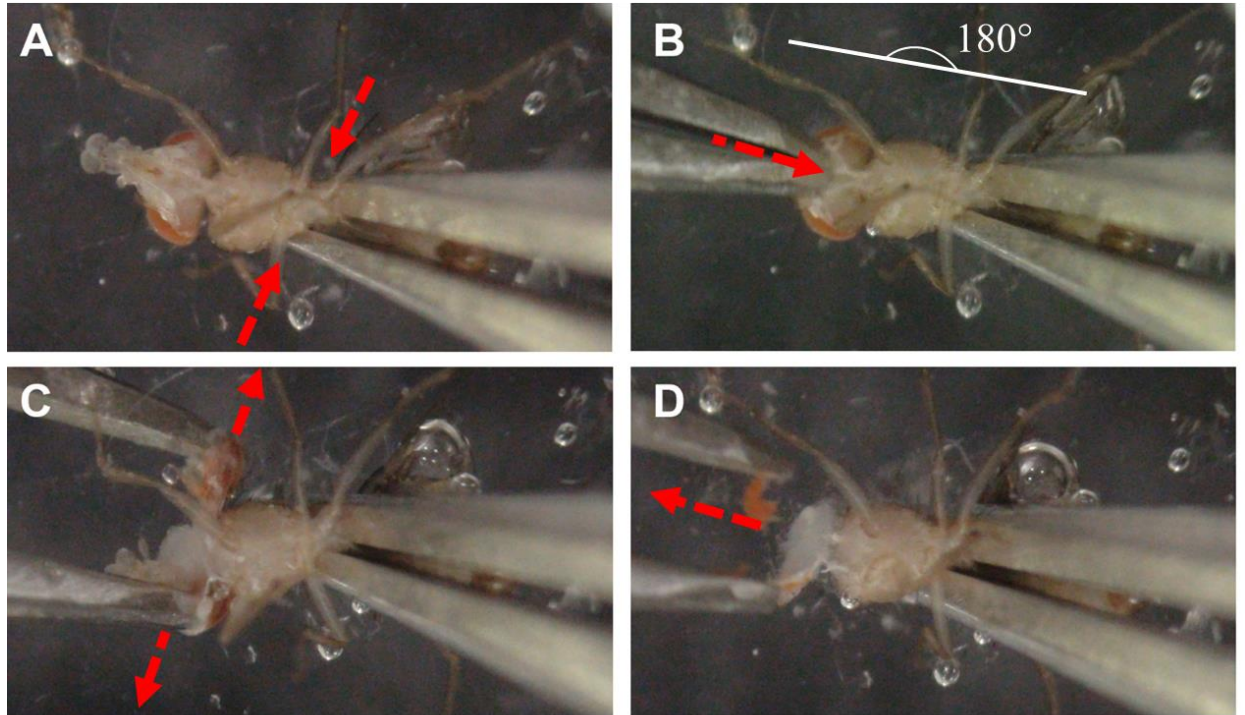
Figure 2.1: Graphical illustration of the dissection protocol for adult *Drosophila* brain.

(A) Flies are positioned with the anterior side upwards, and held by the thorax using the non-dominant hand. Force was gently applied (red arrows) to the forceps to induce backward tilting of the fly head and slight outward extension of the proboscis, exposing the white transparent region below. (B) Forceps are inserted in the transparent region beneath the proboscis, creating a shallow incision. Note that the forceps we use do not have very fine tip ends. (C) Forceps are allowed to come apart through its own force. The momentum generated by opening the forceps removes the eyes and exoskeleton, exposing a relatively clean *Drosophila* brain. Most of the trachea are removed in the process. (D) Excess tissue surrounding the brain is removed for full exposure of the brain proper.
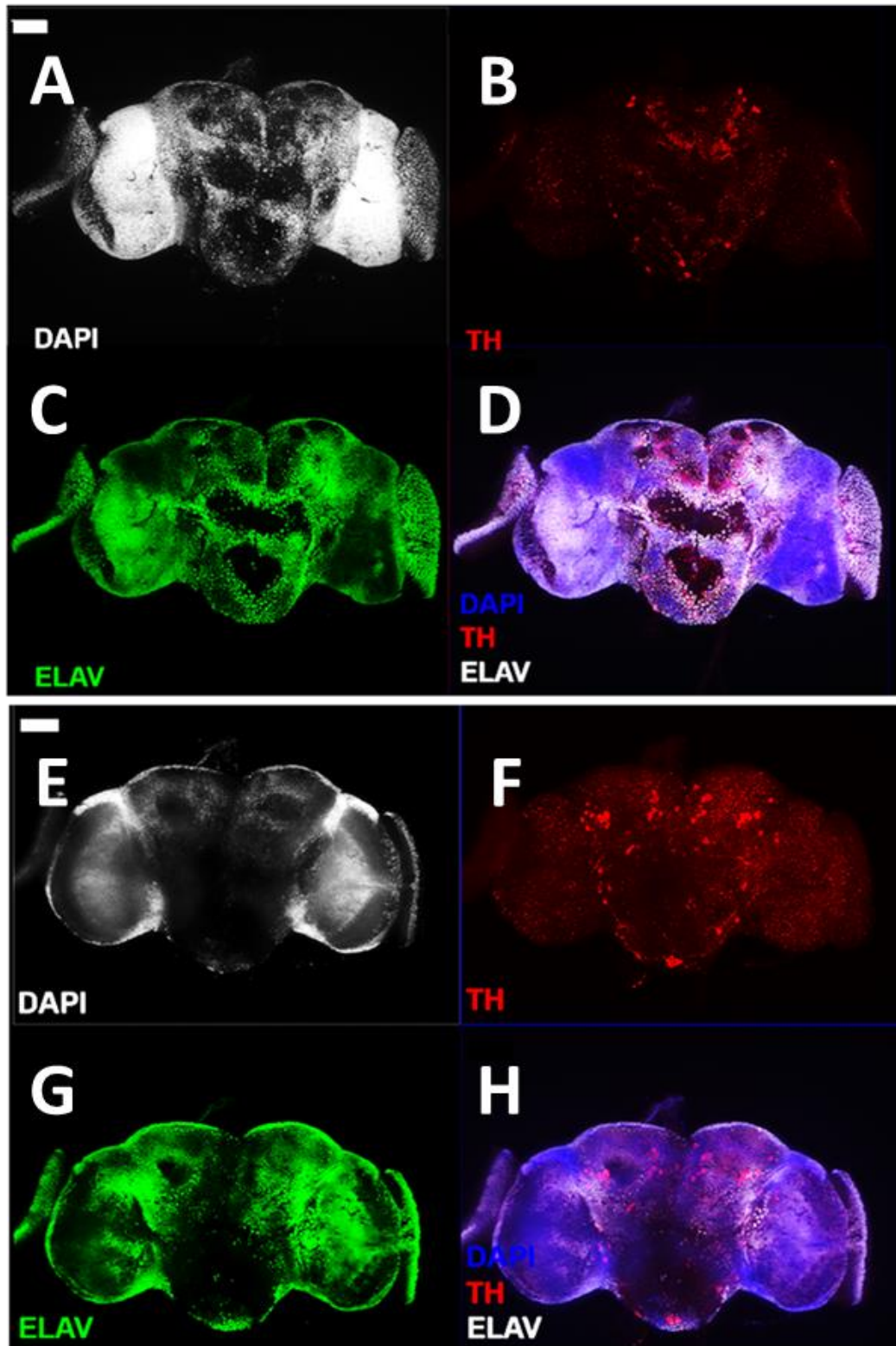
Figure 2.2: Adult fly brain morphologies are preserved

This figure depicts representative images of dissected adult brains, reconstructed using Z-stacked images of the brain region of interest obtained with the compound fluorescent microscope. (A-D) Anterior and (E-H) Posterior views of the same adult brain; (A & E) Cell nuclei were imaged by DAPI staining (white) and (C and G) neurons were labeled by pan-neuronal marker anti-Elav antibodies (green); (B & F) DN are revealed by anti-TH antibodies (red). (D & H) Overlay of images for DAPI, TH and Elav treatment. (E & J) Enlarged view of the brain regions with DN shown in white. All genotypes are adult males of w^{1118} flies. Scale bars = 20 μm.
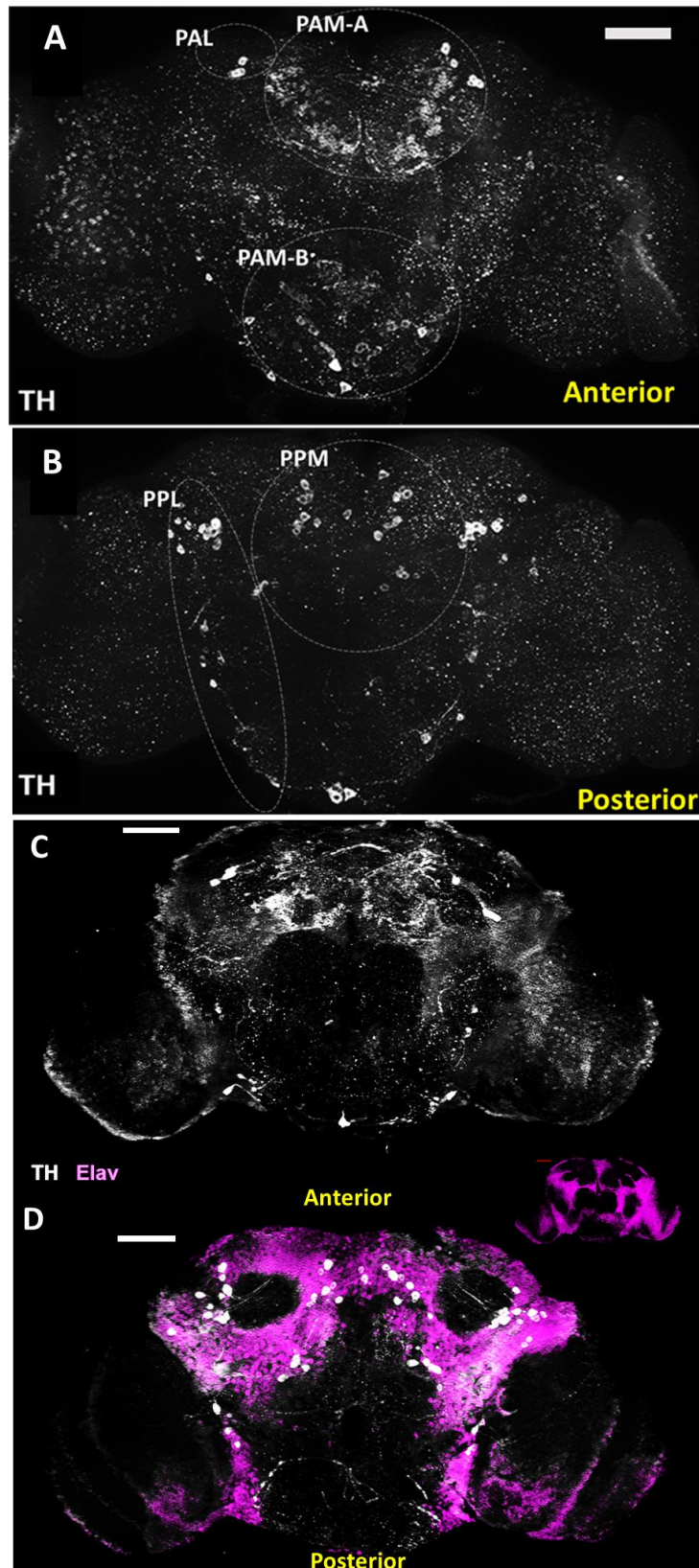
Figure 2.3: DN revealed with anti-TH antibody in the adult male and female *Drosophila* brain (acquired with 20X objective).

(A-D) Anterior (A and C) and posterior (B and D) views of DA neuron distribution in wildtype adult *Drosophila* brain.

PAM cluster neurons are located near the antennal lobe regions. (A & C) Anterior and (B & D) Posterior views of the same adult brain; (A-D) DN are revealed by anti-TH antibodies (red). (D) Overlay of images for TH and Elav treatment. All genotypes are adult (A & B) males and (C & D) females of w^{1118} flies. Scale bars = 20 μm.
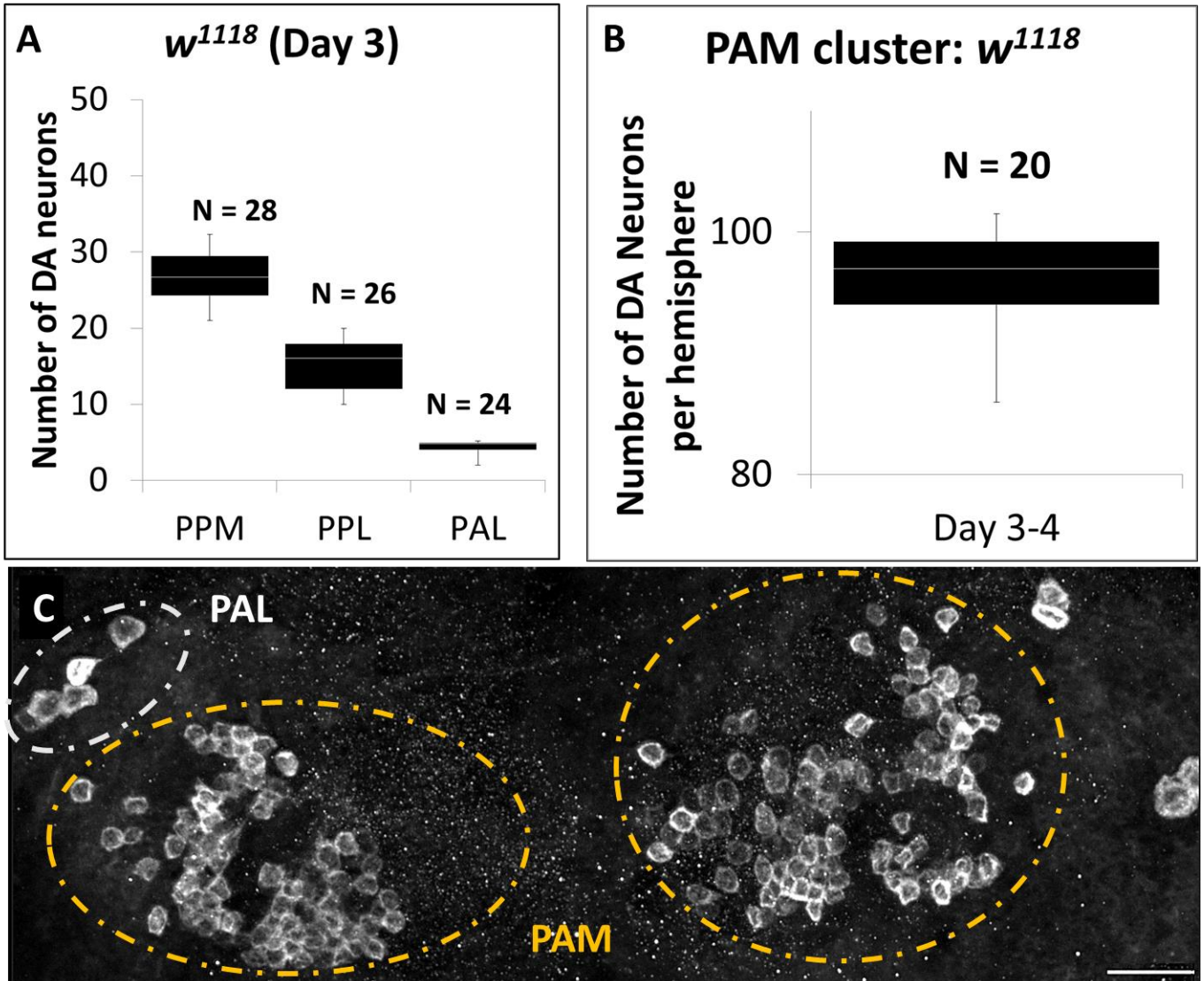
Figure 2.4. Quantification of DN in brains of male adult w^{1118} flies (acquired with 40X objective).

(A-B) Quantification of DN, revealed by anti-TH staining. Data are represented by whisker box plots showing minimum and maximum values as the outliers; as well as the first, second and third quartiles. The second quartile is represented as the mean (average) value. (A) PPM (n = 28) Min: 21, Q1: 24, Average: 27, Q2: 30, Max: 32, PPL (n = 26) Min: 10, Q1: 12, Average: 16, Q2: 18, Max: 25, and PAL (n = 24), Min: 2, Q1: 4, Average: 5, Q2: 5, Max: 10 clusters; and (B) PAM (n = 20) Min: 86, Q1: 94, Average: 97, Q2: 97, Max: 99 cluster of day 3 male w^{1118} flies. (C) A representative projection image showing DN in the PAM and PAL clusters of male w^{1118} flies at day 3. Scale bar represents 20 μm.

2.3   Discussion

With an increasing interest in using adult *Drosophila* brain to study human brain diseases, neuronal circuitry, and higher brain functions, it is important to develop simple and quick methods to harvest intact fly brains for whole-mount analyses. These will be especially important in supporting large-scale brain-based screens.

Our method provides a simple and easy-to-learn approach to dissect out a fly head (often in less than 10 seconds with gained experience) and obtain samples with well-preserved morphology and largely devoid of associated tissues. Our method also significantly minimizes sample loss, which can be a prominent issue in processing brain samples of tiny sizes.

As the dissected brains are still attached to the rest of the fly bodies, they quickly sink to the bottom of the sample tube and are not easily lost during the washing and staining steps. Therefore, our method provides a robust way to perform the washes without losing the brains in the pipette tip.   The brains are then detached after completion of the staining procedure. As shown in the representative images in Figures 2.2-2.3, brains prepared using this protocol produce satisfactory results.

Previous characterization of DN in adult *Drosophila* brains, including fly models of human disease genes, such as *parkin* mutants*,* have largely focused on the PAL, PPL, and PPM clusters with relatively large cell sizes and prominent expression of TH (Kim *et al.*, 2012; Pesah *et al.*, 2004; Trinh *et al.*, 2010; Whitworth *et al.*, 2005; Yang *et al.*, 2006).   However, the majority of DA neurons in the fly brain are found in the PAM clusters, with about 100 DN per hemisphere.

DA neurons in the PAM cluster show reduced protein levels of TH and have smaller cell sizes, in contrast to other DN clusters. DA neurons in the PAM cluster can be clearly imaged at high resolution following our dissection and staining method, which circumvents the need for a confocal microscope. Given the large number of DA neurons in the PAM cluster, our method allows for the incorporation of a larger sample size. We suggest that the DA neurons in the PAM cluster represent a useful system for studying DA biology and model DA-related disorders, such as PD.

The improved microsurgical technique is effective in saving time and providing morphologically preserved, well-structured, brain samples, which is useful in studying the anatomical areas of interest in detail. Visualization of DN in the adult brain serves as a putative strategy to study various genetic manipulations and toxins that can contribute to DN degeneration.

Moreover, our method significantly reduces the dissection time, which is crucial for the investigation of kinase activities *in vivo*.   Our procedure minimizes the time of dissection from 2-5 minutes to less than 10 seconds, which is important to probe for the kinase activity of LRRK2. For instance, the kinetic activities of enzymes, such as PKA and LRRK2, may become compromised in brain samples that are not placed on ice, quickly after dissection.

This three-step method also enhances the brain sample quality by facilitating the removal of almost all trachea and cuticle, which normally interfere with the imaging process. The previously defined adult brain dissection techniques (Luo, L. & Wu, J., 2006 and Sweeney, S. *et al.* 2011) detach the head from the body. The brain

tissues are exposed by carefully holding the anterior and posterior ends of the head. This can prove difficult for students and novice investigators. The simple action of releasing the forceps on the head case, as shown in Figure 2.1c, leaves the brain attached to the body and does not induce damage to the brain.

Critical steps for the protocol involve positioning the fly correctly in the CSF, maintaining the proper angles when removing the exoskeleton from the fly head, and providing the right amounts of force required in performing each step. In the event that the head is removed from the body, it is recommended to hold the head from the dorsal side of the heads while using the forceps in the dominant hand to remove the head case. It is also not required that the investigator performs the protocol in less than 10 seconds.

Overall, the investigator must pay careful attention not to squeeze the abdomen too tightly, as this will only damage the internal organs of the fly. Nevertheless, it is preferable for the investigator to master the procedure in dispensable flies before attempting to work on the experimental samples. Also, the best way to assess for changes in neuronal survival is to count the neurons on each thin section of the z-stack, which is particularly relevant for studying the PAM cluster.

Although our method significantly reduces the time required to perform each dissection, it is limited, in that, it is difficult to maintain consistent forces across experimental trials. The technique requires a significant amount of focus from the investigator and a lot of time to master. It is also complicated by the fact that hands

become tired after performing the experiments for long periods of time. Hence, it is recommended for the investigator to take breaks during the experiments.

Finally, brain studies of the adult fly often require imaging cells on both sides of the same brain. For example, DA neurons are present in clusters of both the anterior and posterior sides of the brain. However, due to its thickness, the side away from the light source usually yields weaker signals and less clear images.

Mounting the samples in between two cover slides allows for the convenient flipping of the brains, which is useful in imaging both sides of the same brain with similar signal intensities. Figures 2.2-2.3 show images of DA neurons in both sides of fly brains, resulting in a relatively comparable signal intensity and imaging quality.

In our experience, the apotome function from a Zeiss compound fluorescence microscope can significantly reduce the background signal from imaging the fly brains. Although the confocal microscope produces images with more details, higher magnification and better quality, it is often time-consuming and costly.

This is especially true for imaging a large number of thick samples that require series of Z-stack section for clear 3-D reconstruction and deconvolution analysis. In this perspective, the apotome function represents a fast and cost-effective alternative for producing images of sufficient quality (e.g., images in Figures 2.2 and 2.3), which may become applicable for the imaging of other organ types of other species.

3   NEURONAL COMPOSITION OF THE PAM CLUSTER

3.1   <u>Introduction</u>

In mammals, the DA-synthesizing neurons are organized into nine discrete clusters that project to different regions of the brain and modulate diverse types of neurological activities (Konrad and Marsh, 1987; Lauvrak *et al.*, 2005; Lee *et al.*, 2008; Lundell and Hirsh, 1994). Notably, not every cluster is equally vulnerable to pathological conditions. In particular, the progressive loss of DN in PD patients primarily occurs in the pars compacta of the substantia nigra (SNPC), a region with a high density of DN (Damier *et al.*, 1999; Gibb and Lees, 1991). Yet, the cause for such selectivity is unknown.

In Chapter 1, I introduced how *Drosophila*, a classic genetic model organism, can be employed to study the regulation and function of DA and to model related neurological disorders including PD (Waddell, 2010; Wangler *et al.*, 2015; Yamamoto and Seto, 2014). Resembling those in mammals, the DA neurons in fly brains are distributed in clusters in a relatively stereotypical pattern (Figure 1A) with distinct axonal projections that modulate discrete brain functions, including locomotion, motivation, sleep and arousal, as well as learning and memory (Bjorklund and Dunnett, 2007; Mao and Davis, 2009; Waddell, 2010).

Notably, the majority of DA neurons in fly brains are contained in two protocerebral anterior medial (PAM) clusters, with about 100 neurons per hemisphere (Budnik and White, 1988; Mao and Davis, 2009). Although these PAM cluster DA

neurons mainly project to the medial lobes of the mushroom bodies, distinct subsets of DA neuron projections have been shown to innervate different regions of the medial lobes and mediate a diverse set of distinct functions. These include reward signals for short- and long-term memories and startle-induced locomotion(Burke *et al.*, 2012; Huetteroth *et al.*, 2015; Liu *et al.*, 2012; Mao and Davis, 2009; Riemensperger *et al.*, 2013; Yamagata *et al.*, 2015).

Although these functions are linked to monoamine neurotransmission, it is not clear whether the relatively tightly packed PAM cluster also contains other catecholamine synthesizing neurons apart from DN. In this chapter, I will present an in-depth characterization of the types of neurons present in a relatively understudied area of the adult fly brain.

In *Drosophila,* the cellular machineries involved in DA synthesis and regulation, such as DA transporters dVMAT and dDAT, synthetic enzymes dTH and dDDC are also highly conserved. The Gal4-based enhancer trap lines have been indispensable for anatomical and functional dissection of neuronal circuitry in the fly brain (Brand and Perrimon, 1993; Jenett *et al.*, 2012).

To characterize the tools useful in studying the PAM cluster in detail, we compared several existing Gal4 lines and further generated a new *vmat*-Gal4 driver line and an endogenous GFP-tagging line for *vmat* gene that expresses VMAT-GFP fusion protein from its own native genomic loci. Both the *vmat*-derived reporter lines can largely recapitulate the endogenous expression pattern of *vmat* gene, including its prominent expression in the PAM cluster neurons.

Analyses of these lines reveal that, in addition to the predominant DN, the PAM cluster also contains a small number of octopamine neurons. This raises an interesting possibility that DA and octopamine neurons in the PAM cluster might form a functional circuitry to mediate brain functions, such as learning and memory.

3.2   Results

3.2.1   Distribution of DA Neurons and DA in the Adult *Drosophila* Brains

TH controls the rate-limiting step in DA synthesis and is an enzyme that is specifically expressed in DA neurons. Using immunofluorescent staining with anti-TH antibody on whole-mount adult brains, we analyzed the presence and distribution of DA neurons in the protocerebrum from w^{1118} flies (as shown in Figures 2.2 and 2.3). We grouped the DA neurons into different clusters, largely following an early designation scheme (Mao and Davis, 2009) (Fig. 1.3A).

Consistent with previous reports (Mao and Davis, 2009), 3-day-old fly brains have an average of 27 DN (n = 28, SD = 0.93) in the PPM cluster in the whole brain; 97 DA neurons (n = 20, SD = 1.01) in each of the two PAM clusters (Figure 3.1 G); 16 DN (n = 26, SD= 0.96) in each of the two PPL clusters; and 5 DA neurons (n = 24, SD = 0.31) in each of the two PAL cluster (Figure 3.1 H).

Anti-TH staining also revealed the relatively smaller sizes and weaker levels of TH expression in DA neurons of the PAM cluster (e.g., highlighted in dashed cycle in Figure 3.1E and F) as compared to those in other clusters, such as the neighboring PAL cluster (yellow arrows in Figure 3.1E and 2F).

Although DA neurons in PAM clusters are tightly packed, we noticed stretches of TH-negative areas (yellow arrows in Figure 3.1C and 3.1D). Additionally, in some brains we found that DN in PAM clusters are tightly packed together, while in others, they are more dispersed (Figure 3.1E and F).

3.2.2 Expression of multiple DA Pathway Gal4 Drivers in the PAM Cluster Neurons

We next examined a collection of Gal4 lines involved in the synthesis of DA, derived from the *th* and *ddc* genes; and those involved in the regulation of DA, derived from the *dat* gene. Gal4-expressing cells were labeled with membrane-associated fluorescent protein reporters including UAS-mCD8::GFP, UAS-mCD8::RFP or UAS-Lamin::GFP, and double stained with anti-TH and anti-GFP or anti-RFP antibodies.

A *TH-Gal4* line, generated using a ~11kb genomic DNA fragments from the d*th* gene that covers ~4.3 Kb of its 5' regulatory region in addition to about 7Kb of its coding and 3' UTR region, has been used extensively to monitor DN in the fly brains (Friggi-Grelin *et al.*, 2003).

DDC controls the last step of DA synthesis, converting L-Dopa to DA (Figure 1.3B). In addition to DA, DDC is also required for the synthesis of neurotransmitters serotonin from L-5-hydroxytryptophan, and thus it serves as a marker for both DA and serotonin neurons. A *DDC-Gal4* line, generated using a 7.5kb genomic DNA fragment encompassing the d*Ddc* gene, has been used to examine and manipulate DA and serotonin neurons in the fly brains (Li *et al.*, 2000).

Consistent with previous reports (Friggi-Grelin *et al.*, 2003; Liu *et al.*, 2012; Mao and Davis, 2009), for DA neurons in the PAM cluster, a majority can be labeled by DDC-Gal4 but only a small number of them are positive for *TH-Gal4* (data not shown). DA-specific DAT functions to recycles synaptic DA back into the cytosol of DA neurons and terminate DA action (Torres *et al.*, 2003).

A PAM-specific Gal4 driver, *R58E02-Gal4,* was generated using a 1,235 bp fragment from the first intron region of d*Dat* gene (Liu *et al.*, 2012; Pfeiffer *et al.*, 2008). Double labeling with mCD8-RFP (Figure 3.3A-D) or Lamin-GFP (Figure 3.2 C and E) reporters and anti-TH antibody labels the projections from the DA neurons and reveal that a majority of neurons in the PAM clusters are positive for both markers.

Specifically, the *R58E02-Gal4* are expressed in the majority of TH-positive neurons (white arrows in Figure 3.2E), in addition to a small number of TH-negative neurons (yellow arrows in Figure 3.2E) in the PAM cluster. Note that the *R58E02-Gal4* expression is absent from other DN clusters (e.g., PAL neurons in Figure 3A) in the brain, as previously reported (Liu *et al.*, 2012).

Thus, similar as to the *TH-Gal4* and *DDC-Gal4* lines, the genomic fragment used to make the *R58E02-Gal4* construct lacks the full regulatory elements controlling the proper expression of the native d*Dat* gene in the brain. Consistent with the previous reports (Liu *et al.*, 2012; Mao and Davis, 2009), *R58E02-Gal4*-positive neurons mainly project to the medial lobes of the mushroom bodies, as revealed by the membrane-bound mCD8-RFP reporter and double stained for mushroom body-specific anti-FasII antibody (Figure 3.3 A-D).

Recent studies reveal a reinforcement circuitry for learning and memory through DA and octopaminergic neurons in *Drosophila* brain (Burke *et al.*, 2012; Huetteroth *et al.*, 2015). Consistent with this finding, an α-adrenergic-like octopamine receptor OAMB (Octopamine receptor in mushroom bodies) is highly expressed in a subset of DN in the PAM cluster (Han *et al.*, 1998), a pattern that is also captured by

the *R48B04-Gal4* driver line, whose expression is controlled by a genomic fragment from the *oamb* promoter regions (Huetteroth *et al.*, 2015; Jenett *et al.*, 2012; Yamagata *et al.*, 2015).

Examination of the *R48B04*-Gal4 line confirmed its expression in about 80% of TH-positive DN, in addition to a small number of TH-negative neurons within and around the PAM cluster (examples indicated by yellow arrows in Fig. 3.4C). Additionally, *R48B04-Gal4* also labels some cells within the optic lobes, as previously reported (data not shown) (Huetteroth *et al.*, 2015).

Notably, *R48B04-Gal4* expressing neurons innervate almost all the mushroom body structures, including both the vertical lobes and the horizontal lobes (compare the trident-like structure on Figure 3.5 with the mushroom body structures revealed by anti-FasII staining in Figure 3.3B). This is in contrast to the rather restricted projection to primarily the medial lobes by the *dDat* promoter-derived *R58E02-GAL4* line (Figure 3.3D), which closely resembles the results obtained from independent *oamb-Gal4* lines, harboring the complete promoter regions of *oamb* gene (El-Kholy *et al.*, 2015). These results are also in line with the broader expression of *oamb* gene, observed outside the PAM cluster neurons (Figure 3.5A and B).

3.2.3 MiMIC-derived VMAT-Gal4 and VMAT-GFP lines recapitulate the Endogenous VMAT Expression Pattern

To generate *vmat*-derived marker lines that can label DA and other monoamine neurons in the brain, we utilized the recently developed Minos-mediated integration cassette (MiMIC) technique *(Nagarkar-Jaiswal et al., 2015a; Nagarkar-Jaiswal et al., 2015b; Venken et al., 2011).* We used a coding intronic insertion MI07680

for EGFP tagging of endogenous VMAT, that we called *VMAT^MI-GFP*; and a 5' UTR intronic insertion MI03756 for creating a VMAT-Gal4 line, that we called *VMAT-Gal4^MI03756*.

More specifically, the MI03756 line is inserted in the 5' regulatory region of *vmat*, in-between the first two non-coding exons. We then examined the expression pattern of the *VMAT-Gal4^MI03756* along with UAS-Lamin::GFP, which marks the nuclear membrane and thus allow more clear identification of individual cells. The *VMAT-Gal4^MI03756* line shows similar expression pattern as endogenous dVMAT proteins (Figure 4 and data not shown).

Importantly, in the PAM cluster, which is prominently labeled by the *VMAT-Gal4^MI03756*, all TH-expressing DN are positive for Lamin-GFP reporter (white arrows in Fig. 4F). Outside of the PAM cluster, except for a cluster of DN around the esophagus region in the ventral brain, almost all the other TH-expressing neurons were labeled by *VMAT-Gal4^Mi03756*, including numerous cells within the optic lobes and the clusters of DN in the protocerebrum (Figure 3.6A-B).

MI07680 is inserted in a coding intron in-between exon 5 and 6 near the 3' of *vmat* gene, thus the expression of EGFP tagged gene is controlled by the native regulatory elements. Indeed, the VMAT-EGFP fusion protein expressed from *VMAT-EGFP^MI07680* line closely mirrors the expression pattern of endogenous dVMAT protein (Figure 3.7).

For example, VMAT-EGFP co-localizes with all the TH-positive DN in the PAM clusters and in other brain regions (white arrows in Fig. 3.7C and data not shown). Together, they support that both the MiMIC-derived *VMAT-Gal4^MI03756* driver and the

VMAT-EGFP[MI07680] line can largely recapitulate the endogenous expression pattern of *vmat* gene, and thus can be used as new tools to analyze DA and other monoamine neurons in *Drosophila*.

3.2.4 **VMAT-positive PAM cluster is primarily composed of DA and octopamine neurons**

Examination of the two VMAT reporter lines also revealed that, within the PAM clusters, a number of VMAT-expressing neurons do not express TH (yellow arrows in Figure 3.6F and 3.7C and 3.9C), suggesting that besides DN, the PAM cluster also contains other types of monoamine neurons. Notably, these TH-negative PAM neurons show relatively higher levels of VMAT expression and mostly have larger cell sizes when compared to the neighboring TH-positive neurons within the same cluster, as observed in both VMAT-EGFP[MiI7680] and *VMAT-GAL4[MI03756]* lines (yellow arrows in Figures 3.6F, 3.7C and white arrowheads in Figures 3.9A-D and 3.10 D).

These "VMAT-expressing, TH-negative" neurons are unlikely to be histaminergic, which mainly utilizes histamine as a neurotransmitter for photo-transduction in the eye (Hardie, 1987; Sarthy, 1991). To determine their identities, we next performed co-immunofluorescence studies on the adult brain from the two VMAT reporter lines. Staining with anti-Serotonin antibody revealed no serotonin-positive neurons in the PAM cluster (data not shown), which is consistent with the previous studies on the distribution of serotonin neuron that largely exclude its presence in the PAM cluster region (Liu *et al.*, 2012; Sitaraman *et al.*, 2008; Valles and White, 1988).

Given that serotonergic and histaminergic neurons are not present in the PAM cluster, it suggests that octopaminergic neurons, another class of monoamine

producing neurons, could be part of this PAM cluster. The neuronal TDC2 enzyme is required for the synthesis of octopamine from precursor tyrosine (Figure 1.3B), and a *TDC2-Gal4* line has been used to label octopamine neurons (Cole *et al.*, 2005; Monastirioti *et al.*, 1996).

Co-labeling with anti-TH antibody revealed about fifteen *TDC2-Gal4* expressing cells located within or near the TH-positive PAM cluster (Figure 3.8A and 3.9A, indicated by yellow arrows in Figure 3.8C). This group of *TDC2-Gal4* neurons are reminiscent of the "anterior superior medial (ASM)" cluster of octopamine neurons described in a previous study using the same *TDC2-Gal4* (Busch *et al.*, 2009), located near the similar region.

Furthermore, most of these *TDC2-Gal4* positive neurons also have relatively larger cell sizes. Together, they suggest that the "VMAT-expressing, TH-negative" cells in the PAM cluster are octopamine origin. Consistent with this conclusion, when the mito-RFP reporter driven by *TDC2-Gal4* was expressed in VMAT-EGFP[MI07680] brains, mito-RFP signal largely overlapped with the GFP-positive cells (white arrows in Figure 3.9A-D and 3.10D). Collectively, they support that the "VMAT-expressing, TH-negative" neurons in the PAM cluster are octopamine neurons, and the PAM cluster is primarily comprised of DA and to a lesser extent octopamine neurons.
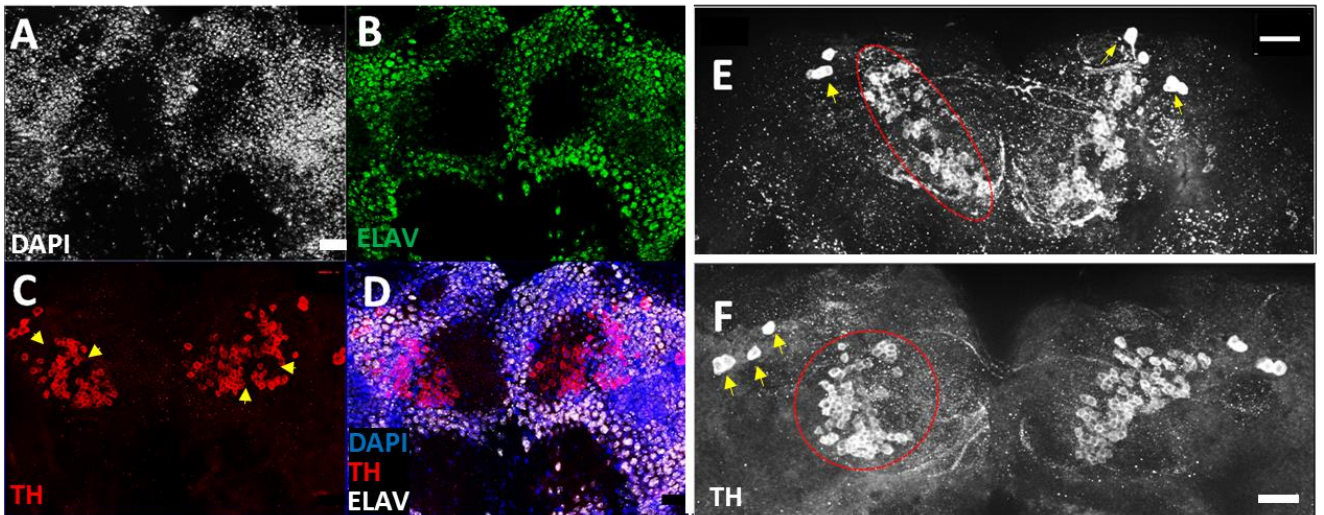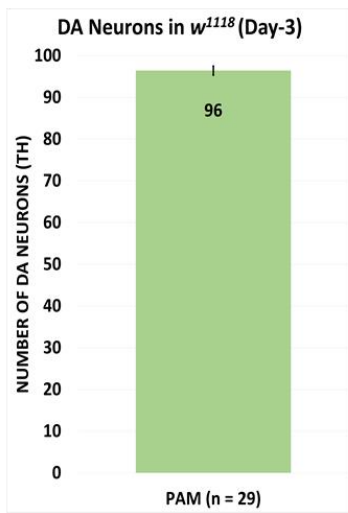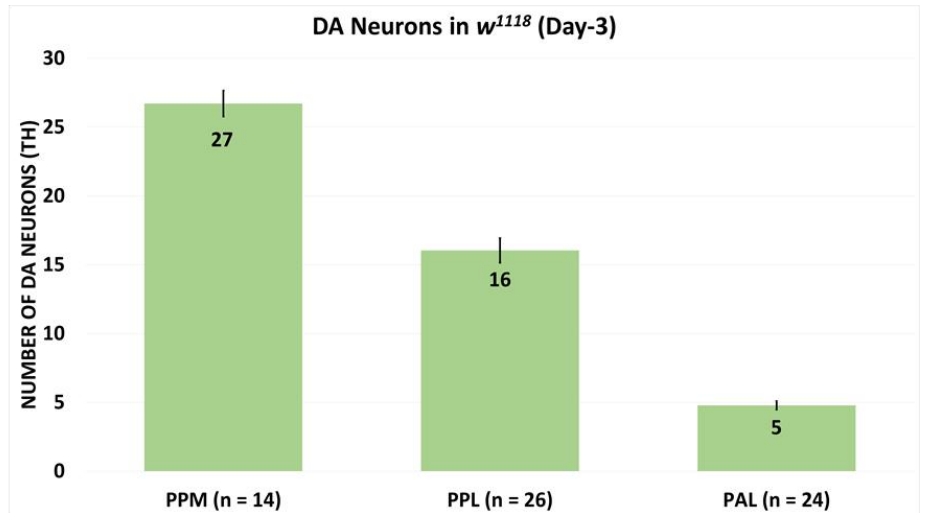
Figure 3.1: DA system in adult *Drosophila* brain.

DN in the PAM cluster region of adult *Drosophila* brain.

(A-D) immunofluorescent imaging of 3-day-old male brains visualized with DNA dye DAPI for cell nuclei (A, white), pan neuronal marker anti-ELAV antibody (B, green), anti-TH antibody for DN (C, red), and their overlaid images (D). Yellow arrows in (C) indicate apparent gaps among the TH-positive neurons in PAM clusters. PAM cluster neurons are located near the antennal lobes.

(E and F) Examples of variable distribution pattern of DN in the PAM clusters (outlined by red dashed lines) from two individual adults, revealed by anti-TH antibody. PAM cluster DN in (E) are more dispersed than those in (F). Yellow arrows in E and F point to PAL cluster of DN. (G) Quantification of DN in the PAM cluster. There is an average of 96 DN per hemisphere in 3-day-old (n = 20, SD= 1.01). (H) Quantification of DN in PPM, PPL, and PAL clusters at day 3. There is an average of 27 DN in the PPM cluster (n = 28, SD = 0.93) from the whole brain, as well as 16 and 5 DN per hemisphere in PPL *(n = 26 SD= 0.96)* and PAL *(n = 24,* SD = 0.31), respectively. All genotypes are adult males of w^{1118} flies. Scale bars in (A-F) represent 20 μm, while scale bars in (I and J) represent 50 μm.
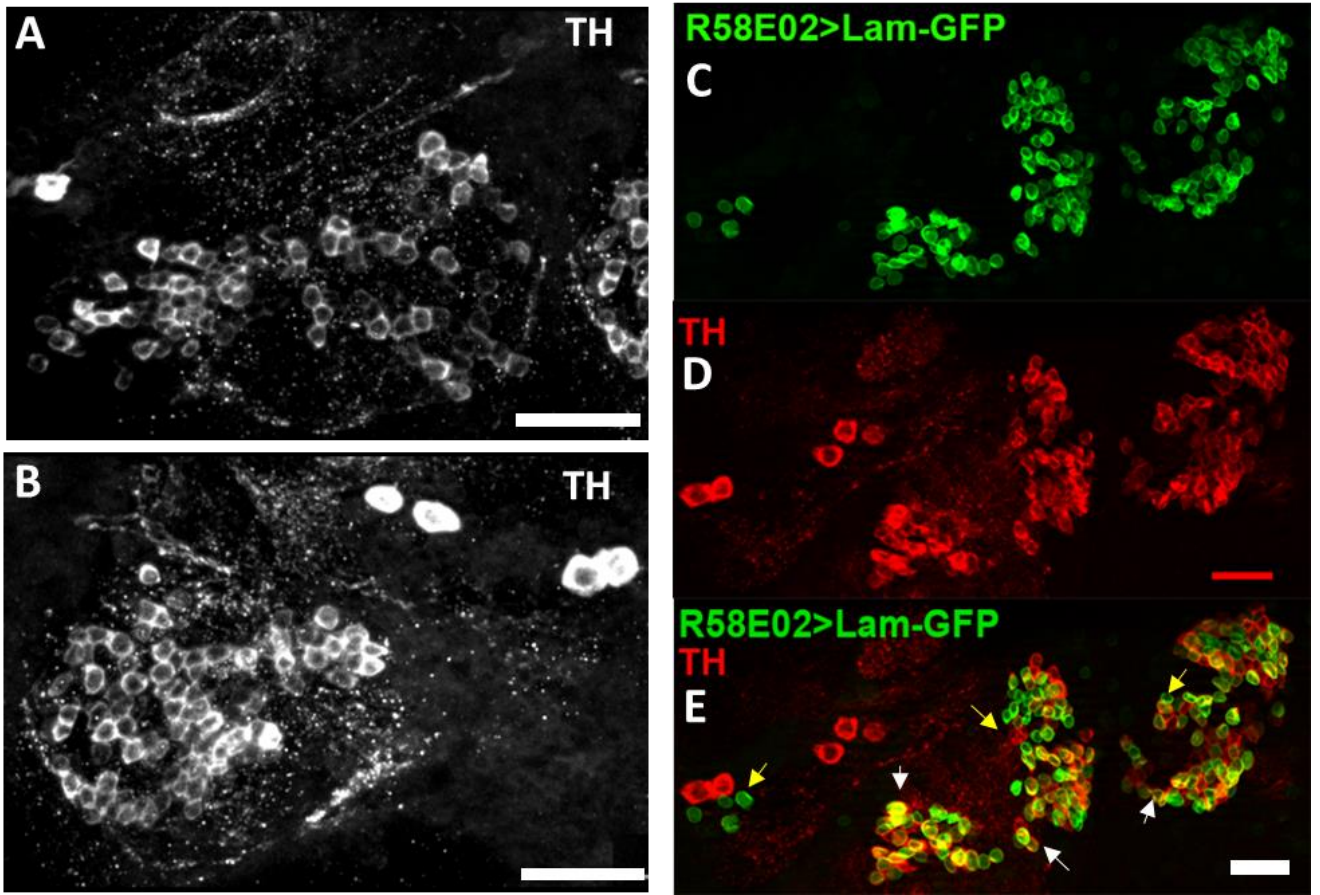
Figure 3.2: Expression patterns of the *R58E02-Gal4* line in the PAM cluster region

(A-B) TH expressing DN in the PAM cluster region of the left and right hemisphere. (C-E) *R58E02-Gal4* is expressed in almost all the DN in the PAM cluster (white arrows in E indicate examples of overlapping expression). Note that some GFP-positive cells do not express TH (yellow arrows in E). All images are from anterior view of w^{1118} male brains. Scale bars in (A-I) represent 20 μm.
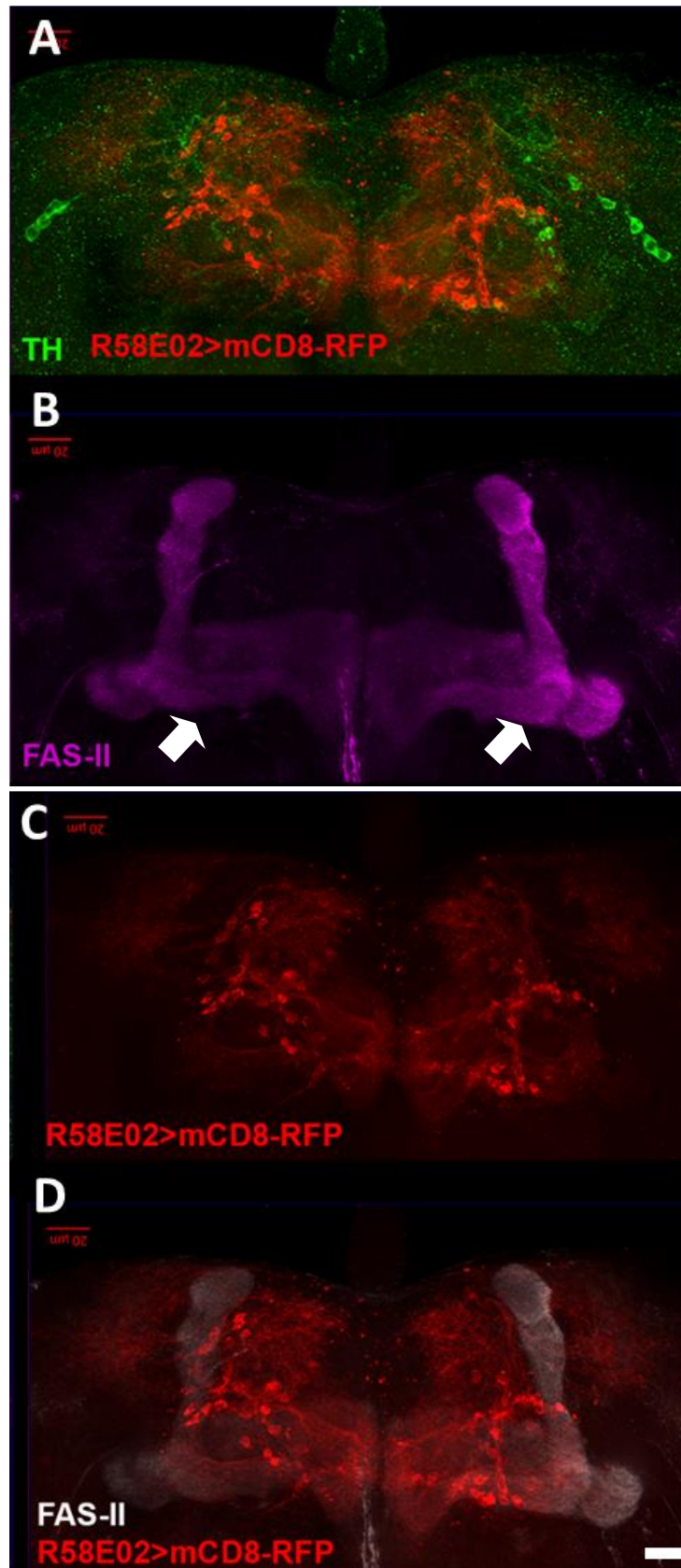
Figure 3.3: Projection patterns of the *R58E02-Gal4* line in the PAM cluster region

The projection patterns of the Gal4 line in the PAM cluster was revealed mCD8-RFP reporters (red in A-D). The brains were also co-stained for anti-TH antibody (green in A). *R58E02-Gal4* line mainly projects to the medial lobes (white arrows) in the mushroom bodies , as revealed by the overlap between the mCD8-RFP reporter (red) and the mushroom body marker anti-Fas II (cyan in B and white in overlaying image D). All images are from anterior view of w^{1118} male brains. Scale bars in (A-I) represent 20 µm.
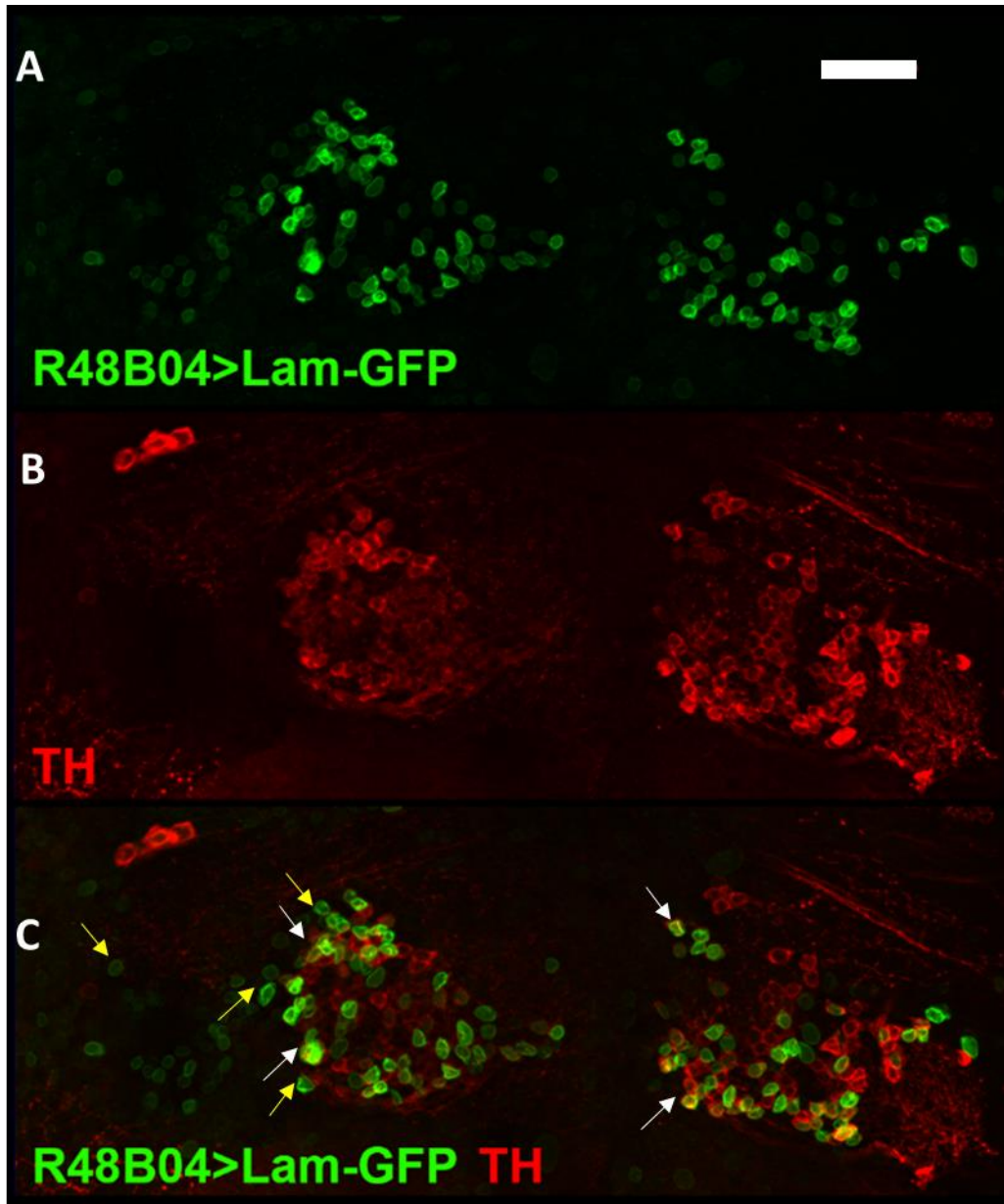
Figure 3.4: Overlapping but distinct expression patterns of Oamb-GAL4

(A-C) *R48B04-Gal4* line is expressed in only a subset of DN (white arrows) in the PAM cluster, in addition to some neighboring non-DN (yellow arrows) nearby (C). In (C) white arrows indicate examples of cells co-expressing both TH and GFP markers, while yellow arrows indicate GFP-expressing cells that are negative for TH.   All images are from anterior view of w^{1118} male brains. Scale bars in (A-C) and (D-E) represent 20 μm and 50 μm, respectively.
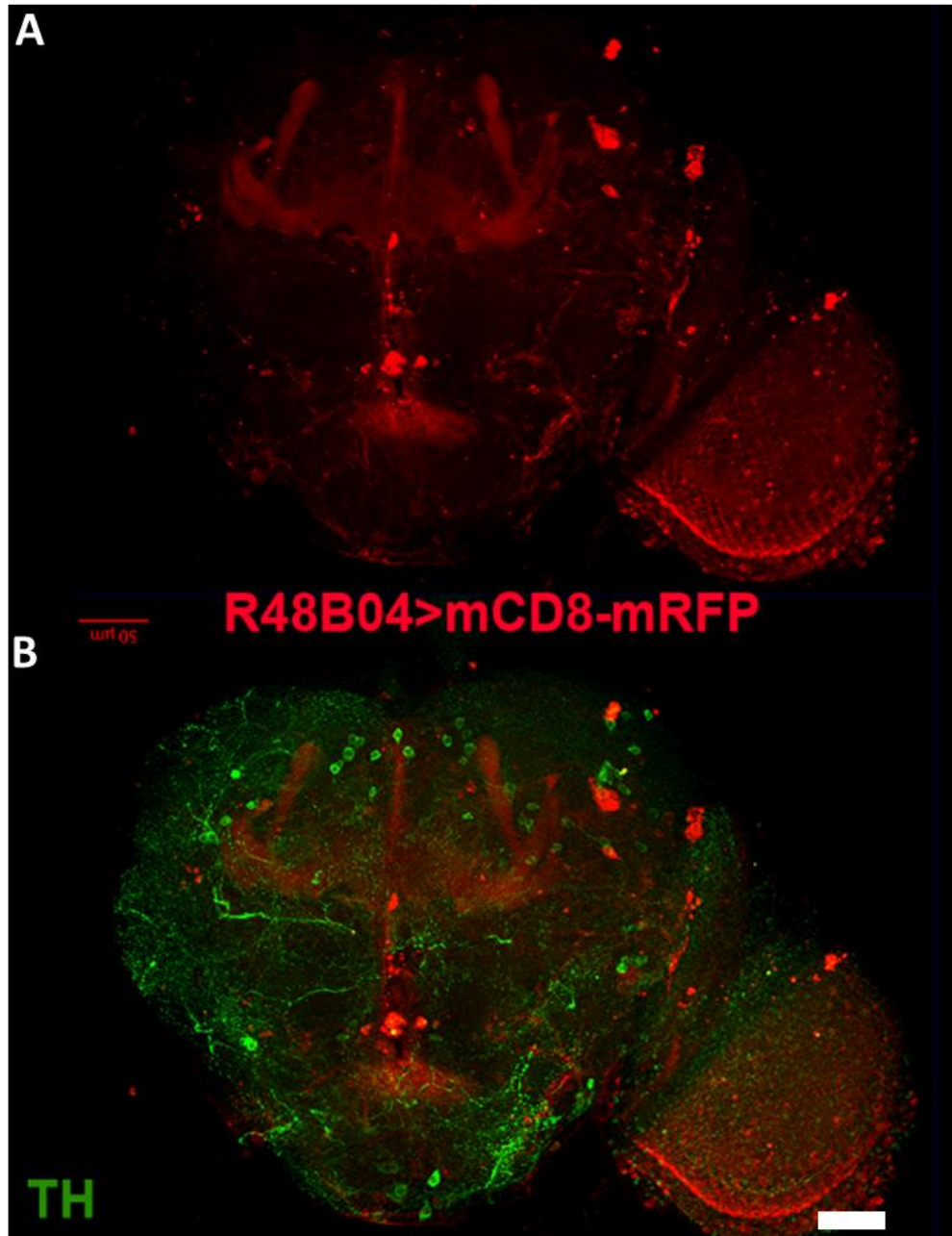
Figure 3.5: Overlapping but distinct projection patterns of Oamb-GAL4

(A-B) *R48B04-Gal4* projects to both lateral and vertical lobes of the mushroom bodies.

The expression and project patterns of the Gal4 line in the PAM cluster was revealed by Lamin-GFP (green in B) and mCD8-RFP (red in D) reporters, respectively, as indicated. The brains were also co-stained for anti-TH antibody (green in E, and red in B), as indicated. All images are from anterior view of w^{1118} male brains. Scale bars in (A-C) and (D-E) represent 20 μm and 50 μm, respectively.
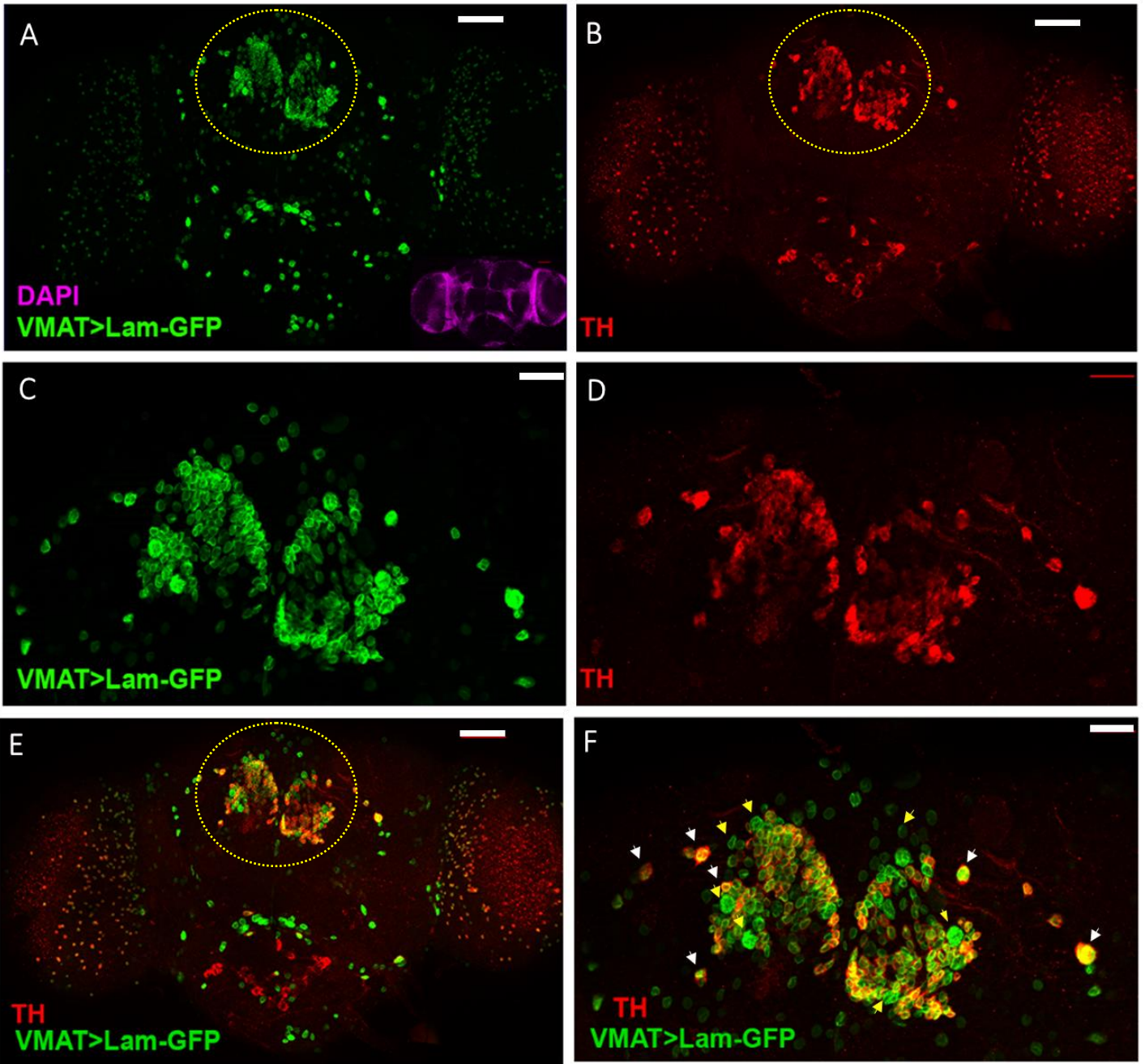
Figure 3.6: Expression pattern of *VMAT-Gal4* line in adult brains

Fluorescence images of an adult brain expressing Lamin-GFP reporter (green) driven by *VMAT-Gal4*, co-stained with anti-TH (red) antibody. Except for cells around esophageal region at the ventral brain, almost all the TH-expressing cells in the adult head and optic lobes overlap with Lamin-GFP. (C, D & F) High-magnification view of the PAM regions (highlighted in yellow dashed circles in (A)). All TH-positive neurons co-express Lam-GFP (examples as indicated by white arrows in F). Also note the existence of non-DArgic neurons in the PAM cluster (examples as highlighted by yellow arrows). Purple insert in (A) shows DAPI staining for cell nuclei to outline the overall morphology of the whole brain. Images are from anterior of the brain. All genotypes are adult males of w^{1118} flies. Scale bars = 50 µm in (A-C) and 20 µm in (D-F).
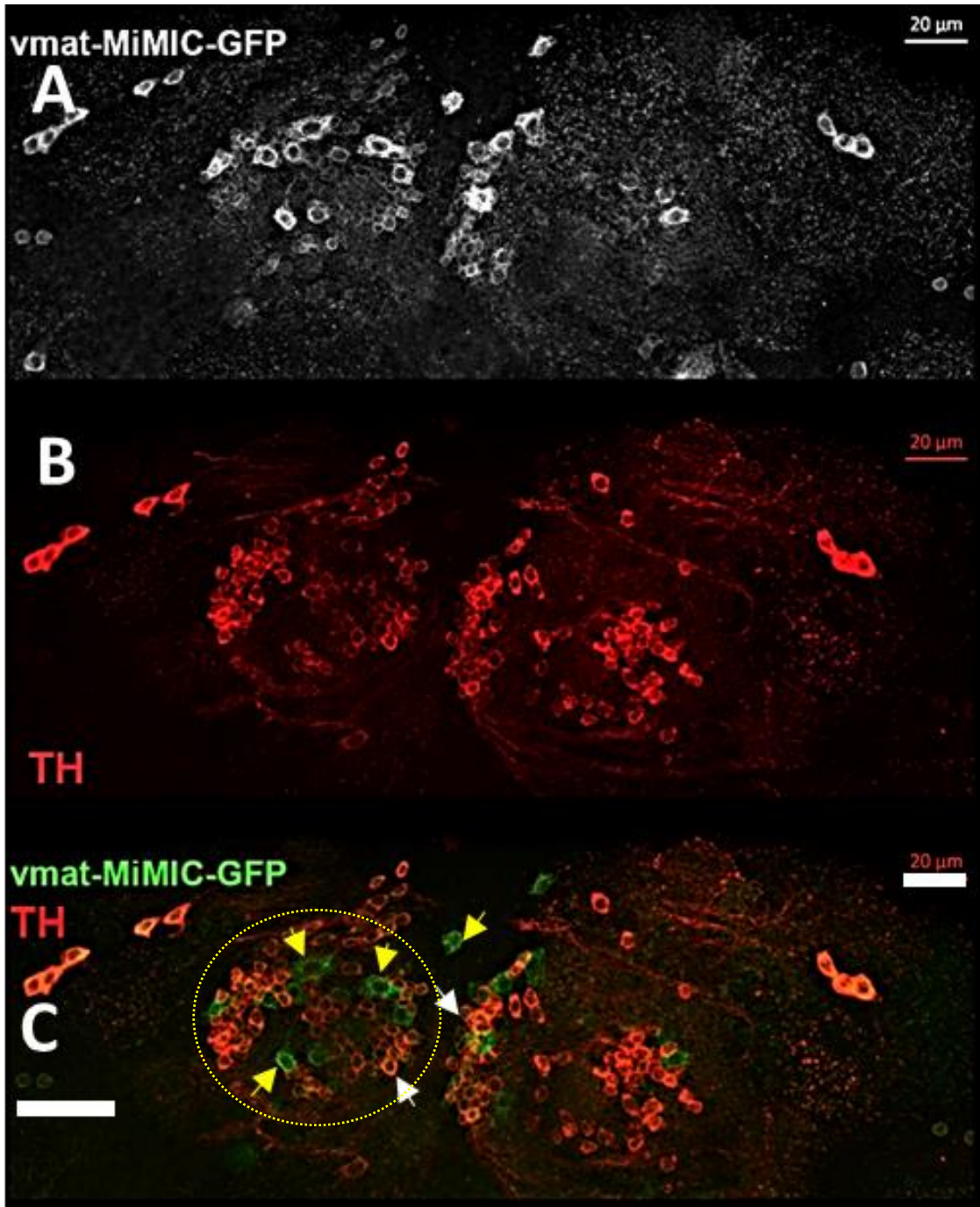
Figure 3.7: Octopamine neurons in the PAM cluster of VMAT-Mi-GFP

(A-C) Expression pattern of VMAT-GFP tagging line in the PAM region showing its predominant overlap with the majority of DN, as revealed by anti-GFP (A, white) and anti-TH (B, red) antibodies and their overlaying images (C).   Note the presence of TH-negative cells (yellow arrows in C) in the middle of the GFP-expressing PAM cluster.
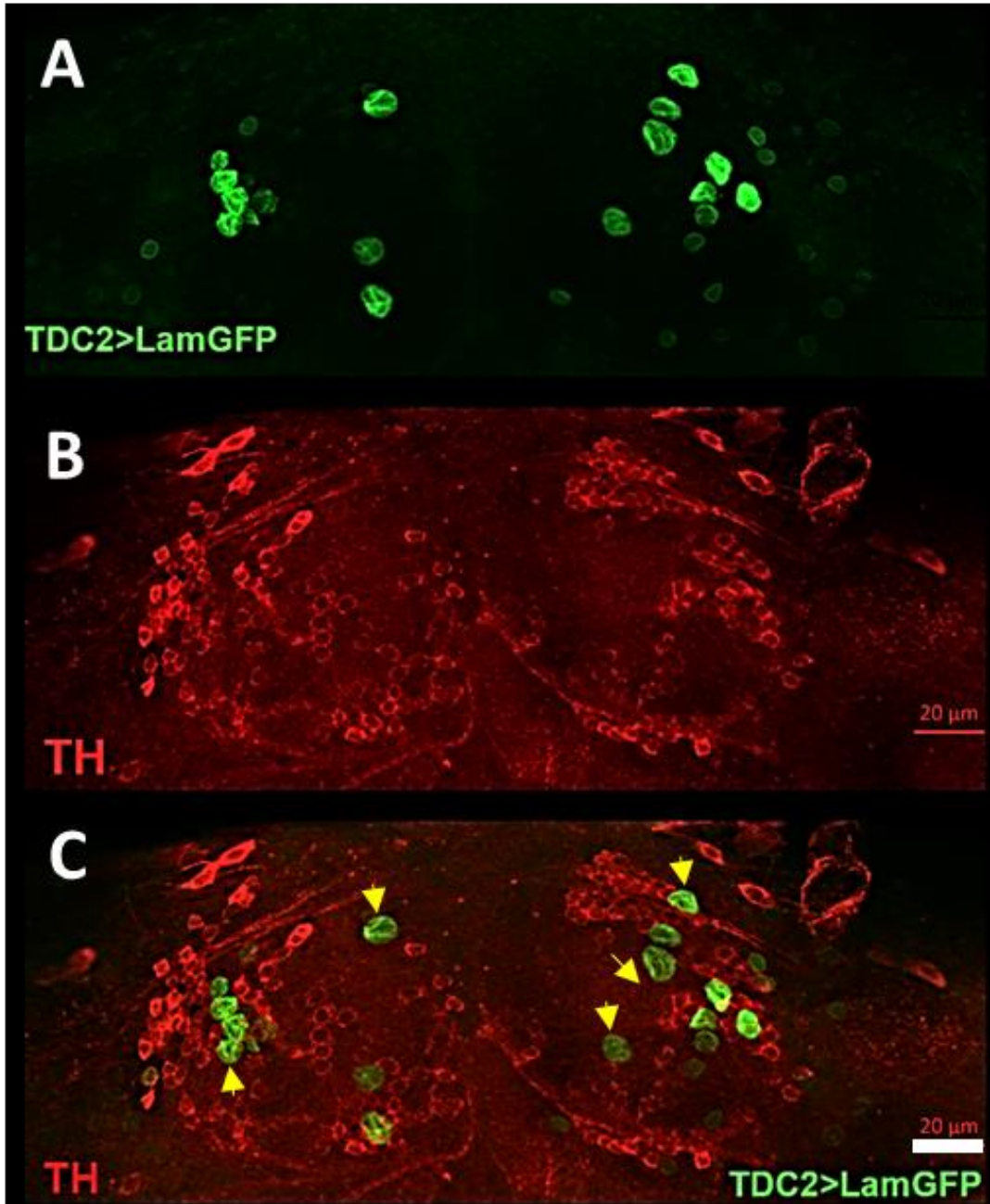
Figure 3.8: Octopamine neurons in the PAM cluster of VMAT-Mi-GAL4

(A-C) Distribution of octopamine neurons in the PAM cluster, revealed by the expression of Lam-GFP (green in A) reporter driven by *TDC2-Gal4*. Note the localization of octopamine neurons (green in A, C), also highlighted by yellow arrows in C, with the region outlined by dashed lines shown at higher magnification in C), showing larger cell sizes, within and around the TH-expressing DN (red in B and F) in the PAM cluster.

All images are anterior view of the brain. All genotypes are adult males of w^{1118} flies. Scale bars = 20 µm in (A-F) and 50 µm in (G-J), respectively.
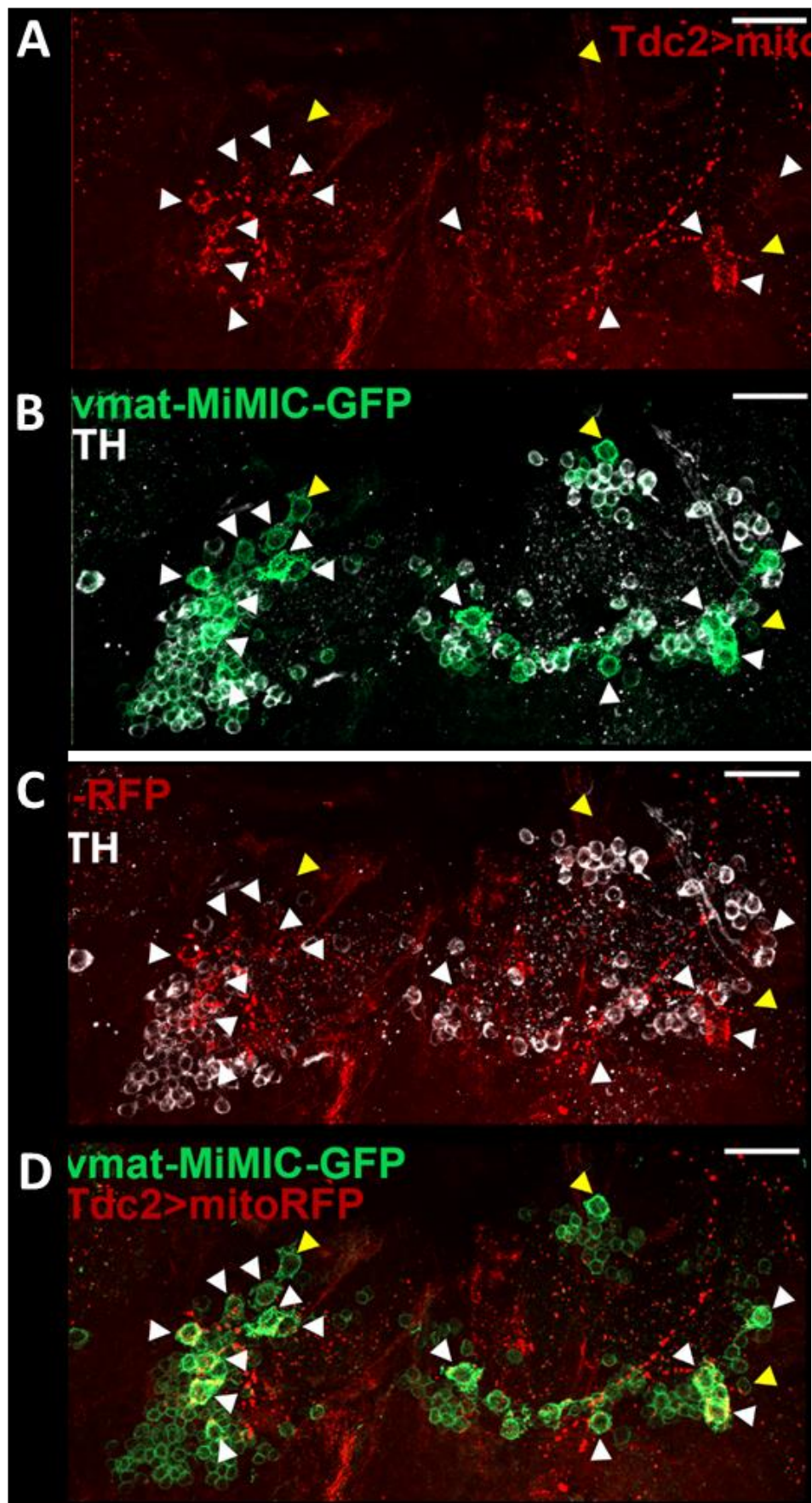
Figure 3.9: Zoom-in of octopamine neurons in the PAM cluster

(A-D) Overlapping expression of *TDC2-Gal4* driver and VMAT-GFP reporter in the PAM cluster, as revealed by UAS-mito-RFP reporter (red in A, C, and D) and anti-GFP antibody (green in B, and D), respectively, co-stained with anti-TH (white in B and C) for DN. (B-D) Overlaying images of (B) anti-TH and anti-GFP, (C) anti-TH and anti-RFP, as well as (D) anti-GFP and anti-RFP staining. White arrowheads indicate "TH-negative, VMAT-GFP-expressing" neurons that overlap with *Tdc2-Gal4*-expressing cells, supporting that they are octopaminergic.

All images are anterior view of the brain. All genotypes are adult males of w^{1118} flies. Scale bars = 50 µm in (A-D).
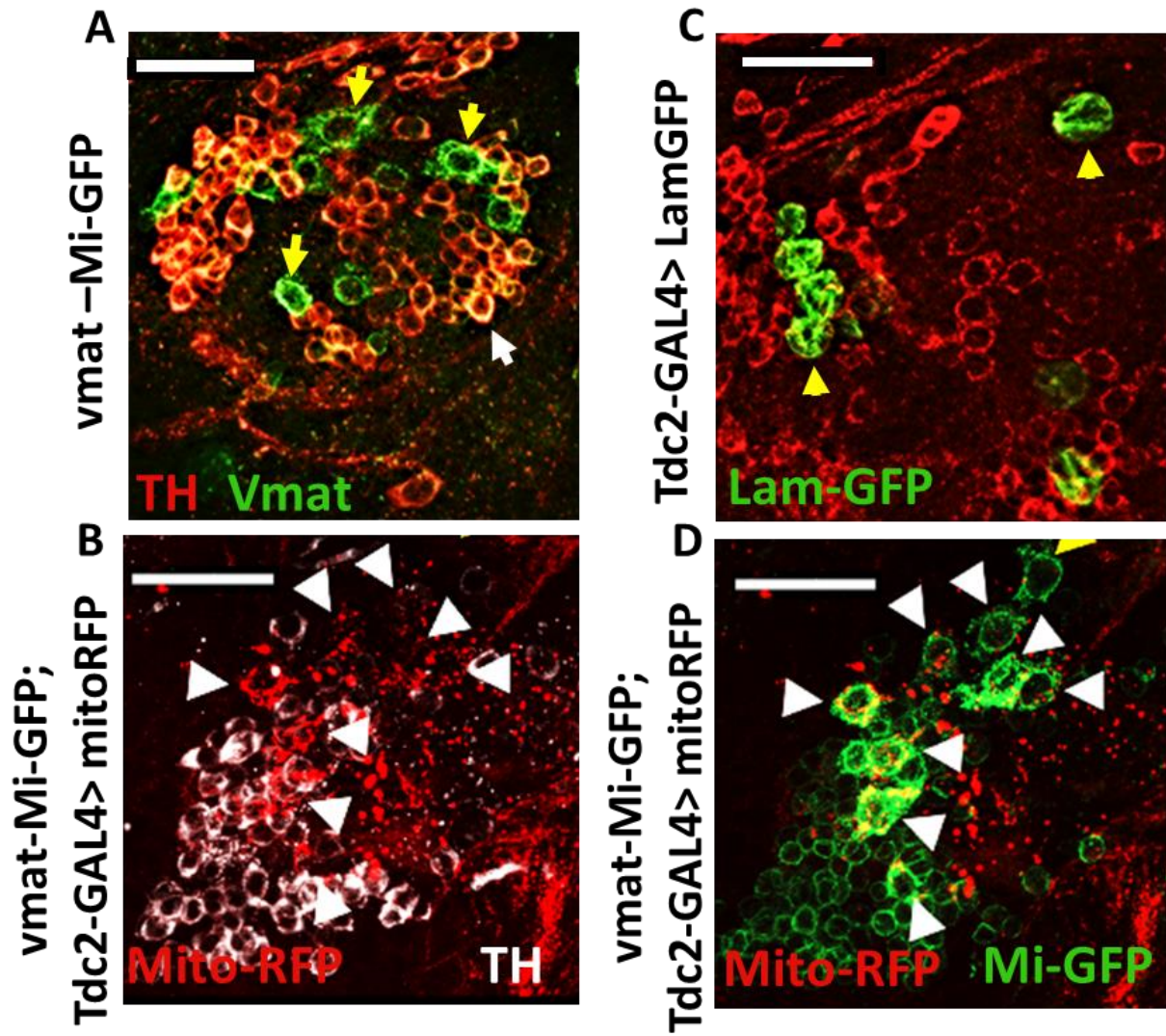
Figure 3.10: Zoomed-in view of octopamine neurons in the PAM cluster

(A-D) shows the high-magnification view of the regions highlighted by dashed lines in (Figures 9 C, F, I and J). (A) Zoom in showing expression pattern of VMAT-GFP tagging line in the PAM region showing its predominant overlap with the majority of DN, as revealed by anti-GFP (white) and anti-TH (red) antibodies. Note the presence of TH-negative cells (yellow arrows in A) in the middle of the GFP-expressing PAM cluster.

(C) Distribution of octopamine neurons in the PAM cluster, revealed by the expression of Lam-GFP (green) reporter driven by *TDC2-Gal4*. Note the localization of octopamine neurons (green), showing larger cell sizes, within and around the TH-expressing DN (red) in the PAM cluster.

(B and D) Zoom in of anti-GFP and anti-RFP staining. Overlapping expression of *TDC2-Gal4* driver and VMAT-GFP reporter in the PAM cluster, as revealed by UAS-mito-RFP reporter (red) and anti-GFP antibody (green in D), respectively, co-stained with anti-TH (white in B) for DN. White arrowheads indicate "TH-negative, VMAT-GFP-expressing" neurons that overlap with *Tdc2-Gal4*-expressing cells, supporting that they are octopaminergic.

All images are anterior view of the brain. All genotypes are adult males of w^{1118} flies. Scale bars = 20 µm in (A and C) and 50 µm in (B and D), respectively.

3.3   <u>Discussion</u>

In this chapter, we focus on the cellular characterization of the PAM cluster, a small defined region in the adult fly brain that contain the majority and also the highest concentration of DN, with a total of about 200 out of all the ~280 DN in the brain (Budnik and White, 1988; Mao and Davis, 2009). The PAM clusters are often not extensively analyzed in many DA-related studies in *Drosophila*, which might be due to the difficulty in examining the DN in the PAM cluster with a relatively weaker TH-expression level and smaller cell sizes.   Examination of the existing DA-related Gal4 lines shows variable patterns of expression of these drivers in the PAM cluster.

Using the MiMIC-based gene conversion approach, we established a new VMAT-Gal4 driver and an endogenously tagged VMAT-EGFP line and showed that these lines recapitulate the expression pattern of endogenous VMAT.   Gnerer J. *et al.* recently reported a VMAT-T2A-Gal4 driver line, as well.   However, they applied the revised T2A-protein trap method to incorporate the *Gal4* gene into the same MI07680 line, and it has not been determined whether this inserted T2A cassette disrupts the normal splicing and translation of VMAT (Gnerer *et al.*, 2015).

In contrast, the MI03756 line is inserted in the 5' regulatory region of *vmat*, in-between the first two non-coding exons, thus the established *VMAT-GaAL4^{MI03756}* line may not interfere with the translation of the encoded VMAT proteins. Additional studies are needed to compare the expression pattern of these two *VMAT-GAL4* lines and their effects on the expression of native VMAT proteins. Since the *vmat*-derived lines are expressed in all monoamine neurons (Figure 3.6 and data not shown) they

would be useful tools for dissecting the anatomic connections and functional interactions among these monoamine neurons in *Drosophila* brain.

An interesting question about the relatively tightly packed PAM clusters is that, apart from harboring the majority of DN, whether they contain other neuronal cell types and whether they operate together as an integrated functional unit in modulating animal behaviors. By analyzing the two VMAT-marker lines, we show that, in addition to containing the majority of DN, VMAT-positive PAM cluster also contains a small number of octopamine neurons.

Interestingly, recent studies have demonstrated functional connections between octopamine and DA signaling in various high functions, such as memory formation and sleep/wakefulness regulation. For instance, it has been shown that octopamine neurons mediate wakefulness by connecting with DN of the PAM clusters, and an increase of octopamine signaling leads to an increase in wakefulness of the animal due to excess DA release in the brain (Crocker and Sehgal, 2008).

4 CHARACTERIZATION OF THE *DROSOPHILA* HOMOLOGUE OF THE *VESICULAR MONOAMINE TRANSPORTER 2* AND ITS ROLE IN PD PATHOGENESIS

4.1 Introduction

Animal models of PD show a loss of VMAT2 activity, a deficiency that is not observed in monkey models with acute destruction of DN of the brain induced by DA neuron toxin, MPTP (Pifl *et al.*, 2014). Conversely, in both mouse and *Drosophila*, targeted overexpression of VMAT2 and dVMAT2 protects DA neurons from MPTP and other environmental toxicants (Inamdar *et al.*, 2013; Lawal *et al.*, 2010; Lohr *et al.*, 2014).

Furthermore, the catechol-based structure of DA makes it into a chemically labile molecule and a potential toxin. When exposed to free oxygen in a pH-neutral cytosol, DA can be spontaneously oxidized to toxic by-products, such as quinone and NM, and induce the production of ROS (Graham *et al.*, 1978; Hastings *et al.*, 1996; Spencer *et al.*, 1998; Stokes *et al.*, 1999; Sulzer and Zecca, 2000). Because of this, DA-associated neuronal toxicity has long been suspected to play a significant role in PD pathogenesis (Goldstein *et al.*, 2013).

Lastly, higher levels of dVMAT2 expression or activity have been implicated with increased protection against PD in humans (Brighina *et al.*, 2013; Glatt *et al.*, 2006). Together, they support the hypothesis that PD might be "a vesicular DA storage disorder" (Lohr and Miller, 2014; Pifl *et al.*, 2014). These observations raise an

intriguing question as to whether defective VMAT and the resulting disruption of intracellular DA handling can act as a trigger to initiate and/or accelerate DA neuron degeneration in *parkin* mutant animals, which, by themselves do not show an overtly manifestation of DA neuron degeneration.

We tested this hypothesis using *Drosophila*, a model organism with well-characterized DN system and highly conserved mechanisms for DA synthesis and intracellular handling (Yamamoto and Seto, 2014).   The protocerebrum of wildtype adult flies contains about 220 DN (see Chapter 3).

Just like in mammalian brains, DA neurons are distributed in nine clusters with distinct projection patterns, which are thought to mediate discrete brain functions. The majority of the DA neurons, about 100 out of the total 120 reside in the PAM clusters of each hemisphere.

These particular DA neurons mainly send their projections to the mushroom bodies, the structure involved in learning and memory in *Drosophila* (Mao and Davis, 2009). Besides DA neurons, the PAM clusters contain about thirty mutually exclusive octopamine neurons (manuscript in preparation), which is particularly important for our study, since we are interested in determining whether DA neuron loss is specific to DN (Tito *et al.*, under review).

Importantly, both dVMAT and dParkin genes are highly conserved in *Drosophila* and the corresponding mutant lines have been established and extensively characterized. Flies lacking the *parkin* gene are viable but show severe mitochondria defects in muscle and reproductive tissues, together with abnormal levels of oxidative

stress and immune responses (Greene *et al.*, 2005; Greene *et al.*, 2003; Whitworth *et al.*, 2005). Adult *vmat* mutant flies are also homozygous viable with highly reduced levels of DA and other monoamines. However, there is no apparent loss of DN in flies mutated for either d*parkin* or d*VMAT* genes (Greene *et al.*, 2003; Simon *et al.*, 2009). Conversely, overexpression of VMAT in *Drosophila* leads to increased monoamine storage in vivo and altered motor and other amine-linked behaviors (Chang *et al.*, 2006; Rana *et al.*, 2013), while higher level of dParkin can extend adult lifespan (Chang *et al.*, 2006; Rana *et al.*, 2013).

Here, we have also re-examined the gain- and loss-of-function phenotypes of VMAT gene in *Drosophila*. We show that ectopic expression of dVMAT2 can induce darker pigmentation of adult cuticles, a phenotype normally associated with increased DA synthesis and secretion, supporting an additional specific role of VMAT2 in facilitating DA release.

Conversely, lack of dVMAT causes a significant loss of total DA, including the complete lack of detection in the mushroom bodies that are prominently enriched with DA in wildtype flies. DA become conspicuously accumulated in the soma of PAM clusters neurons that innervate the mushroom bodies, a phenotype not observed in wildtype flies. Although there is no apparent loss of DA neurons in flies mutated for *VMAT*, additional removal of *parkin* results in an age-dependent loss of DA neurons primarily in the PAM cluster, while the total levels of DA also become further reduced.

Together, our data support a critical role of VMAT2 in vesicular packaging of DA and the devastating effects of altering its function *in vivo*. Disrupting VMAT function

potentiates selective degeneration of DN in PD-associated *parkin* mutant. Moreover, given the observation that DA distribution in the PAM cluster neurons shows particular sensitivity to VMAT activity, it suggests an intrinsic difference in the dynamics of intracellular DA handling among different DA clusters, which might be partially responsible for the selective vulnerabilities of DN in the aging brain.

4.2   Results

4.2.1   Characterization of new *dVMAT* Mutant Alleles

Previous studies have shown that flies lacking the *VMAT* gene can survive as adults despite significantly reduced levels of monoamines, including DA, serotonin and octopamine in the brain (Simon *et al.*, 2009). Phenotypically, female adults devoid of *VMAT* are sterile and display prominent accumulation of mature eggs in the ovary, one of the most recognizable phenotypes, a defect caused by the loss of norepinephrine-like octopaminergic signaling that controls egg retention and egg laying.

The existing *VMAT* mutant alleles are mostly derived from *dVMAT^{p1}*, a null mutant allele with no detectable level of VMAT protein in the homozygous animals. *dVMAT^{p1}* is generated from a P-element insertion in the last coding exon of *VMAT* gene that disrupts its proper expression (Simon *et al.*, 2009).

From a large-scale MiMIC insertion screen, we identified two novel MiMIC lines that are inserted in the d*VMAT* gene (Nagarkar-Jaiswal *et al.*, 2015a; Nagarkar-Jaiswal *et al.*, 2015b; Venken *et al.*, 2011). Mi07680 is located in an intron in-between two coding exons near the C-terminus of *VMAT*.

Applying the Recombinase-Mediated Cassette Exchange (RMCE) method to this line, we generated an eGFP-tagging line named as *VMAT^{eGFP-Mi07680}* that has an eGFP epitope fused in-frame with the endogenous VMAT protein at a location near its 10th transmembrane domain. Mi03756, another MiMIC line, is inserted in the first intron of d*VMAT*, in-between the first two non-coding exons.

Using the RMCE method to insert a Gal4-expression cassette into the Mi03756 site, we established a VMAT-Gal4 trap line that we called *VMAT-Gal4^Mi03756*. In these two MiMIC-derived lines, the expression of both dVMAT-eGFP fusion protein and Gal4 are under the control of the native regulatory elements of *VMAT* gene. Indeed, both lines can faithfully recapitulate the endogenous expression pattern of *VMAT* (Tito, *et al.*, 2016, manuscript under review), thus serving as new tools for studying VMAT expression and function in *Drosophila*.

Both *VMAT-Gal4^Mi03756* and *VMAT-eGFP^Mi07680* lines are homozygous lethal before eclosion, with no viable adult progenies found. However, when crossed with the null *dVMAT^p1* allele, they produced trans-heterozygous progenies that hatched at the expected ratio and adults were viable up to 75 days (Fig. 4.5), suggesting that the lethality is due to background mutations that existed or were spontaneously generated in these lines.

Furthermore, the trans-heterozygous females from both crosses are sterile with prominent egg retention phenotype, which is a characteristics of *VMAT* loss of function mutants (Fig. 4.1B). Quantification of the egg laying efficiency showed that the females with *dVMAT-Gal4^Mi03756* trans-heterozygous over *dVMAT^p1* (*dVMAT-Gal4^Mi03756* / *dVMAT^p1*) hardly laid any eggs in the first 20 days after they hatched, and afterwards only produced a smaller number of eggs as compared to the age-matched controls (Fig. 4.1C).

The d*VMAT-eGFP^Mi07680*/d*VMAT^p1* trans-heterozygous females laid few if any egg over a 40-day period, similar as that reported for the homozygous null *dVMAT^p1*

line (Simon *et al.*, 2009). Consistently, there was a significant reduction of the levels of DA in adult heads of the *dVMAT-eGFP^Mi07680* /*dVMAT^p1* trans-heterozygous flies, as revealed by HPLC quantification, with the degree of reduction comparable with that reported in the null *dVMAT^p1* homozygous flies (Simon *et al.*, 2009). Together, these data suggest that both MiMIC lines are novel loss-of-function alleles of *VMAT*. *dVMAT-eGFP^Mi07680* behaves as a strong mutant allele similar to the null *dVMAT^p1* line, while *dVMAT-Gal4^Mi03756* acts as a weaker *VMAT* mutant allele.

In the *VMAT-Gal4^Mi03756* line, the inserted Gal4-expression cassette likely disrupts the regulatory elements of VMAT gene, altering the expression pattern or levels of endogenous VMAT protein. Indeed, we noticed that although the overall expression pattern of *dVMAT-Gal4^Mi03756* in the brain closely mirrors that of endogenous VMAT, it is conspicuously absent from expression in the esophagus region that VMAT normally presents (Tito, *et al.*, 2016, manuscript under review).

In the *VMAT-eGFP^Mi07680* line, the VMAT-eGFP fusion protein is expressed in a pattern almost identical as the endogenous VMAT. However, the eGFP epitope is inserted in the dVMAT protein at a position very close to its 10th TM domain, potentially disrupting its proper folding or substrate binding ability, resulting in a nonfunctional transporter.

4.2.2   Differential Rescue Efficiency by VMAT Isoforms and DAT

We next examined the effect of overexpressing VMAT in *Drosophila* tissues. In mammals, two VMAT genes with distinct expression patterns are present: the brain-specific VMAT2 and the more ubiquitously expressed VMAT1 (Peter *et al.*, 1995).

Drosophila has only one VMAT gene in its genome but produces two protein isoforms, dVMAT2 and VMAT-B, due to alternative splicing of the last exons encoding its very C-terminal sequences (Greer *et al.*, 2005). Accordingly, the two dVMAT isoforms share the majority of their sequences, including the regions responsible for substrate binding.

Their sequences differ only at their very C-termini, where the respective short stretches of sequences are responsible for the proper subcellular distribution and trafficking of the respective VMAT isoforms. However, these two VMAT isoforms do have distinct expression patterns: dVMAT2 is expressed in all catecholamine synthesizing neurons (DA, 5-HT and octopamine) in the central nervous system, whereas dVMAT-B is expressed in a restricted subset of glial cells in the eye and regulates the vesicular package of histamine, the predominant neurotransmitter in fly visual system (Chang *et al.*, 2006; Greer *et al.*, 2005; Romero-Calderon *et al.*, 2008).

To facilitate the overexpression study, we generated UAS-based transgenic fly lines for the two dVMAT isoforms and also for DAT to serve as a control. For convenient detection of the ectopically expressed proteins, the transgenes were tagged at their N- or C-terminus with eGFP epitope. To verify that the eGFP-tagged VMAT isoforms are functional, we tested their ability to rescue the *VMAT* mutants.

Since the *VMAT-Gal4^{Mi03756}* driver line largely recapitulates the expression pattern of endogenous VMAT gene, we used it to direct the ectopic expression of VMAT-eGFP and eGFP-dDAT transgenes. Female flies trans-heterozygous for *VMAT-Gal4^{Mi03756} and dVMAT^{p1}* alleles were sterile and hardly laid any eggs before day 20. However, in the presence of either of the dVMAT isoforms, the egg-laying defect was

almost completely rescued, demonstrating that both eGFP-tagged dVMAT isoforms are functional and the *VMAT-Gal4*^{Mi03756} line is a loss-of-function allele of VMAT gene.

Although both dVMAT isoforms from the transgenes rescued *dvmat* mutants, they exhibited subtle differences in their rescue efficiency, with dVMAT-B showing a more effective rescue than that by dVMAT2. Specifically, for the flies rescued by dVMAT-B, they laid eggs at a similar rate as the age-matched controls from the very beginning after their hatching. However, for flies rescued by dVMAT2, the female adults only become as effective in egg-laying as controls about 8 days after they hatched. Interestingly, although DAT was originally employed in the experiment as a control for VMAT, it also exhibited a weak but significant rescue ability, as *VMAT* mutant females overexpressing DAT begun to lay small number of eggs a few days after their hatching.

Although DAT normally locates on the plasma membrane to reuptake extracellular DA back into the cytosol, a higher level of ectopically expressed DAT might lead to promiscuous subcellular localization as well as non-specific binding and transport of other monoamines such as octopamine, partially supplementing the transport function normally carried out by endogenous VMAT.

4.2.3 Ectopically expressed dVMAT2 facilities DA release from Epithelial Cells

In *Drosophila*, in addition to DN in the nervous systems, epithelial cells also synthesize DA, which controls the pigmentation of adult cuticles (Neckameyer and White, 1993; Wittkopp *et al.*, 2003; Wright, 1987). During the late pupae stage, before eclosion, DA is secreted from the epithelial cells underneath the forming cuticle, where they are oxidized to Dopa and polymerized to form yellow melanin.

Consistently, when *pannier*-Gal4 driver was used to express dsRNA against DA-synthesis enzymes TH or DDC in epithelium along a longitudinal dorsal domain covering the thoracic and abdominal segments, they induced a clear stripe of de-pigmented cuticles in the adult dorsal notum, largely along the *panier* expression domain (Calleja *et al.*, 2000). Earlier studies have shown that the level of VMAT is not detectable in epithelial cells, and flies lacking *VMAT* do not have cuticle pigmentation defect (Greer *et al.*, 2005; Simon *et al.*, 2009).

Indeed, *VMAT* mutant flies with *VMAT^{p1}* trans-heterozygous over *VMAT-Gal4^{Mi03756} or VMAT-eGFP^{Mi07680}* alleles also have normal pigmented cuticles. Further, targeted depletion of VMAT or DAT by RNAi through *panier*-Gal4 driver did not cause any cuticle effect. Together, they confirm that VMAT is not necessary for the secretion of epithelium-derived DA. Currently it is still not clear how DA is trafficked and released from epithelial cells, and whether a vesicular-based mechanism is involved.

It was also reported that overexpression of dVMAT2 using different Gal4 drivers such DDC-GAL4 does not induce apparent cuticle or pigmentation phenotypes (Chang *et al.*, 2006). However, interestingly, when DDC-Gal4 was used to direct ectopic expression of dVMAT2, it induced darker pigmentation in adult cuticles.

Such pigmentation effect is specific to VMAT2, as it is not observed in flies overexpressing DAT or VMAT-B, even at higher dosages. In addition, the pigment phenotype is also dosage-dependent, as animals with additional copies of UAS-dVMAT2 transgene and/or DDC-Gal4 driver show darker cuticles.

Moreover, co-expression of TH, the rate-limiting enzyme for DA synthesis, or halving the dosage of *ebony* (data not shown), an enzyme involved in DA metabolism, all could enhance the dVMAT2-induced dark pigmentation phenotype, suggesting that the darker pigment effect is associated with increased levels of DA. DDC-Gal4 is expressed in both DA and serotonin neurons and also in epithelial cells(Li *et al.*, 2000). Importantly, neuronal-specific overexpression of DVMAT2, such as by *elav*-Gal4 driver, do not cause dark pigmentation, indicating that the effect is due to DA from epithelial origin (data not shown). Together, these data suggest that although VMAT is not required for the package and release of DA from epithelial cells, the presence of dVMAT2 is sufficient to facilitate the extracellular release of pre-existing DA, potentially by promoting its vesicular packing.

4.2.4   Differential Subcellular Dynamics of dVMAT2 and dVMAT-B proteins

It is surprising that overexpression of VMAT-B, even at higher-dosage, did not induce dark pigmentation phenotype as DVMAT2, although they both can rescue the *dvmat* mutant phenotypes and share majority of their protein sequences, including the substrate binding domain. The two VMAT isoforms differ only at their very C-terminal sequences, which have been shown to modulate their subcellular trafficking and localization(Fei *et al.*, 2007; Greer *et al.*, 2005; Grygoruk *et al.*, 2014; Grygoruk *et al.*, 2010).

Considering this, we further investigated the subcellular distribution patterns of the two VMAT isoforms. In the brain, the majority of cells have small cell bodies and the sizes of SVs are too small to be clearly visualized by standard immunofluorescent

imaging. Accordingly, we employed the salivary gland, a secretory tissue with large cell sizes, as a heterologous system to mimic neuronal cells for the study.

The secretory cells in salivary glands are highly polarized epithelial cells that synthesize large amount of glue proteins, which are normally packaged and stored inside large-sized granules (Biyasheva *et al.*, 2001; Fraenkel and Brookes, 1953). At late 3rd instar larval stage, upon stimulation by the peaked ecdysone signal, these glue granules migrate to the apical side of the cells where they fuse with plasma membrane in a Ca^{2+}-dependent manner to release the glues into the lumen, which are subsequently pumped out of the body to attach late stage larvae that enter metamorphosis onto solid surfaces.

Thus, both neurons and salivary gland cells are highly polarized secretory cells with several shared properties, including vesicular storage of their contents (glue proteins or neurotransmitters), the polarized transport of the vesicles (granules or SVs), as well as the activity (hormonal stimulation and calcium)-dependent fusion of the vesicles with the specialized domains in plasma membrane (apical membrane or synapse) for their content release. It has been further suggested that, in neurons, the synaptic terminus from projected axons corresponds to the apical side of epithelial cells where activity-dependent membrane fusion and regulated content-release occur. By contrast, the peri-synaptic region that DAT normally resides to re-uptake extracellular DA bears more similarity to the basal-lateral membranes of the epithelial cell (Rodriguez-Boulan and Powell, 1992; Torres *et al.*, 2003).

When DAT and VMAT isoforms were ectopically expressed in the salivary gland cells, DAT mainly located to the basal-lateral plasma membrane, but was conspicuously absent from the apical side of the membrane and from structures inside the cell. In contrast, both dVMAT2 and VMAT-B both were largely absent from basal-lateral membrane but instead primarily localized on the vesicular membranes inside the cell, in addition to their prominent enrichment on the apical side of the membrane.

Thus, when ectopically expressed in the polarized salivary gland cells, VMAT and DAT likely employ similar mechanisms as in neurons for their proper sorting and trafficking to their appropriate destinations, with VMAT being trafficked specifically to the vesicular membrane that enclose the secretory granules, whereas DAT being targeted to basal-lateral plasma membrane. Noticeably, although both dVMAT2 and VMAT-B show similarly vesicular localization inside the cell, dVMAT2 exhibits a more polarized subcellular localization pattern than VMAT-B.

More specifically, the majority of dVMAT2-positive granules were clustered near the apical side of the cell, as compared to a more dispersed distribution of VMAT-B in the cell. Such an observation, combined with their different overexpression effects on cuticle pigmentation, raising the possibilities that dVMAT2 not only is important for vesicular package of monoamines, but also can potentiate membrane fusion and content release. Additionally, it is possible that dVMAT2 is actively trafficked to granules and SVs that are fusion-competent, the ones that are being positioned in proximity to the fusion active sites on the plasma membrane.

4.2.5 Loss of VMAT leads to increased cytosolic accumulation of DA but does not cause loss of DA neurons

Consistent with a previous report, quantification by HPLC analyses revealed a significant reduced level of total DA in *dvmat* mutant brains (Simon *et al.*, 2009). In an early study, it has been shown that DA neurons develop normally in *dvmat*^{p1} mutant flies and do not exhibit apparent degeneration as the fly ages (Simon *et al.*, 2009).

However, this study only focused on a small group of DA neurons from the PAL and PPL cluster, but did not analyze the PAM clusters that contain the majority of DA neurons in the brain. To obtain a more comprehensive evaluation of the role of VMAT on the development and survival of DA neurons, we expanded the study to more DA clusters in the brain, including the PAM clusters.

The viability of *VMAT* mutant flies was found to be highly sensitive to their cultured conditions and genetic background (Simon *et al.*, 2009). To minimize such background effect on the survival of DA neurons, we performed the studies on *VMAT* mutant flies trans-heterozygous for *VMAT*^{p1} and *VMAT*^{eGFP} alleles, two strong *vmat* alleles that were each derived from an independent parental line of different genetic background.

Examination with anti-TH antibody revealed that in both the PAM cluster and several other clusters we examined, there was no significant loss of DA neurons between young and 30-day-old *VMAT* mutant flies transheterozygous for *dvmat*^{p1}/*dvmat*^{eGFP}. For example, in each PAM cluster, there are on average 89 DA neurons in 3-day-old *VMAT* mutant flies as compared to about 91 DA neurons in 30-day-old *VMAT* mutant flies.

To examine the effect of VMAT on the distribution of DA in adult brains, we next performed immunofluorescent staining with anti-DA antibody. In most of the DA neuron clusters such as PAL and PPL of wildtype flies, anti-DA staining clearly recognized the soma of individual DA neurons, indicating a significant retention of DA in the cell bodies of these neurons.

One noticeable exception is in the PAM clusters, where anti-DA staining hardly revealed any individual cell bodies, despite the fact that it contains the majority of DA neurons in the brain. Instead, there is a prominent enrichment of DA in the mushroom bodies (MBs), the primary target of innervation by DA neurons from the PAM clusters. Such an observation implies that the majority of DA produced by the PAM cluster cells are effectively packaged and delivered out of the soma into the axonal termini, which is in contrast to the clear retention of DA in the soma of the neighboring PAL cluster cells.

Besides the mushroom bodies, there is also an extensive and widespread distribution of DA throughout the brain, including its heavy enrichment in the commissures that connect the two brain hemispheres and around the esophagus region. In *VMAT* mutants, the elaborate and extensive distribution of DA in the brain was abolished, and the signal intensity of DA in almost all the brain regions was greatly reduced, including a complete loss of DA in the mushroom bodies, in agreement with the significantly reduced levels of total DA as revealed by HPLC study.

However, for DA neurons in the PAM cluster, their soma became clearly labeled by anti-DA staining, in contrast to their lack of immunoreactivity in wildtype background, indicating a significant accumulation of cytoplasmic DA in these cells in the absence of VMAT. Additionally, DA was also still clearly present in the soma of most

DA neurons in other clusters such as the neighboring PAL and in the large commissures connecting two sides of the brain. These findings suggest that vesicular-package of DA is absolutely required for its distribution out of the soma into the projected axons.

Further, considering the apparent difference between the PAM and other DA clusters in the subcellular distribution of DA, both in wildtype and under *VMAT* mutant background, it raises a possibility that the dynamics of handling intracellular DA are different between DA neurons of different brain clusters.

4.2.6 Normal Distribution Patterns but Reduced Levels of DA in *parkin* mutant brains

We next examined the effect of *parkin* depletion on the distribution of DA in adult brains. It has been shown that *parkin* mutant flies do not manifest apparent loss of DA neurons, despite their prominent mitochondria defects and oxidative stresses (Greene *et al.*, 2005; Greene *et al.*, 2003).

Similar as to *VMAT*, the viability of *parkin*-deficient flies is highly sensitive to different genetic background and can be altered by disturbance in a variety of cellular pathways such as mTOR, protein synthesis, metal clearance and oxidative responses (Humphrey *et al.*, 2012; Kim *et al.*, 2012; Ng *et al.*, 2012; Ottone *et al.*, 2011; Saini *et al.*, 2011; Tain *et al.*, 2009; Whitworth *et al.*, 2005; Zhu *et al.*, 2015). Considering this, we focused the study on flies that are trans-heterozygous for two strong *parkin* loss-of-function alleles, *parkin*$^{\Delta 21}$ and *parkin*^{f01950} derived from independent parental lines with different genetic background (Pesah *et al.*, 2004).

When different DA clusters were examined by anti-TH staining, there was no apparent loss of DA neurons in these *parkin* mutant flies. For example, in both 3- and

30-day-old *parkin* mutants, anti-TH staining could clearly identify about 90 DA neurons in each of the PAM clusters, similar as that in *VMAT* loss of function flies.

Interestingly, although anti-TH staining revealed no apparent loss of DA neurons in *parkin* mutant flies, the immunoreactivity for DA were significantly reduced, which is especially apparent in the mushroom bodies, although the pattern of DA distribution in *parkin* mutant brains was similar as that in wildtype, including its characteristic enrichment in mushroom bodies, in a region around esophagus and in large commissures connecting two brain hemispheres. Such an observation suggests that Parkin directly or indirectly regulates DA production and/or its subcellular package and delivery in the brain.

4.2.7 Significant loss of DA neurons in the PAM cluster of flies lacking both VMAT and Parkin

We next examined whether the altered DA subcellular distribution associated with VMAT depletion can become a toxic factor in *parkin* deficient background. To test this, we generated adult flies carrying both *VMAT* and *parkin* mutations. Additionally, to obtain comparable results with flies from similar genetic background and also to minimize background effect, we used the same $VMAT^{p1}$ and $VMAT^{eGFP}$ alleles to remove native VMAT gene and $parkin^{D21}$ and $parkin^{f01950}$ alleles to delete Parkin.

Flies trans-heterozygous for $parkin^{D21}/parkin^{f01950}$ flies are viable with a mean life span of 22 days, with 80% of them die by day 28. The mean life span of $VMAT^{p1}/VMAT^{eGFP}$ adults is at day 55, with 80% of them die by day 62. The mean life span of *VMAT/parkin* double mutants (genotype "w^{1118}; $VMAT^{p1}/VMAT^{eGFP}$; $parkin^{D21}/parkin^{f01950}$") double mutant flies was slightly shortened to day 22, with 80%

of them die by around day 29. We therefore focused the remaining studies on aging flies primarily to 22-day-old adults.

We first examined the presence of DA neurons by anti-TH staining. In 3-day-old young flies of "*VMAT/parkin*" double mutants, cell bodies of DA neurons were clearly recognizable for all the clusters we examined, including the PAM, PPM, PAL and PPL. The number of DA neurons was similar in *VMAT/parkin* double mutants as those in *VMAT* or *parkin* single mutant alone. By day 22, for *VMAT/parkin* double mutants, the cell bodies of DA neurons in the PAL, PPM and PPL clusters were clearly recognizable by anti-TH staining, and their number were largely the same as those in the young flies, and also similar as the single mutants of the same ages.

However, in the PAM clusters, the number of DA neurons were significantly reduced, from an average of 92 DA neurons per PAM cluster in day 3 to about 72 by day 22, a significant 30% reduction. Additionally, there was a noticeably big variation on the number of DA neurons per PAM cluster among individual flies, and the signal intensity of anti-TH staining also became markedly lower.

Examination of these animals with anti-DA antibody revealed a more dramatic change in "*VMAT/parkin*" double mutants flies. When processed in parallel, the signal intensity for DA became almost completely diminished from the brains of the "*vmat;parkin*" double mutant animals even in 3-day-old flies, in contrast to the characteristic patterns of DA distribution that were clearly present in either of the mutants alone.

Taken together, our findings reveal that simultaneous loss of VMAT and Parkin causes a significant perturbation of DA production and/or metabolism in the brain accompanied by an accelerated loss of DA neurons especially in the PAM clusters.

4.2.8 Selective loss of DA neurons in the PAM cluster of d*vmat;parkin* double mutant flies

The noticeable loss of the DA neurons in the PAM cluster raised a question whether other cell types in this cluster were also affected in "*VMAT*/*parkin*" double mutant flies. In addition to its majority composition of DA neurons, the PAM cluster also contains a small number of octopamine neurons, which can be identified as the cells that express VMAT transporter but not the DA synthesis enzyme TH.

We used the established $VMAT^{eGFP}$ genome tagging line, which expresses a nonfunctional VMAT-GPF fusion protein that faithfully recapitulate the endogenous expression pattern of VMAT gene in the brain, to both disrupt native VMAT function and to label all the endogenous VMAT-expressing cells. We specifically quantified the number of octopamine neurons (i.e., "VMAT-eGFP positive, TH-negative" cells) in the PAM clusters by double-labeling of the $VMAT^{p1}$/$VMAT^{eGFP}$ brains with anti-TH and anti-eGFP antibodies.

In the "*VMAT*/*parkin*" double mutant flies (genotype: "w^{1118}; $VMAT^{p1}$/$VMAT^{eGFP}$; $parkin^{D21}$/$parkin^{f01950}$"), despite the loss of DA neurons in the PAM clusters, octopamine neurons (i.e., "VMAT-eGFP positive, TH-negative") were still clearly present and their number was similar as that observed in *VMAT* mutant alone of the same age (genotype: w^{1118}; $VMAT^{p1}$/$VMAT^{eGFP}$), suggesting that the cell loss is more restricted to DA neurons within the PAM cluster.
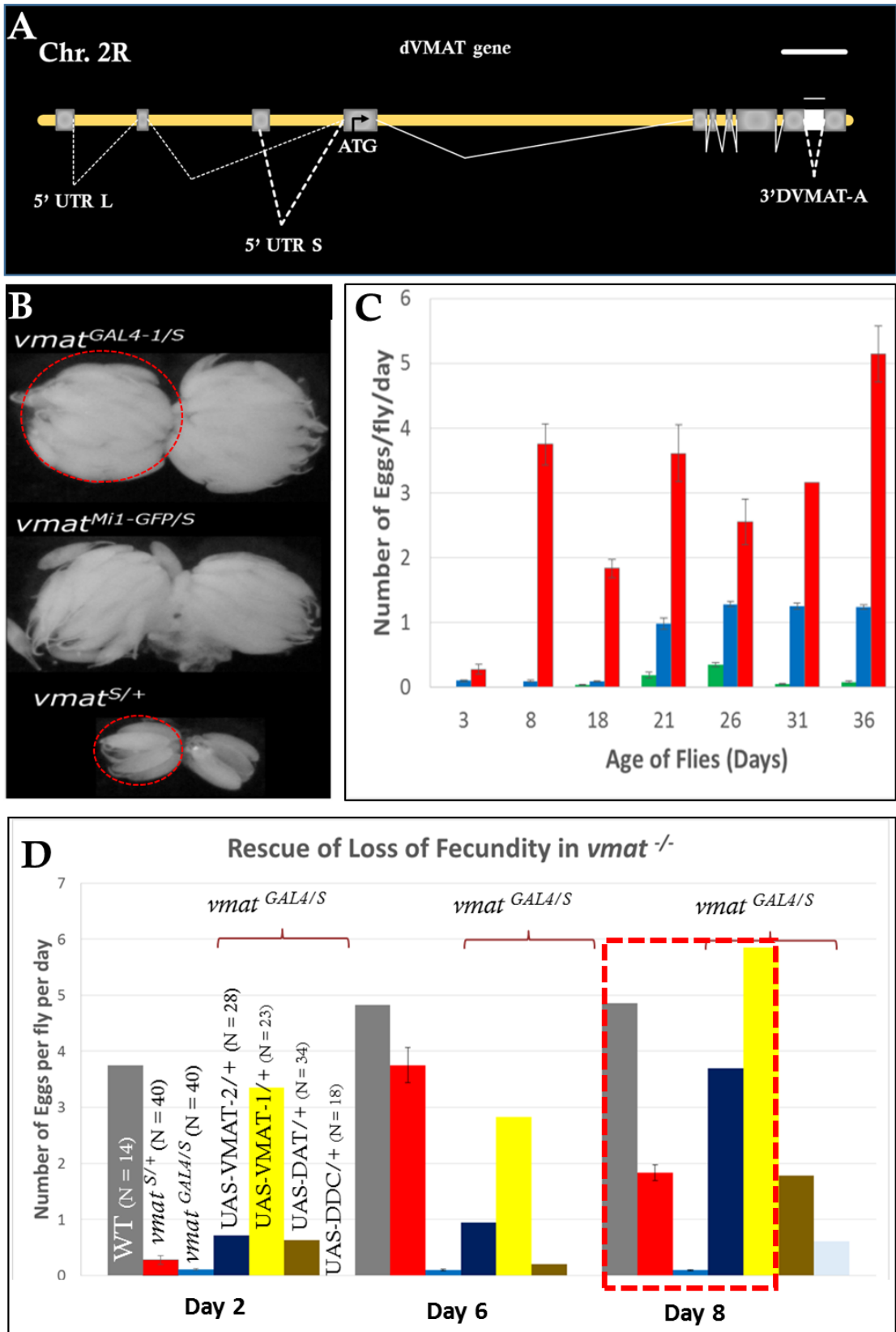
Figure 4.1: New MiMIC-derived insertional lines disrupt VMAT function

(A)   Schematics of *Drosophila VMAT* gene structure. Gray boxes indicate exons and filled boxes represent protein coding regions. White dashed lines near the C-terminus of VMAT gene indicate the alternative splicing sites that produce the dVMAT2and VMAT-B protein isoforms. Inverted triangles indicate the sites of insertion by the two MiMIC-lines.

(B)   The characteristic egg retention phenotype associated with the new *VMAT* alleles derived from the MiMIC lines. The ovaries were dissected from 8-day-old females adults carrying transheterozygous *VMAT* mutations: the null *VMAT^P* allele over the *VMAT^{Gal4}* line (top, genotype: *w^{1118}*; *VMAT^{p1}*/*VMAT^{Gal4}*), *VMAT^P* allele over the *VMAT^{eGFP}* line (middle, genotype: *w^{1118}*; *VMAT^{p1}*/*VMAT^{eGFP}*), or over a wildtype control (bottom, genotype: *w^{1118}*; *VMAT^{p1}*/+). Notice the dramatic accumulation of mature eggs in the top two *VMAT* mutants.

(C)   Quantification of the egg laying efficiency by *VMAT* mutant females, plotted as the average number of eggs produced per day by one female over a 36-day timespan. Flies that were transheterozygous with the null *VMAT^P* allele over the *VMAT^{eGFP}* line (green) laid almost no eggs during the study, while the *VMAT^P*/*VMAT^{Gal4}* flies (blue) laid eggs much later and produced fewer eggs than the heterozygous *VMAT^P*/+ control (green).

(D)   Rescue of the egg-laying defect in the transheterozygous *VMAT^P*/*VMAT^{Gal4}* females through the ectopic expression of eGFP-tagged dVMAT2, VMAT-B and DAT transgenes. The transgene expression was driven by the *VMAT^{Gal4}* trap line, which expresses Gal4 driver under the control of the native VMAT regulatory elements.

Genotypes: WT (w^{1118}, brown column), heterozygous $VMAT^P$/+ control (red), transheterozygous $VMAT^P$/$VMAT^{Gal4}$ mutants (green column), transheterozygous $VMAT^P$/$VMAT^{Gal4}$ mutants co-expressing dVMAT2-eGFP (dark blue column, w^{1118};$VMAT^P$/$VMAT^{Gal4}$; UAS- dVMAT2-eGFP/+), transheterozygous $VMAT^P$/$VMAT^{Gal4}$ mutants co-expressing VMAT-B-eGFP (yellow column, w^{1118};$VMAT^P$/$VMAT^{Gal4}$; UAS-VMAT-B-eGFP/+), transheterozygous $VMAT^P$/$VMAT^{Gal4}$ mutants co-expressing eGFP-DAT (brown column, w^{1118};$VMAT^P$/$VMAT^{Gal4}$; UAS-eGFP-DAT/+), transheterozygous $VMAT^P$/$VMAT^{Gal4}$ co-expressing DDC (light blue column, w^{1118};$VMAT^P$/$VMAT^{Gal4}$; UAS-DDC/+).

A — DA Levels (Young, Old) bar chart for vmat-/- (2), vmat Cyo (2), w1118 (2)

B — 5HT Levels (5HT Levels Young, 5HT Levels Old) bar chart for vmat-/- (2), vmat Cyo (2), w1118 (2)
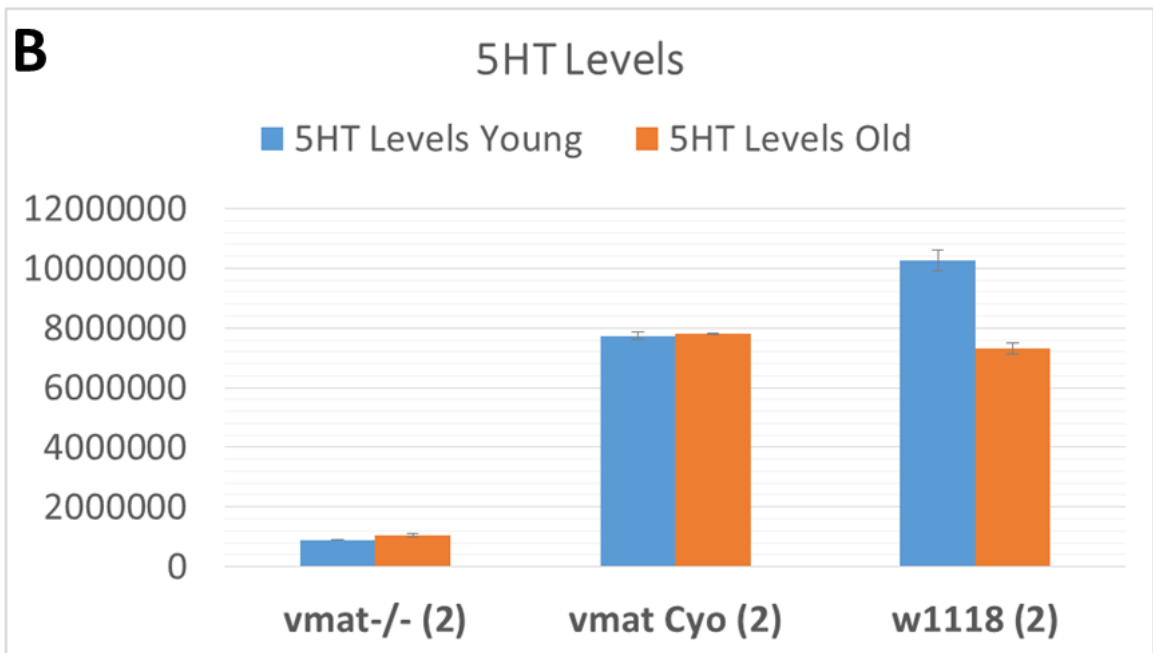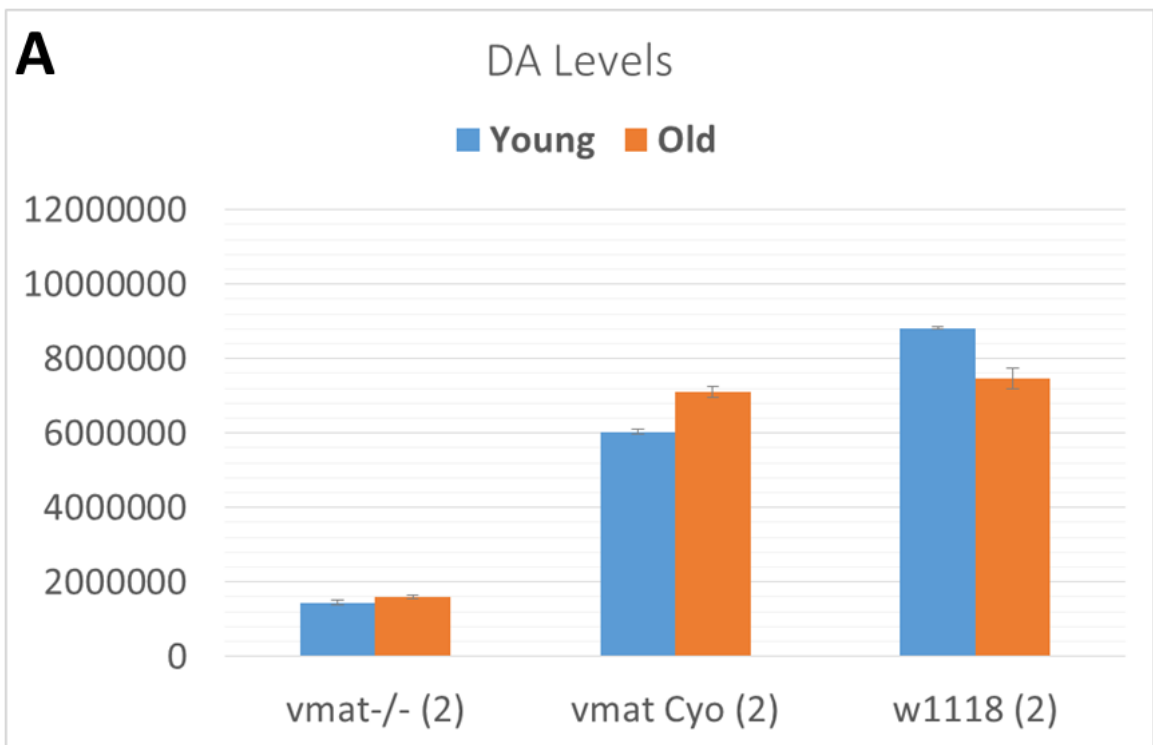
Data generated by Hirsh Lab at the University of Virginia

Figure 4.2: New MiMIC-derived insertional lines reduce DA and 5HT synthesis

Significantly reduced levels of total DA (A) and 5HT (B) in the brains of *VMAT* mutant adults, as quantified by HPLC from the following genotypes at day 3 (blue columns) and day 22 (orange columns): wildtype control (w^{1118}), heterozygous *VMAT* control (w^{1118}; *VMAT*^{eGFP}/*Cyo*), and transheterozygous *VMAT* mutants (w^{1118}; *VMAT*^{eGFP}/ *VMAT*^{P}).
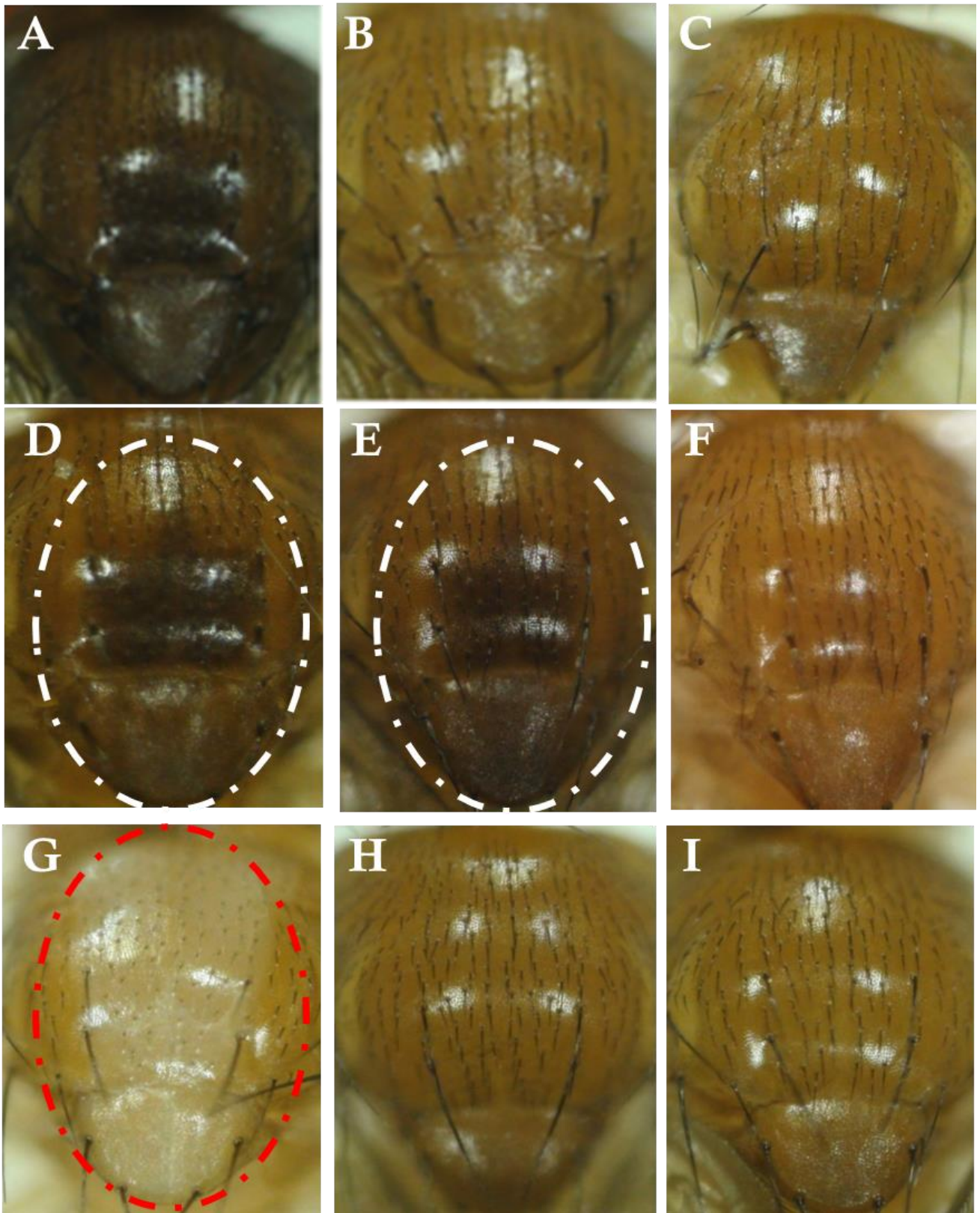
Figure 4.3: Ectopic expression of dVMAT2 induces darker cuticle pigmentation

Bright-field images of the notum from 3-day-old adult flies.

(A-F) Ectopic expression of dVMAT2 (A, D), but not VMAT-B (B,F) or DAT (C), by DDC-Gal4 driver induces darker pigmentation in adult cuticle.

(A-C) Flies carried two copies of DDC-Gal4 with two copies of the UAS-transgenes. Genotypes: (A) w^{1118}; DDC-Gal4, UAS- dVMAT2-EGFP/ DDC-Gal4, UAS- dVMAT2-EGFP. (B) (A) w^{1118}; DDC-Gal4, UAS-VMAT-B-EGFP/ DDC-Gal4, UAS-VMAT-B-EGFP. (C) w^{1118}; DDC-Gal4, UAS-EGFP-DAT/ DDC-Gal4, UAS- EGFP-DAT.

(D) Flies carried one copy of DDC-Gal4 driver with two copies of the UAS-transgenes. Genotypes: (D) w^{1118}; DDC-Gal4, UAS- dVMAT2-EGFP/ UAS- dVMAT2-EGFP. Note that it showed lighter pigmentation than flies in (A) that carried two copies of DDC-Gal4 driver. (E and F) Co-expression of TH enhanced the dark pigmentation effect induced by (E) dVMAT2but not (F) VMAT-B. (E) A fly that co-expressed dVMAT2and TH showed similar level of dark pigmentation as fly in (D) that with two copies of UAS- dVMAT2-EGFP transgene.

Flies carried only one copy of DDC-Gal4 and one copy of UAS- dVMAT2-EGFP (data not shown) have lighter pigmentation that in (D) and (E). Genotype: w^{1118}; DDC-Gal4, UAS-dVMAT2-EGFP/ UAS-TH. (F) A fly that co-expressed TH with VMAT-B showed normal pigmentation as in wildtype. Genotype: w^{1118}; DDC-Gal4, UAS-VMAT-B-EGFP/ UAS-TH.

(G-I) VMAT and DAT are not required for cuticle pigmentation. Depletion of (G) TH, but not (H) VMAT or (I) DAT, led to de-pigmentation of adult cuticle. The knock down of target gene expression along the dorsal cuticle region was achieved by expressing

dsRNA constructs against the respective target genes using the *panier*-GAL4 driver. Genotypes: (G) *w^1118; panier*-GAL4/+; UAS-TH^dsRNA/+. (H) *w^1118; panier*-GAL4/+; UAS-VMAT^dsRNA/+; (I) *w^1118; panier*-GAL4/+; UAS-DAT^dsRNA/+.
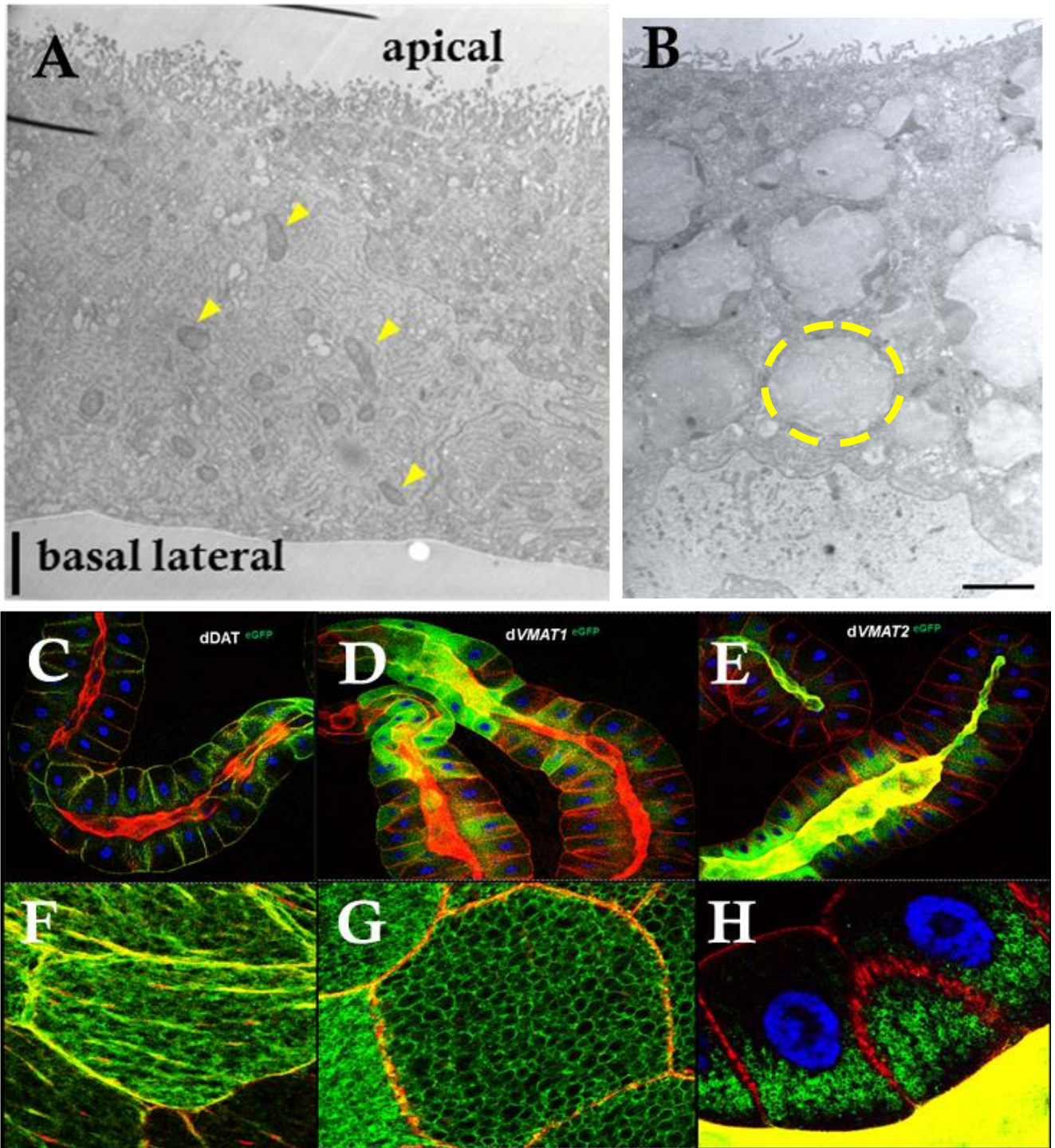
Figure 4.4: Secretory salivary gland cells as a heterologous system to study the subcellular localization of DA transporters

(A and B) Images of the highly-polarized structure of salivary gland epithelial cells by transmission electronic microscope (TEM) from (A) an early 3rd instar stage larva, before the initiation of massive synthesis of glue proteins showing mitochondria with yellow arrows, or from (B) a late 3rd instar larva that showed the presence of many glue granules of large sizes in the cell (representative unit within a dashed circle). Apical side of the cells (top) is characterized by the presence of extensive microvilli that project into the lumen of the salivary gland.

(C-H) Subcellular localization of ectopically expressed (C, E) DAT, (D, G) dVMAT2and (E, H) VMAT-B in salivary glands from late third-instar larvae. The EGFP-tagged transporters were revealed by anti-GFP antibody (green), overall tissue morphology and cell membrane were labeled by phalloidin staining (red) for filamentous Actin (F-Actin) and cell nuclei by DAPI staining (blue). Salivary glands at this stage produce large numbers of secretory granules that are filled with glue proteins.

(C-E) Overview of the salivary glands. The lumens are highlighted by the F-Actin (red) highly enriched on the apical side of the cells. (C) DAT is localized to the basal-lateral membrane where it co-localizes with F-actin, but is largely excluded from the apical region of the cells surrounding the lumen.

(D and E) Both dVMAT2 (D) and VMAT-B (E) are mainly localized to the vesicular membrane on the granules inside the cell and are also highly enriched on apical side of the plasma membrane surrounding the lumen. Compared to VMAT-B-positive granules (D), granules positive for dVMAT2show a more polarized distribution (D), being heavily

concentrated to the apical side of the cells and conspicuously absent from the basal side, a pattern that is more apparent in close-up view of the cells in (H).

(F-H) Close-up view of individual cells from salivary glands in (C-E), respectively. (F) A close-up view of the membrane surface on the basal side of a cell (center). DAT is enriched on cell-cell junction where it co-localizes with F-Actin (red) and shows an uneven distributed pattern on the membranes surface, likely due to its preference for lipid raft-rich membrane structures. Note that the image also captured the area just below the basal surface of two neighboring cells (bottom part of the image), where no vesicular-location of DAT was observed (compare it with the large number of GFP-positive vesicles in G).

(G) A close-up view of an area below the basal surface of a cell expressing VMAT-B, which was heavily enriched on the vesicular membrane of the granules that filled the cell. (H) A cross-section view of the middle region of two cells, including both their apical and basal-lateral sides, with the cell nuclei (blue) sitting in the middle.

dVMAT2 positive granules are highly enriched on the apical surface (bottom, as revealed by the intense yellow color showing the co-localization of dVMAT2-GFP with F-Actin in the lumen area, both at high protein levels). dVMAT2 positive granules are also enriched in apical half of the cells below the lumen, but are prominently absent from the basal half of the cells.

A part of a third cell sitting in between these two cells was also captured, showing a region below its lateral surface and close to its apical lumen region that is filled with GFP-positive granules. Note that in all the three cells, dVMAT2-EGFP is clearly absent

from the basal-lateral membrane labeled by F-Actin. In all cells, *patched*-GAL4 was used

to direct the target gene expression in salivary glands. Genotypes: (A and B). Orange R.

(C and F) w^{1118}; *ptc*-GAL4/+; UAS-EGFP-DAT/+. (D and G): w^{1118};*ptc*-GAL4/+; UAS- VMAT-

B-EGFP/+. (E and H): w^{1118}; *ptc*-GAL4/+; UAS- dVMAT2-EGFP/+. Scale bars: 20 μm.
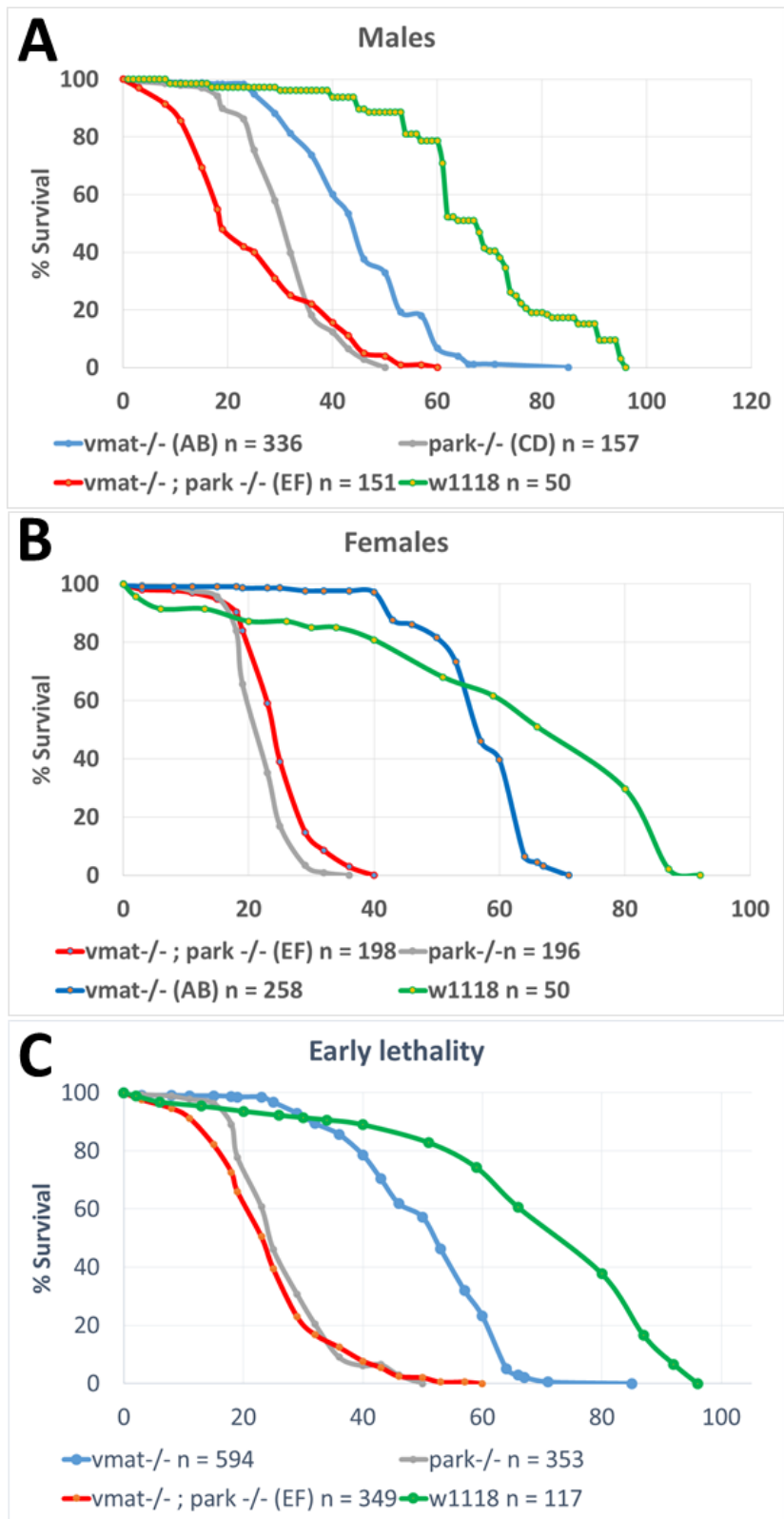
Figure 4.5: Early lethality in double mutants due to *parkin* mutation.

(A-C) Representative life-span curves of (A) male and (B) female adult flies mutated on VMAT (blue), *parkin* (grey) or *vmat/parkin* double mutants (red). (C) Average of the life-span curves for males and females. Flies were kept at a density of 20-25 flies per sex and vial on standard fly food and passed every 3 to 4 days.   Dead flies were counted every passage.   Results show a 50% survival rate of 22 days to *VMAT/parkin* double mutants.
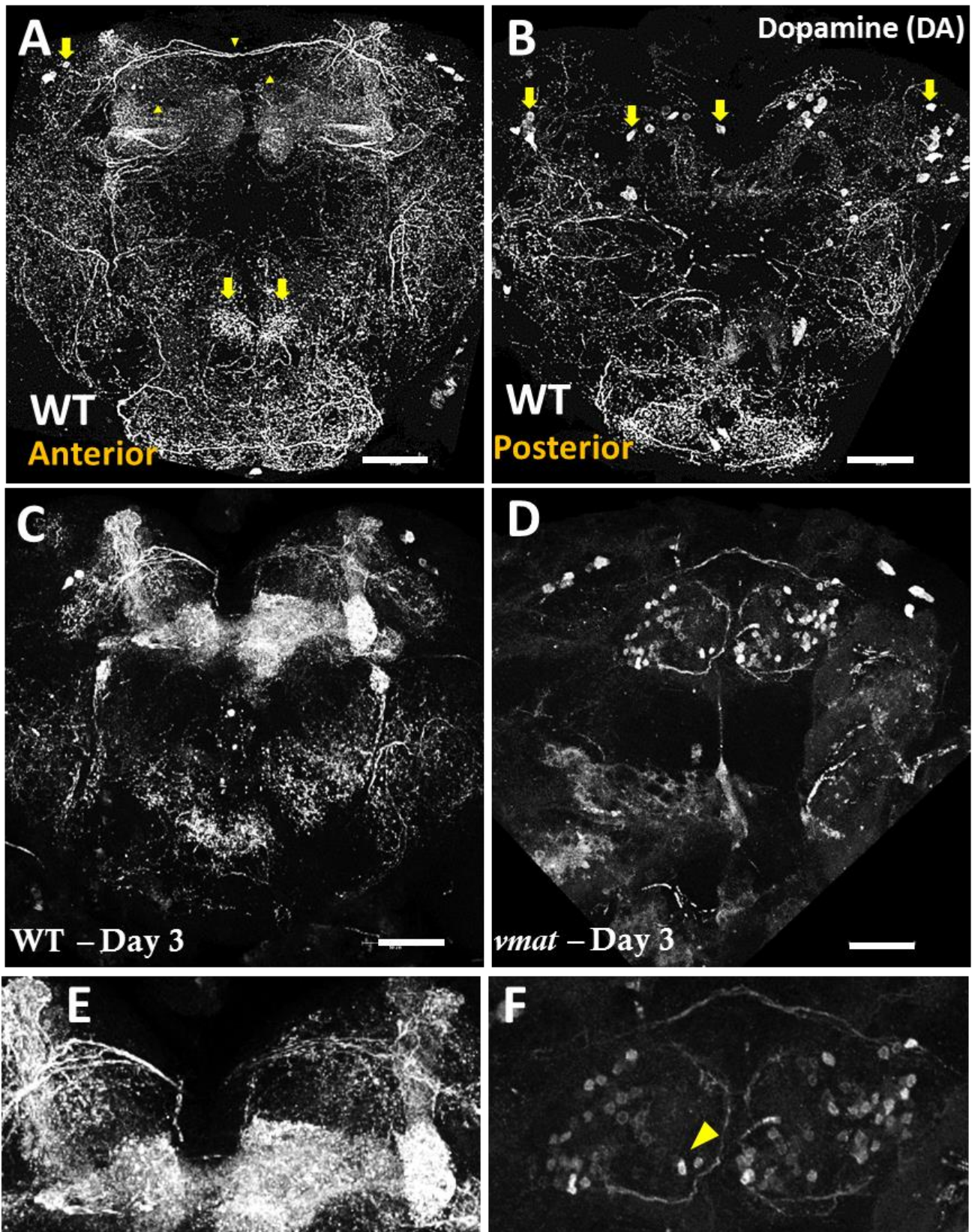
Figure 4.6: Distribution of DA in wildtype and *parkin* and *VMAT* mutant brains*

(A and B) Anterior (A) and posterior (B) view of DA distribution in 3-Days old wildtype adult *Drosophila* brains.

DA shows extensive distribution throughout the brain, with characteristic enrichment in the large commissures (arrowheads) connecting the two brain hemispheres, the mushroom bodies and a region around esophagus (arrows). For DA neuron clusters including PAL, PPL and PPM, DA is clearly present in the soma of the cells (arrow), however it is undetectable in the soma of DN in the PAM clusters (arrowheads). * DA immunohistochemistry performed by Hirsh Lab. Image projection performed by Antonio Tito.
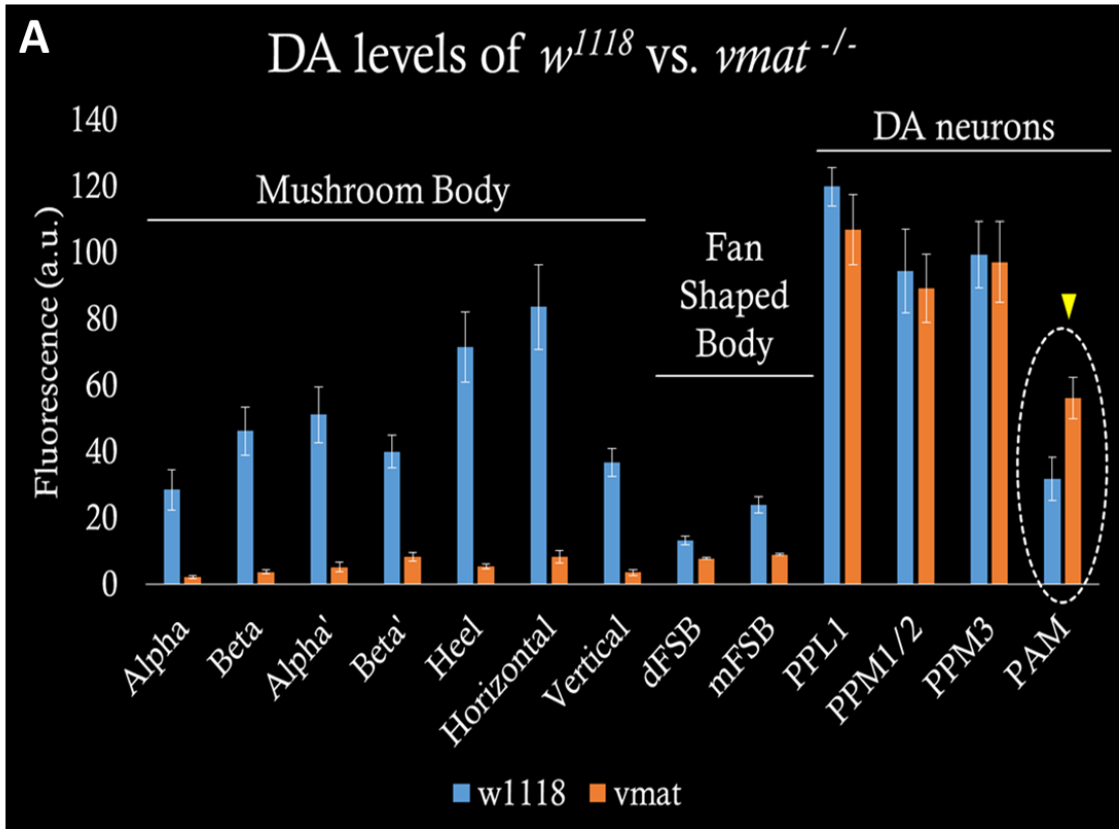
Figure 4.6: Quantification of DA and Serotonin in 3-Days and 22-Days old flies*

(A) Quantification of DA signal intensity in different areas of the brain of wildtype (blue bars) and *VMAT* mutant (orange bars) flies using a DA antibody. The levels of DA were significantly lower in all regions examined of *VMAT* mutant than in wildtype (indicated by yellow arrowhead),

Genotypes: (A-C): w^{1118} (wildtype control), w^{1118}; $VMAT^{eGFP}$/ $VMAT^{P}$ (*vmat* mutant), w^{1118}; $VMAT^{P}$ / *CyO* (*vmat* control). * DA signal analysis performed by Hirsh Lab and confirmed by Antonio Tito.
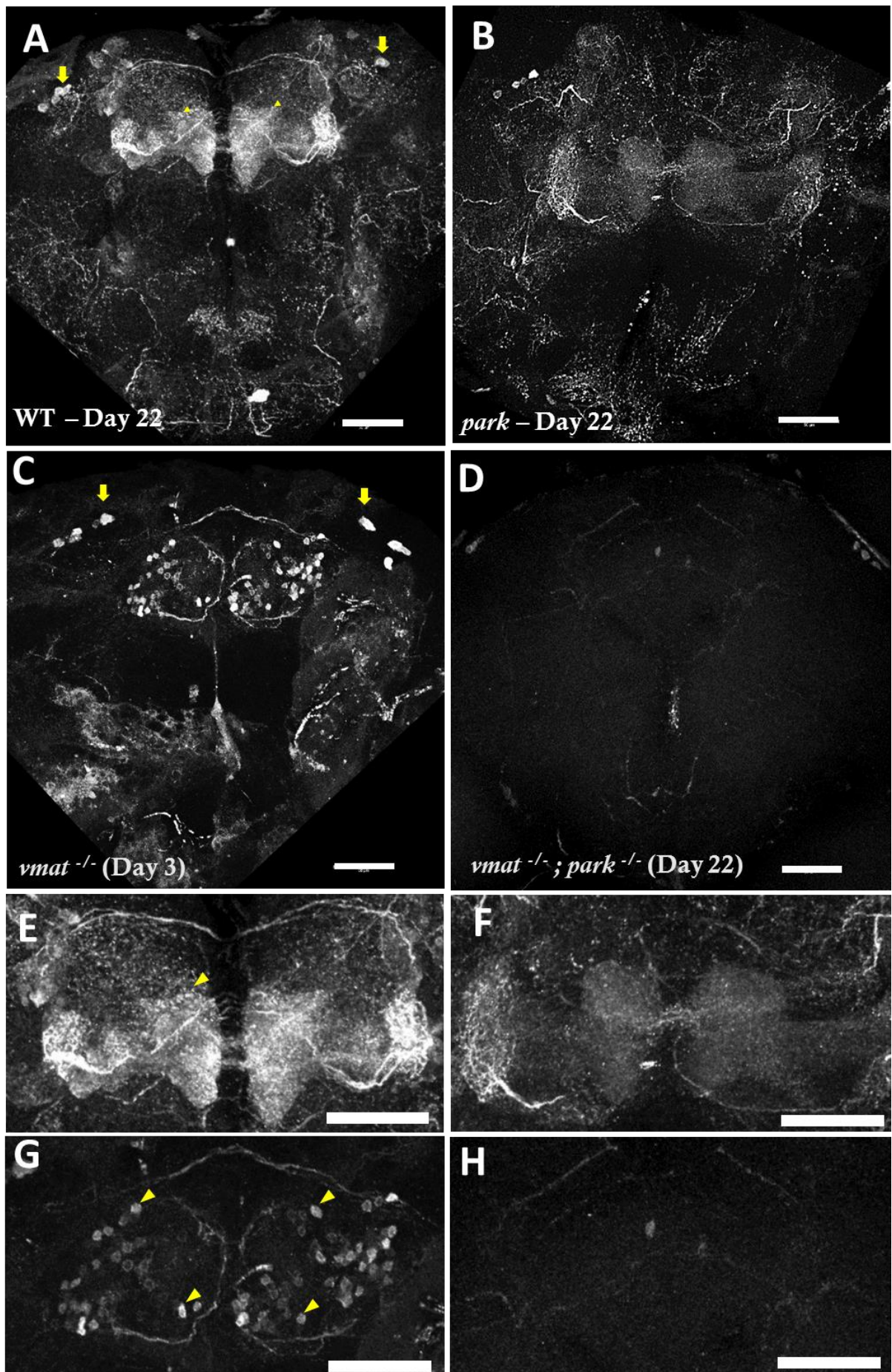
Figure 4.7: Distribution of DA in WT, *park, vmat*, and *vmat; park* mutants*

(A-D) Anterior view of DA distribution in 22-day-old adult brains (*vmat* mutant are 3-days old) and (E-H) close-up view of the mushroom body and PAM cluster regions.

(A and E) Wildtype. DA is prominently present in the giant commissures, the mushroom bodies, around the esophagus region as well as in the soma of PAL neurons (arrows), but is absent from the soma of DN (arrowheads) in the PAM clusters.

(C and G) *VMAT* mutant. DA is absent from the mushroom bodies and the region around the esophagus as well as in the soma of PAL neurons (arrows in C), but the soma of DN in the PAM cluster became clearly labeled by DA immunoreactivity (arrowheads in G).

(B and F) *parkin* mutant. DA shows similar distribution pattern as in wildtype, including its enrichment in the mushroom bodies and the region around the esophagus, is absent from the soma of DN in the PAM cluster. However, the levels of signal intensity from DA immunoreactivity become significantly weaker.

(D and H) *"VMAT; parkin"* double mutant. The signal intensity from anti-DA staining became barely detectable throughout the brain. DA signal is observed in PAL cluster neurons. Genotypes: (A and E): w^{1118} (wildtype control). (C and G) w^{1118}; $VMAT^{eGFP}$/ $VMAT^P$. (B and F) w^{1118}; $park^{\Delta 21}$/ $park^{f01950}$. (D and H) w^{1118}; $VMAT^{eGFP}$/ $VMAT^P$; $park^{\Delta 21}$/ $park^{f01950}$ Scale bar: 50 μm. * DA immunohistochemistry performed by Hirsh Lab. Image projection performed by Antonio Tito.
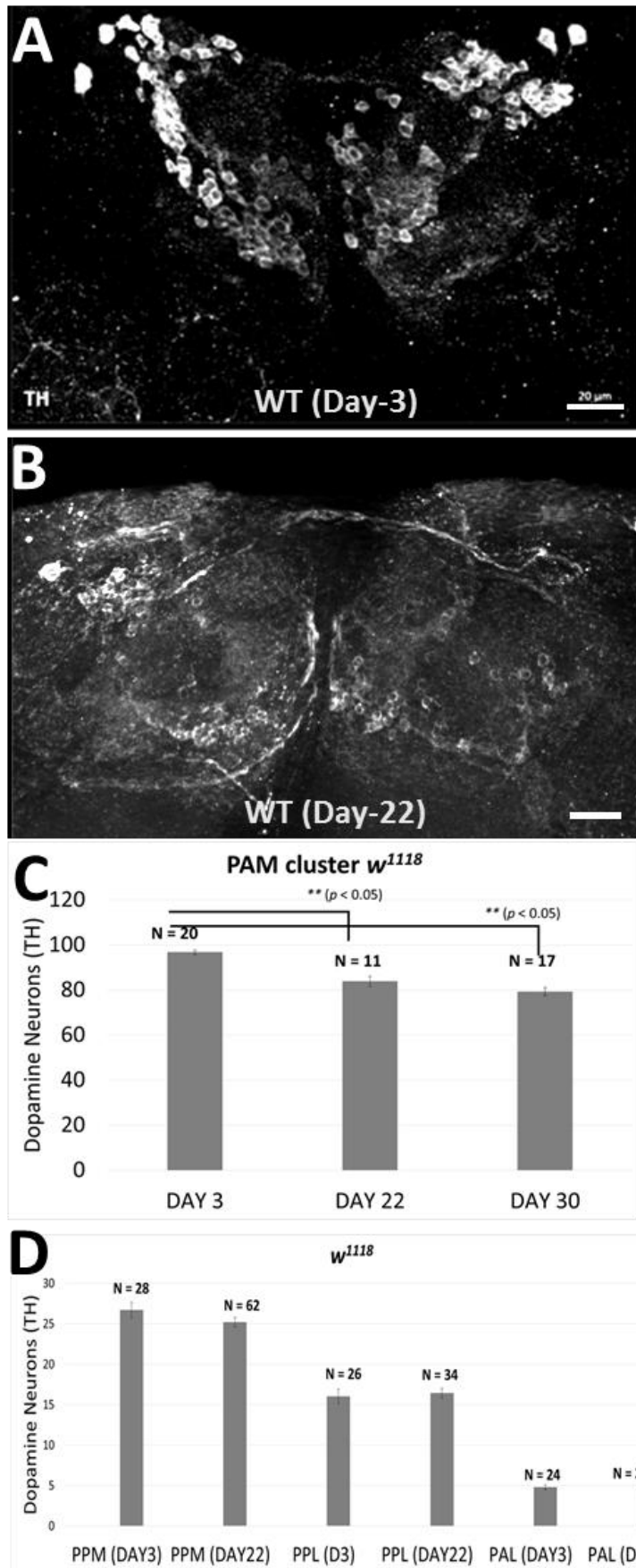
Figure 4.8: Loss of DN in aged *w¹¹¹⁸* (WT) flies

(A-D) Representative images of DN of w^{1118} in the PAL and PAM clusters in (A-D) 3- and (E-H) 22-day-old adult brains, as revealed by anti-TH antibody staining. (A and E) Wildtype flies.

(C-D) Quantification of the number of DN in (C) PAM and (D) PPM, PPL, and PAL brain clusters. For wildtype control, there were no significant change between young and aged flies in all clusters, except for PAM cluster, which showed a 15% reduction in the number of DN.

Genotypes: (A-D): w^{1118} (wildtype control). Scale bar: 20 μm.
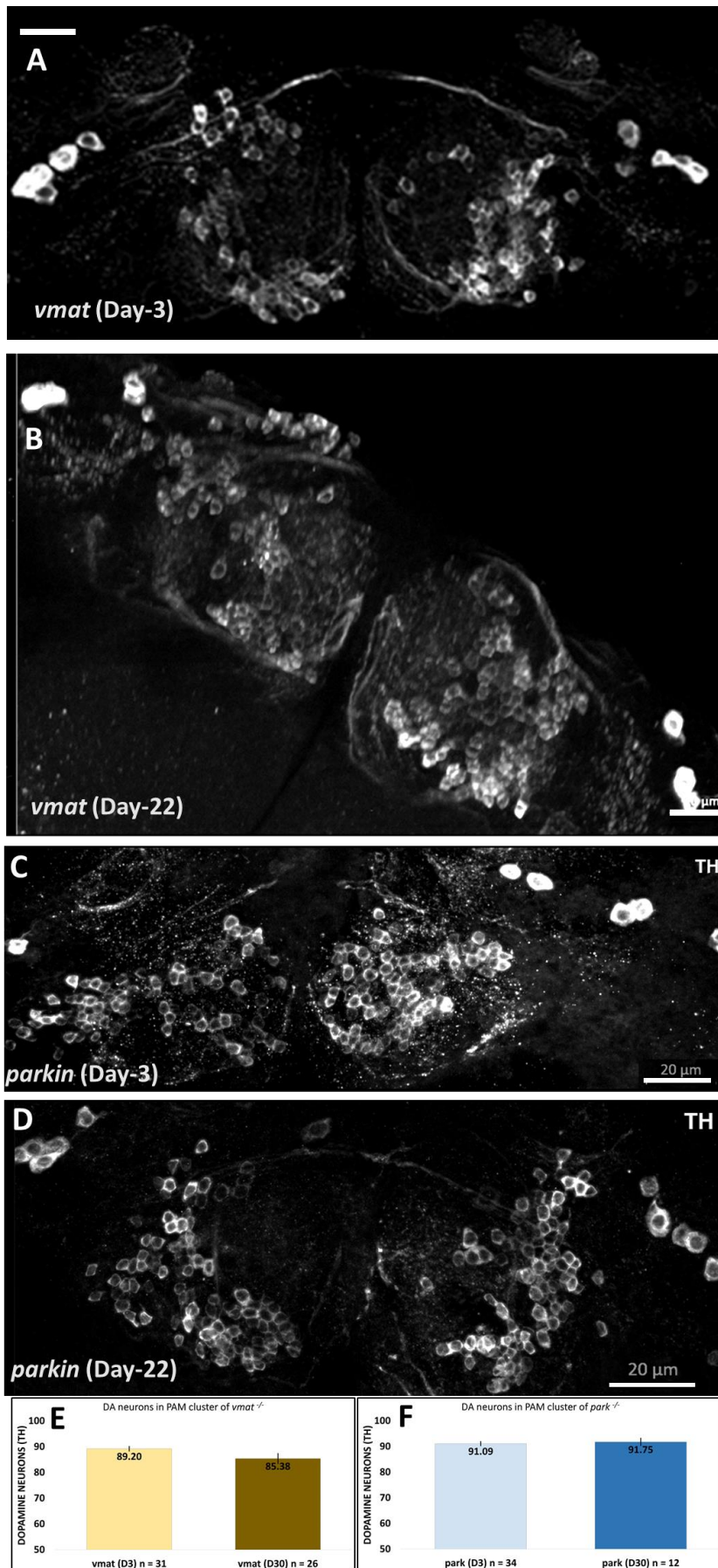
Figure 4.9: No apparent loss of DN in aged *VMAT* or *parkin* single mutant flies

(A-D) Representative images of DN in the PAL and PAM clusters in (A and C) 3- and (B and D) 22-day-old adult brains, as revealed by anti-TH antibody staining.

(A and B) *VMAT* mutant and (C and D) *parkin* mutant flies.

(E and F) Quantification of DN in different brain clusters.

Genotypes: (A and B): w^{1118}; $VMAT^{eGFP}$/ $VMAT^P$. (C and D) w^{1118}; $park^{\Delta 21}$/ $park^{f01950}$.

Scale bar: 20 μm.
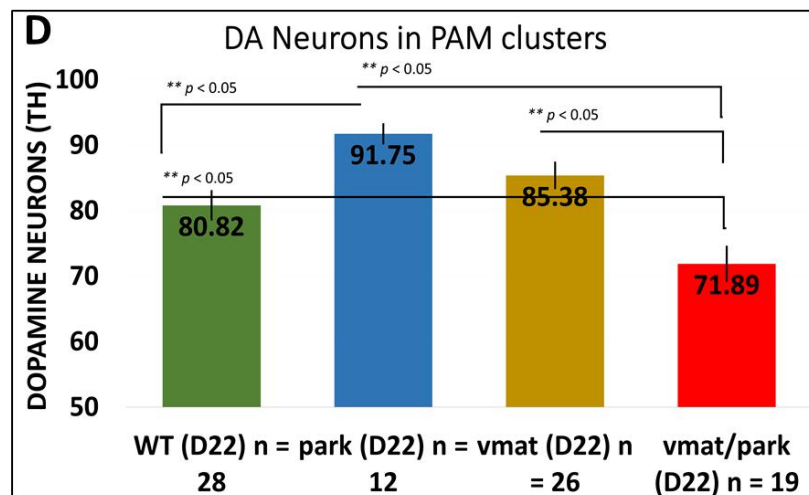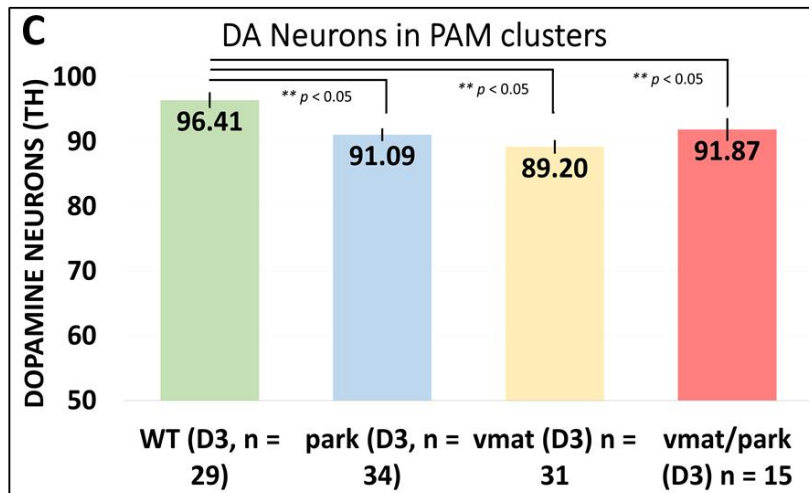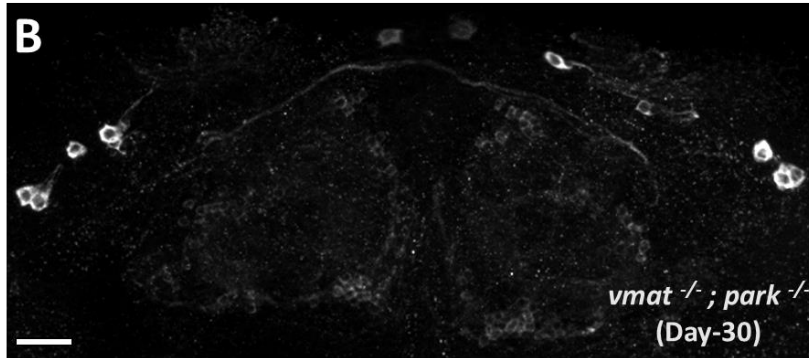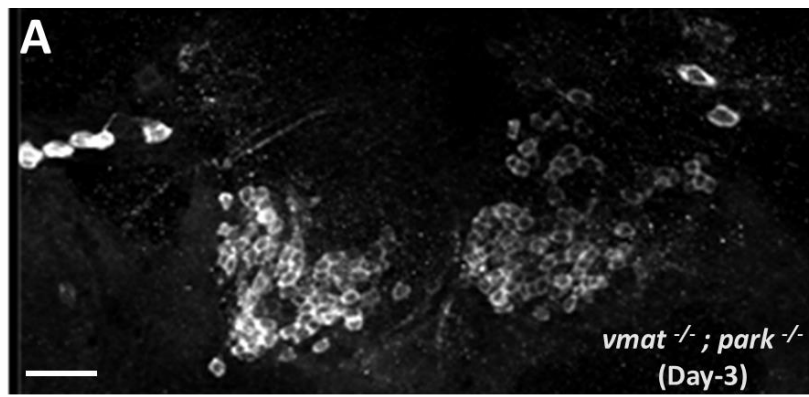
Figure 4.10: Age-dependent loss of DN in the PAM clusters in flies mutated for both *VMAT* and *parkin*

(A and B) Representative images of DN in the PAL and PAM clusters in the brains of (B) 3-day-old or (C) 22-day-old "*VMAT/parkin*" double mutant adults. DN in the PAM clusters were clearly recognizable by anti-TH antibody staining in the 3-day-old brains, but many became unrecognizable in 22-day-old brain, although DN in the neighboring PAL clusters (arrows) were clearly present.

(C and D) Quantification of the number of DN in different brain clusters. For wildtype control or flies carrying *VMAT* mutant alone or *parkin* mutant alone, there were no significant changes between young and aged flies in all the cluster examined. In the *VMAT/parkin* double mutant flies, there was a significant loss of DN in the PAM cluster in aged flies compared that in young ones, while the number of DN in other clusters largely remained the same.

Genotypes: (B and C) w^{1118}; $VMAT^{eGFP}/VMAT^P$; $park^{\Delta 21}/park^{f01950}$

Scale bar: 20 μm.
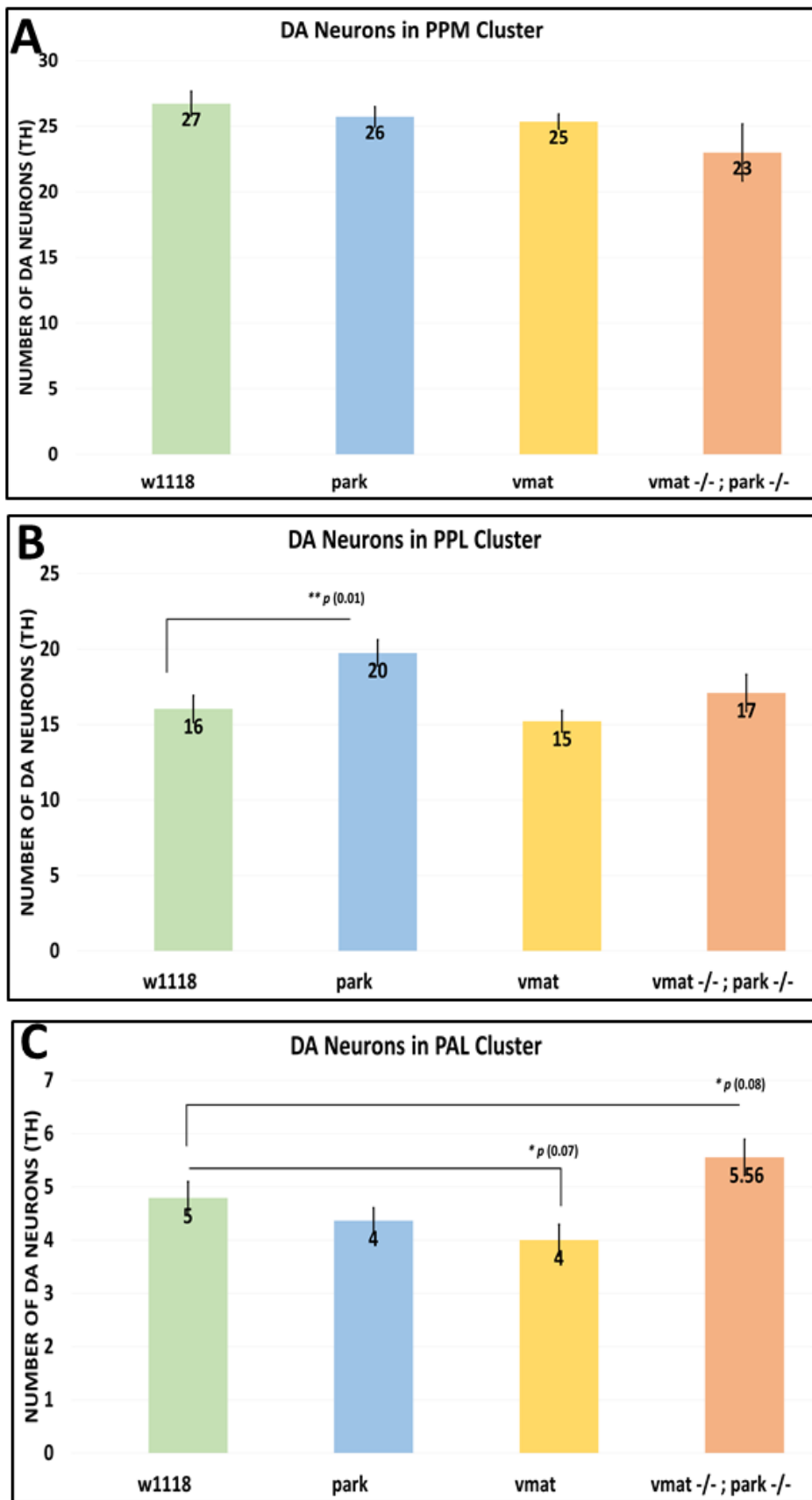
Figure 4.11: Quantification of DN in the PPM, PPL, and PAL clusters of Day-3 fly brains.

(A-C) Quantification of the number of DN of (A) PPM, (B) PPL, and (C) PAL clusters of 3-day-old WT, *vmat, parkin,* and "*VMAT/parkin*" double mutant adults.

There were higher number of neurons in the PPL cluster of *parkin* mutant flies, compared to wildtype, and no significant changes in all the other clusters examined.

For *vmat* mutant flies, there was a trend for a loss in the number of DA neurons in the PAL cluster, and no significant changes in all the other clusters examined.
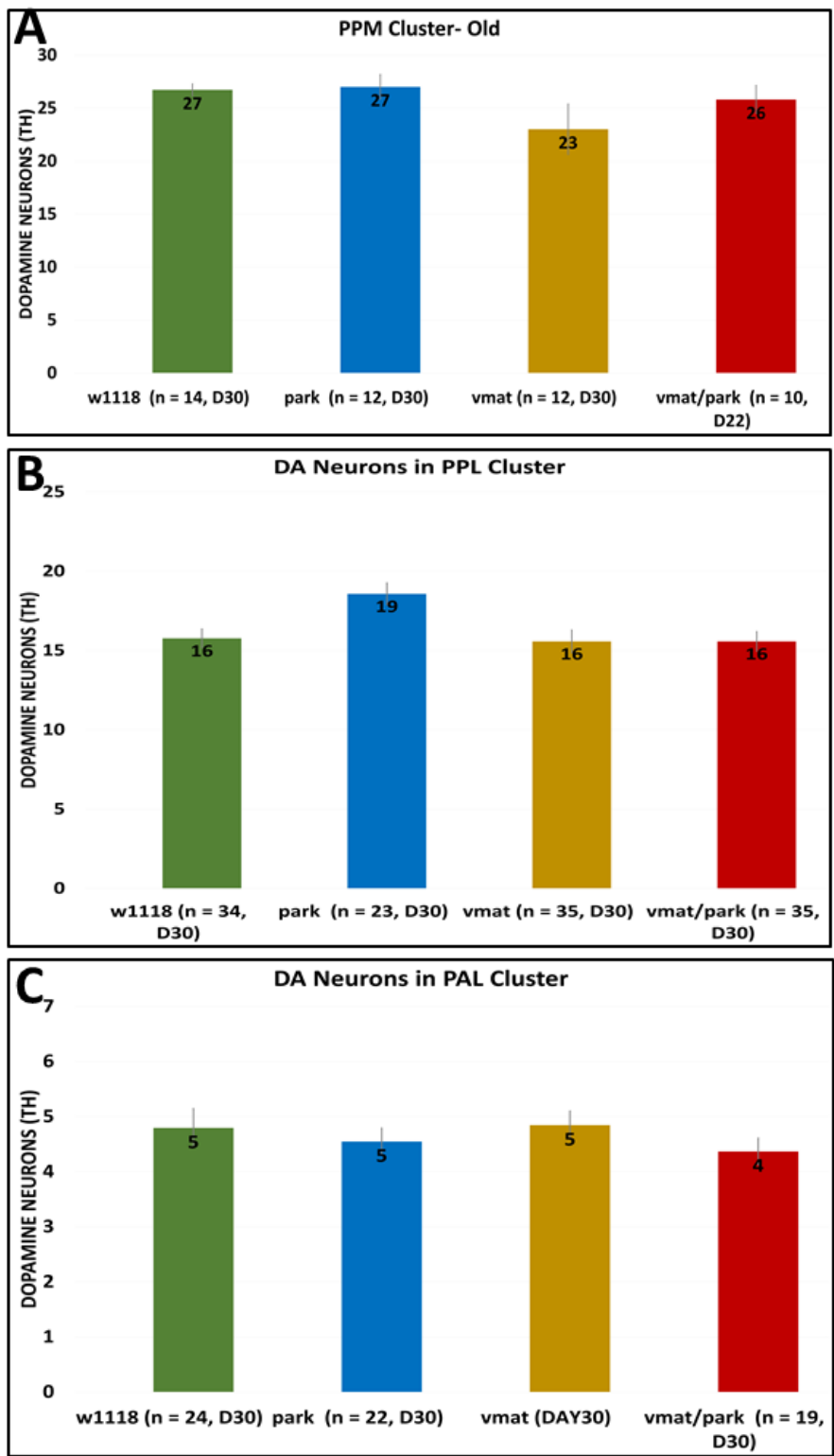
Figure 4.12: Quantification of DA neurons in the PPM, PPL, and PAL clusters of Day-22 fly brains

(A-C) Quantification of the number of DA neurons of PPM, PPL, and PAL clusters of (B) 3-day-old w^{1118}, *vmat*$^{-/-}$, *parkin*$^{-/-}$, and "*VMAT/parkin*" double mutant adults.

In wildtype control or flies carrying *VMAT* mutant alone or *parkin* mutant alone, there were no significant changes between aged flies in all the clusters examined.
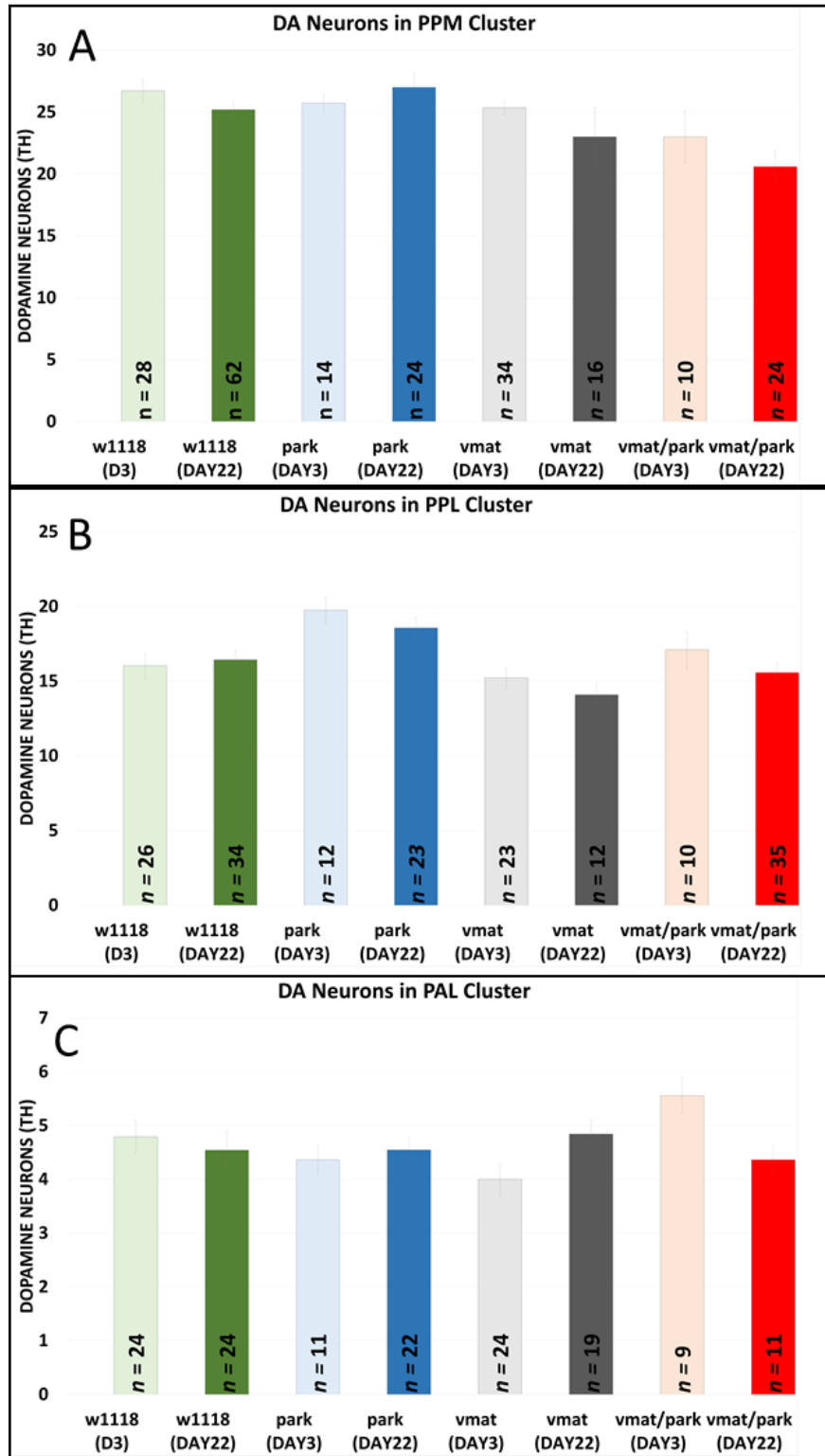
Figure 4.13: Quantification of DA neurons in the PPM, PPL, and PAL clusters of Day-3 and Day-22 fly brains

(A-C) Quantification of the number of DA neurons of PPM, PPL, and PAL clusters of 3-day-old and 22-day-old w^{1118}, $vmat^{-/-}$, $parkin^{-/-}$, and "*VMAT/parkin*" double mutant adults.

In wildtype control or flies carrying *VMAT* mutant alone or *parkin* mutant alone, there were no significant changes between young and aged flies in all the clusters examined.
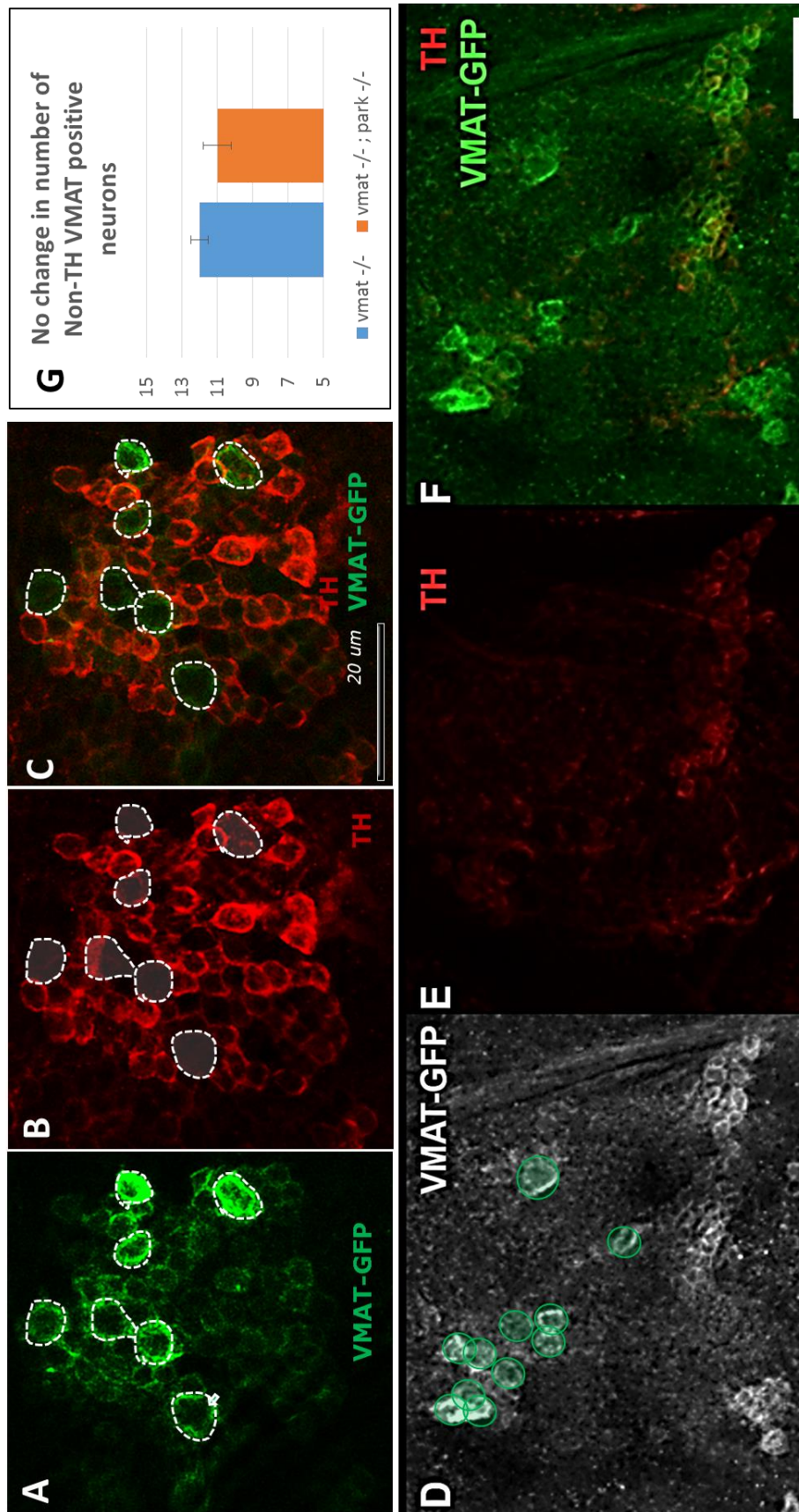
Figure 4:14: No apparent loss of octopamine neurons in the PAM cluster in flies lacking both *VMAT* and *parkin*

(A-F) Projected images of brain region covering the PAL and PAM clusters in 22-day-old

(A-C) d*VMAT* single mutant (genotype: w^{1118}; $dVMAT^{eGFP}$/ $VMAT^P$) or (D-F)

d*VMAT*/d*Parkin* double mutant flies (genotype: w^{1118}; $dVMAT^{eGFP}$/ $dVMAT^P$; $dpark^{\Delta 21}$/

$dpark^{f01950}$). d*VMAT*^{eGFP} is a VMAT genome-tagging line, which expresses a

nonfunctional VMAT-GFP fusion protein in a pattern mirroring that of endogenous

VMAT protein from wildtype flies.

(A-C) In 22-day-old d*VMAT*^{eGFP}/ $dVMAT^P$ flies, the VMAT-expressing cells were revealed

by (A) anti-GFP antibody (green) and DN by (B) anti-TH antibody (red). DN express both

TH and VMAT. Within the PAM clusters, octopamine neurons are identified as cells that

express VMAT but not TH (highlighted by white dashed lines). These octopamine

neurons also have relative larger cell sizes and higher level of VMAT expression as

compared to the TH-expressing DN within the same cluster.

(D-F) In 22-day-old d*VMAT*/d*Parkin* double mutant flies, most of the "GFP-positive, TH-

negative" octopamine neurons were still present (highlighted by white dashed lines).

The signal intensity for both TH and VMAT-GFP were apparently diminished in most

other cells there.

(G) Quantification of the number of octopamine neurons within the PAM clusters in 22-

day-old *VMAT* single mutant (blue bar, Genotype: w^{1118}; $dVMAT^{eGFP}$/ $VMAT^P$) or the

VMAT/parkin double mutant (orange bar. Genotype: w^{1118}; $dVMAT^{eGFP}$/ $dVMAT^P$;

$dpark^{\Delta 21}$/ $dpark^{f01950}$) flies, which shows no significant difference between the two

genotypes. Scale bar: 20μm.

4.3 Discussion

VMAT is essential for the proper vesicular storage of monoamines and their regulated release. Increasing evidence have linked VMAT dysfunction with PD. In this study, we have re-examined the gain- and loss-of-function phenotypes of the sole *vmat* homolog in *Drosophila*. Our results suggest that dVMAT2 (a homologue of dVMAT2) potentially confers a previously unexplored unique activity in promoting DA release and that the C-terminal sequences in the two encoded VMAT isoforms, not only determine their differential subcellular localizations, but also induce content release.

Additionally, we show that the fly's secretory epithelial systems, such as hypodermal tissues and salivary glands, can be useful heterologous systems to study the activity and subcellular trafficking of DA transporters. Moreover, by examining DA distribution in WT and d*vmat* mutant animals, we find intrinsic differences in the dynamics of intracellular DA synthesis within DA neurons of the PAM clusters compared to DA neurons from other clusters.

Loss of dVMAT causes severe loss of total DA levels and a redistribution of DA in the whole brain. Lastly, removal of both dVMAT and dParkin result in the selective loss of DA neurons in the PAM clusters, but not in octopaminergic neurons; supporting a potential involvement of cytosolic DA in selective degeneration of DA neurons. Overall, our results implicate a differential intracellular DA handling mechanism that, when dysfunctional, may contribute to the regional specificity in PD.

4.3.1   Comparison with the previous human Parkin Mutant/VMAT-RNAi Study

A previous study by Sang *et al.* showed that depletion of d*VMAT* in *Drosophila* through RNAi, enhances the defects associated with the overexpressed human Parkin mutants, including DN loss in adult fly brains (Sang *et al.*, 2007). These findings demonstrate the importance of VMAT in protecting cells from DA toxicity. However, it is important to note, that the underlying mechanisms of cellular defects studied in that report, is very different from the ones analyzed in our study.

Firstly, while our study used loss-of-function *dParkin* as the sensitized background to study DA toxicity and a protective role of VMAT; the previous study focused on overexpressed human *Parkin* mutants, which does not recapitulate the loss-of-function phenotypes of d*Parkin* mutant animals nor exhibits the traits of a dominant negative mutant. Rather, human *parkin* mutants likely cause cellular toxicity through an unknown gained function, as pointed out by the investigators of this study.

Secondly, in agreement with other studies on VMAT mutants in both mouse and *Drosophila* (Caudle *et al.*, 2007; Fon *et al.*, 1997; Simon *et al.*, 2009; Takahashi *et al.*, 1997; Taylor *et al.*, 2014; Wang *et al.*, 1997), we observed a significant loss of total DA levels and a dramatically altered pattern of DA distribution in the brains of d*VMAT* mutant flies. In contrast, the Sang study showed a significant induction in the level of total DA in flies depleted of VMAT expression with RNAi knockdown.

Lastly, we observed significant loss of DA neurons, primarily in the PAM clusters of flies lacking both endogenous dVMAT and dParkin. Yet, in flies over-expressing human *Parkin* mutants, the degeneration was observed in the DM and DL

clusters. Nevertheless, both studies similarly demonstrate that in different sensitized genetic backgrounds, VMAT plays an important role in protecting cells from the toxicity of cytoplasmic DA.

4.3.2   *Drosophila* Salivary gland as a Heterologous System to study the Sorting and Trafficking Mechanisms for Monoamine Transporters

In *Drosophila*, hypodermal tissues synthesize and secrete DA molecules, which are subsequently oxidized and polymerized, leading to the hardening (sclerotization) and pigmentation of adult cuticles (Neckameyer and White, 1993; Wittkopp *et al.*, 2003; Wright, 1987). Since VMAT expression is not detected in hypodermal tissues and given that VMAT is not required for cuticle formation and pigmentation, it is still unclear as to how DA is packaged and secreted, in and out of epidermal cells.

Nevertheless, it is interesting that ectopic expression of dVMAT2 can induce dark pigmentation in adult cuticles. Such a finding raises a possibility that in epithelial cells, the ectopically expressed dVMAT2 can be properly sorted and trafficked to the surface of endogenous secretory vesicles. It is in these active vesicles that dVMAT2 may function similarly as in the DA neurons: sequestering existing cytosolic DA into the vesicles, thereby inducing extracellular release of its inner contents.

Interestingly, when expressed in epithelial cells in the salivary gland, another heterologous system and a highly polarized secretory tissue, both dVMAT isoforms and dDAT are targeted to subcellular destinations reminiscent to the locations where they normally reside, in their native neurons. For instance, dVMAT primarily localizes on the surface of glue granules and is excluded from basal-lateral plasma membrane, whereas

dDAT resides almost exclusively on the basal-lateral plasma membrane, where it is further enriched at sub-membrane, lipid-raft like domains.

These observations suggest that the secretory epithelial cells employ similar mechanisms as neuronal cells. These may involve the recognition of protein targeting signals embedded in these transporters which execute proper sorting and trafficking of the vesicles.

Salivary glands (SGs) may, therefore, represent an ideal heterologous tissue for imaging-based studies, since it contains big glue granules, with relatively large diameters, often 3-7µm wide. This simple physical attribute makes the SG an important system to dissect the regulatory mechanisms that could potentially mediate subcellular trafficking of these monoamine transporters in the neurons as well.

4.3.3   A Fusion-Promoting Activity by dVMAT2?

It has been shown that the expression levels of neurotransmitter transporters correlate with the number of transporters residing on an SV, as well as the capacity of each vesicle to package neurotransmitters. The later correlates with the increased amplitude (quantal size) of elicited responses, triggered by signals that initiate vesicular release (Daniels *et al.*, 2004; Edwards, 2007; Fei *et al.*, 2008; Pothos *et al.*, 2000; Prado *et al.*, 2006; Song *et al.*, 1997; Tordera *et al.*, 2007; Wilson *et al.*, 2005; Wojcik *et al.*, 2006; Wojcik *et al.*, 2004).

However, the vesicular packaging of DA by VMAT should not be sufficient to promote extracellular DA release, considering existing evidence that both dVMAT2 and VMAT-B are equally capable of packaging monoamines into secretory vesicles, and yet,

only dVMAT2 induce dark cuticle pigmentation. dVMAT2 and VMAT-B share majority of their sequences, including all of the 12 TM domains that determine their substrate affinity and transport activity, and differ on at their very C-terminal sequences, which modulate the trafficking and subcellular localization of the respective proteins (Fei *et al.*, 2007; Greer *et al.*, 2005; Grygoruk *et al.*, 2014; Grygoruk *et al.*, 2010).

Indeed, both VMAT isoforms are functional, *in vivo,* and can fully rescue the female sterility phenotype of *VMAT* mutant flies. Similarly as to mammalian VMAT2, dVMAT2 contains multiple motifs in its C-terminal domain, which are known to be involved in protein endocytosis and sorting, and which are absent in dVMAT-B.

These include the di-leucine sequence, a string of acidic residues and an YXXY tyrosine-based motif (Greer *et al.*, 2005; Grygoruk *et al.*, 2010). Consistent with this, dVMAT2 primarily localizes to intracellular membrane in transfected insect S2 cells, and exhibits much faster endocytosis rate than dVMAT-B (Greer *et al.*, 2005).

However, even for the dVMAT2 derivatives that show aberrant subcellular trafficking, due to mutations in these C-terminal sorting motifs, they still show equal capability as wildtype dVMAT2 in their storage capacity of monoamines, *in vivo*. These findings suggest that subcellular trafficking of dVMAT2 is mutually exclusive from its vesicular activity to package DA (Grygoruk *et al.*, 2014; Grygoruk *et al.*, 2010).

Furthermore, when expressed in the polarized secretory cells of the fly salivary glands, both dVMAT2 and VMAT-B are primarily localized to vesicular membrane, albeit with subtle modifications (see discussion below). Taken together, these observations would suggest that in hypodermal cells, both dVMAT2 and VMAT-B are equally capable

of packaging cytosolic DA into the vesicles. However, since only dVMAT2 is able to induce darker pigmentation, it could be possible that the C-terminal sequence in dVMAT2 confers it with additional functions, such as promoting membrane fusion and/or triggering content release. It will be interesting to determine whether the C-terminal of dVMAT2 can physically interact with proteins involved in membrane fusion, such as the SNARE complex components and their regulators.

4.3.4 <u>Differential Sorting of dVMAT2 and VMAT-B into Vesicles with Unique Properties?</u>

Partially in agreement with the above hypothesis, it is also interesting that, although both the ectopically expressed VMAT isoforms localize to vesicular membrane in salivary gland cells, they show substantial differences. These include dVMAT2 containing granules which exhibit a striking polarized distribution inside the cells, are largely absent in the basal-half of the cells, but are heavily concentrated in close proximity to the apical surface, where membrane fusion and secretion of glue proteins occur. In contrast, although the granules positive for dVMAT-B show polarized distribution toward the apical surface, their distribution is more dispersed.

Additionally, secretory vesicles with different properties also exist, including those act as 'reserve" and those that are more "readily releasable"(Evans and Cousin, 2007; Kidokoro *et al.*, 2004; Paillart *et al.*, 2003; Richards *et al.*, 2000; Rizzoli and Betz, 2005). In neurons, VMATs are localized both to synaptic vesicles (SVs), which are mostly clustered around the active zone at the synapse, and also to large dense-core vesicles (LDCVs), which are highly dispersed throughout the cytosol (Nirenberg *et al.*, 1996, 1997; Nirenberg *et al.*, 1995). Interestingly, resembling that observed for

dVMAT2 in salivary gland cells, overexpression of VMAT2 in mice leads to an increase in vesicle volume, and translocation to the active zones (Lohr *et al.*, 2014).

It is unknown whether salivary gland cells harbor different subtypes of glue granules, such as the ones that store glue proteins, or the ones with less competency for membrane fusion. However, given the apparently differential subcellular distribution pattern of the two VMAT isoforms in salivary gland cells, it is possible that dVMAT2 is selectively trafficked to a subset of granules similar to SVs present in the active zones of neurons.

These vesicles are fusion competent and "readily releasable." On the other hand, dVMAT-B is targeted to a subset of granules resembling the more dispersed LDCVs and/or the SVs in reserve pools. In support of this, dVMAT2 contains amino acid sequences that signal the subcellular localization of the transporter to SVs, but not to LDCVs.

Such sorting signals may also be recognized in salivary gland cells to further refine the trafficking of dVMAT2 among subsets of glue granules with different properties. These signals are embedded in C-terminal sequence of dVMAT2 and are absent from dVMAT-B (Grygoruk *et al.*, 2014; Grygoruk *et al.*, 2010).

It will be interesting to dissect out the functional significance for such subtle changes in the pattern of distribution and identify upstream mechanisms that regulate the precise timing of such events. The GFP-tagged dVMAT isoforms expressed in *Drosophila* salivary gland cells offer a convenient platform to carry out such studies.

4.3.5   Parkin in Regulating DA Homeostasis

In *Drosophila*, extensive characterization of different *parkin* mutant alleles from various scientific groups have produced conflicting results on the health of DA neurons in the adult fly brains (Greene *et al.*, 2003; Pesah *et al.*, 2004). Our studies failed to reveal a prominent loss of DA neurons in the brains of flies that are trans-heterozygous for two strong *parkin* mutant alleles (*parkin*$^{\Delta 21/f01950}$).

However, it is interesting to observe a markedly reduced level of DA staining in *parkin* mutant brains, although its distribution pattern was not altered. Consistent with this finding, early reports described the shrunk morphology and diminished TH immunoreactivity in DA neurons of the DM, as well as reduced level of total DA in *parkin* mutant flies (Cha *et al.*, 2005; Greene *et al.*, 2003).

Such an observation implies an unexplored role of Parkin in maintaining normal DA homeostasis. Since TH expression is not apparently affected by the loss of Parkin, it is unlikely that Parkin modulates DA synthesis by controlling the levels of TH. It is possible that Parkin achieves such regulation, directly or indirectly, through mechanisms that affect DA metabolism, such as glia-mediated sequestration and recycling of DNA, and change in dVMAT expression or activity.

On this latter aspect, it is interesting to note that Glutathione S-transferase Omega 1 (GSTO1), a key antioxidant gene, can act as a potent suppressor of *parkin* mutants and also become significantly up-regulated in d*VMAT* mutant, suggesting a shared functional link between VMAT and Parkin in stress response (Hanna *et al.*, 2015;

Kim *et al.*, 2012). Future studies are warranted to address this interesting question that might bear important implications in understanding Parkin-associated PD pathogenesis.

4.3.6   **Exposed DA Toxicity in *parkin* Mutant Flies**

In d*VMAT* mutant flies, we observed a significant loss of total DA levels, as indicated by both HPLC-ECD and DA immunoreactivity, as well as a profoundly altered distribution pattern of DA in the brain. These findings support the critical role of dVMAT in maintaining DA homeostasis and in the appropriate allocation of DA to discrete brain regions to modulate different brain functions.

The observation of a significant loss of DA neurons in the PAM cluster of d*VMAT*/d*parkin* double mutant flies, support the hypothesis that cytosolic DA can be toxic and its abnormal accumulation can exacerbate the vulnerability of Parkin mutant animals, thereby further disrupting the already perturbed cellular pathways. It is of interest to show that, although TH is clearly present in the brains of young d*VMAT*/d*parkin* double mutant flies, the overall DA immunoreactivity is greatly diminished.

Such a dramatic loss could be due to the additive effect from simultaneous loss of d*VMAT* and d*parkin*, as either mutant alone similarly results in a reduction of DA levels in the brain. As d*parkin* mutants are associated with increase accumulation of abnormal mitochondria and heightened oxidative stress (Greene *et al.*, 2005; Greene *et al.*, 2003), it is possible that cytosolic DA, when left unprotected in the absence of *VMAT*, would become quickly oxidized and/or metabolized to products that are no longer recognizable by the anti-DA antibody. Such a rapid turnover of cytoplasmic DA

would predict a vicious positive feedback cycle that creates a more stressed cellular environment by increasing ROS production, eventually resulting in the degeneration of DA neurons.

In order to obtain a better understanding of how accumulation of cytoplasmic DA can accelerate the degeneration of DA neurons in *parkin* mutant brains, it will be important to characterize the identity and quantity of DA derivatives in fly brains from different genetic background, especially in flies carrying single and double mutations for d*Parkin* and d*VMAT*. Similarly, it will be informative to develop assays that permit *in vivo* examination of the stress pathways activated in these mutant animals. Except for DA itself, the current technique is still not sensitive enough for us to detect DA metabolites from the adult brains (data not shown).

4.3.7 Differential Dynamics in Intracellular Handling of DA and Selective Vulnerability of PAM Cluster DA neurons

It is intriguing that in d*VMAT*/d*parkin* double mutants, the loss of DA neurons is more restricted to the PAM cluster, revealing potential intrinsic difference between DA neurons in different brain regions. Consistent with this finding, among the known DA clusters in the fly brain, the PAM cluster stands out on several aspects.

First, it contains the majority of DA neurons in the protocerebellum, with ~200 out of 280 DA neurons confined within a rather small region in the brain (Mao and Davis, 2009). Additionally, compared to DA neurons in other clusters such as the neighboring PAL, DA neurons in the PAM cluster mostly have relatively smaller cell sizes and lower levels of TH expression, although the underlying mechanism behind these differences are still not clear. Moreover, in wildtype background, although DA is

clearly present in the soma of DA neurons in most of the other clusters such as PAL, it is largely undetectable in the soma of PAM cluster cells.

Importantly, such a difference is unlikely, due to low level of total DA in these cells, as there is an intense enrichment of DA in the mushroom bodies, the structure that is heavily innervated by DA neurons from the PAM clusters. Such an observation would suggest that PAM cluster neurons might in fact contribute the majority of existing DA in the brain.

Thus, the almost absence of DA immunoreactivity in the soma of PAM cluster cells might imply a highly effective packaging and delivery mechanism employed by these cells to transfer the synthesized DA out of the soma and into the axonal terminal target. On the other hand, this pattern of DA distribution in PAM cluster cells is reversed in *VMAT* mutants. PAM cluster neurons show a clear accumulation of DA in their soma, accompanied by an almost complete absence of DA in the mushroom bodies.

Taken together, given the apparent difference in subcellular allocation of DA in cells of the PAM clusters, as compared to cells in most other clusters, suggest intrinsically different dynamics in the intracellular handling mechanisms of DA. These findings indicate that the packaging and delivery of DA in these cells is heavily VMAT-dependent, a finding that becomes further manifested by the loss of d*VMAT*.

Consistent with our finding, in a recent study on a *Drosophila* PD model using another PD gene αSynuclein (αSyn), it was shown that DA neurons within the PAM cluster have higher vulnerability to αSyn toxicity. In particular, the progressive

locomotion deficits induced by pan-neuronally expressed αSyn can be mostly attributed to the degeneration of a subset of fifteen DA neurons in the PAM cluster (Riemensperger *et al.*, 2013).

In humans, PD mainly affects DA neurons of the *Substantia nigra* while largely spare DA neurons in the VTA system (Blesa and Przedborski, 2014). It will be provocative to speculate an underlying similarity between the DA neurons in the SNPC region in human brains and DA neurons in the PAM cluster of *Drosophila* brain. It will be especially interesting to explore whether the intrinsic difference in intracellular handling of DA among different brain clusters play a role in selective degeneration of DA neurons in PD brains.

5   CONCLUSION AND PERSPECTIVES

Ever since Hornykievicz established PD as a DA depletion disease that slowly robs the patient from motor and cognitive faculties, millions of PD patients have been treated with DA based drugs. Although these drugs are quite effective in treating motor symptoms, PD continues to be the most common movement disorder and the second most common neurodegenerative disease. Its detrimental effects are due to cardinal symptoms not manifesting in PD patients until after 70-80% of striatal DA and 40-50% of nigral cell bodies have degenerated. Therefore, understanding the pathogenic events and the associated therapeutic targets will help develop drugs that could potentially slow down, or even reverse, the course of the disease. Despite the unsurmountable efforts to develop palliative treatments for the disease, there are still no effective treatments for such a devastating disorder. One of the major disadvantages of L-Dopa administration is its contribution to the spontaneous onset of dyskinesia, giving clinicians a small treatment window, after which the drug yields off-target effects.

As previously indicated, the neurotransmitter DA is a chemically labile molecule. When exposed to free oxygen in the PH-neutral cytosol, DA can spontaneously oxidize into toxic by-products, like the *o*-semiquinone and 5, 6-indolequinone. The DA metabolites can form protein adducts with alpha synuclein, parkin, and mitochondrial complex I, III, and V. DA neurons employ various mechanisms to prevent the accumulation of toxic products. For example, the enzyme glutathione peroxidase catalyzes the transfer of glutathione to DA *o*-quinone through

the nucleophilic attack of glutathione (Tse *et al.*, 1976) (Bisaglia *et al.*, 2010) (Segura-Aguilar and Lind, 1989).

To suppress the production of superoxide anion and DA *o*-semiquinone, cells can also induce the activity of cytochrome P450, prostaglandin H synthase, lactoperoxidase, DA B-monooxygenase, and tyrosinase (Graham *et al.*, 1978; Hastings, 1995; Baez *et al.*, 1997; Foppoli *et al.*, 1997; Thompson *et al.*, 2000). However, detecting the levels of toxic chemicals in physiological conditions is not trivial since the DA metabolites undergo intramolecular cyclization, causing difficult detection *in vivo* using conventional methods. Hence, other research paradigms must be established to determine the toxic effects of cytosolic DA in DA neurons.

Improving the vesicular storage of L-Dopa derived DA has been postulated to extend the treatment window of the drug and reduce the risk of unwanted effects (see Chapter 1). Growing evidence has implicated DA toxicity and dysfunctional VMAT in PD pathogenesis and the inability of L-Dopa to sustain long therapeutic effects. For instance, reducing VMAT2 activity *in vivo* results in substantial alterations in DA levels.

Mice expressing 5% of wild-type levels of VMAT2 show a remarkable reduction of total DA level in the brain (Want *et al.*, 1997; Caudle WM *et al.*, 2007). Also, the ability of Reserpine to induce the translocation of VMAT2 to non-synaptic reservoirs in neurons, suggests that VMAT2 orchestrates protection against the gradual buildup of toxic DA-adducts in mice (Yelin and Schuldiner, 1995). Therefore, a VMAT2 agonist that can cross the blood brain barrier could potentially have a remarkable therapeutic effect on patients. Pifl *et al.* showed a significant reduction in the VMAT2 ability to fill vesicles

with monoamines in pigmented neurons from mesencephalic tissues of postmortem PD brains (Pifl *et al.*, 2014). Such impairment is also evident in infantile patients harboring a familial *vmat2* mutation (Glatt *et al.*, 2006). Both patient populations exhibited the cardinal symptoms of PD, including loss of motor and cognitive abilities (Glatt *et al.*, 2006).

Conversely, gain-of-function SNPs in the promoter region of the *vmat2* gene confer a reduced risk of developing PD (Brighina *et al.*, 2013). Over-expression of VMAT2 in DA neurons also results in a significant induction in DA synthesis, DA neurotransmission, and protection from MPTP toxicity (Lohr KM *et al.* 2014). Deciphering the role of VMAT2 in genetic models of PD, therefore, will make it plausible to develop targeted therapies that enhance VMAT2 function, replenish DA levels, and improve DA neurotransmission in surviving neurons.

In this study, we performed a detailed investigation of the *VMAT* homolog in the model organism *Drosophila* and further evaluated its role in affecting the selective degeneration of DA neurons in normal and a sensitized d*Parkin*-mutant background. The nervous system of adult *Drosophila* serves as a sophisticated model to study the pathogenic mechanisms of various neurodegenerative disorders. Evidently, exposing fruit flies to the volatile fungal chemical 1-octen-3-ol induces DN degeneration and significantly reduces DA levels in the brains, phenotypes which are rescued by targeted over-expression of dVMAT2 in dopaminergic and serotonergic neurons (Inamdar *et al.*, 2013). The adult *Drosophila* brain is also a powerful model used for investigating cellular mechanisms regulating DA synthesis, packaging, release, and reuptake.

Using *Drosophila* to model age dependent DA neuron loss requires microsurgical techniques that can reliably provide access to brains with excellent morphology. Several easy-to-follow approaches for dissecting adult fly brains have been described (Sweeney *et al.*, 2011; Wu and Luo, 2006). To further simplify the dissection process of adult fly brains, a highly efficient technique taking less than ten seconds, has been introduced to dissect adult fly brains. With the advent of large-scale studies that promise to map out the neuronal circuitry of *Drosophila*, it is foreseeable that our dissection procedure will facilitate the development of high-throughput genetic and drug screens in the adult fly brain.

Furthermore, by examining the ectopic overexpression phenotypes of the two dVMAT isoforms in the salivary glands of the fruit fly, we found that, although both share similar sequences, they have apparent functional differences, regardless of being capable to fully rescue the d*VMAT* mutants. The two proteins are also targeted to different populations of secretory vesicles. To determine the biological significance of specific subcellular localization pattern of the transporters, we also performed a phenotypic assessment from ectopically expression of the transporters in Ddc positive hypodermal cells. DVMAT2 is the only isoform capable of inducing darker cuticle pigmentation, potentially by stimulating an excess in DA release.

Consistently, VMAT2 immunoreactivity was detected in the peripheral blood lymphocytes, further confirming its role in a systemic response to toxic molecules (Amenta *et al.*, 2001). By contrast, loss of d*VMAT* contributes to both a significant reduction in the total levels of DA and a drastically altered distribution pattern of DA in

the adult fly brain. Moreover, DA redistributes from the innervation targets to the soma of DA neurons, a phenotype that is especially prominent in DA neurons within the PAM clusters.

These observations help us reach the following conclusions: (1) Our data support the critical role of VMAT in the homeostasis of cellular DA, which is required for proper delivery of DA to the innervation targets; (2) The efficiency of intracellular handling of DA is different among different clusters of DA neurons in the fly brain; (3) DA neurons in the PAM cluster cells operate a more active VMAT-dependent mechanism to package and deliver cytosolic DA out of the soma.

We also confirmed that removal of either d*VMAT* or *parkin* alone does not cause a significant degeneration of DA neurons in the respective mutant animals. Additionally, loss of *parkin* does cause a significant reduction of the total level of DA but does not alter its distribution pattern in the brain, implicating a role of Parkin in regulating DA homeostasis. Lastly, simultaneous removal of both d*VMAT* and d*Parkin* causes an age-dependent loss of DA neurons primarily in the PAM cluster, in addition to a more dramatically reduced level of DA in the brain. This is the first demonstration linking a dysfunction in dVMAT2 to the selective loss of DA neurons in a region of the adult *parkin* mutant brain that is involved in learning and memory.

Our results further suggest that disruption of VMAT2 function can potentiate the selective degeneration of DA neurons in the mutant background of *parkin,* one of the causative genes of familial juvenile PD. The phenotypes associated with the loss of function of *dvmat,* consisting of a significant reduction in egg laying ability and a

decline in DA and 5HT levels in the fly brain (Figure 4.1), serve as functional readout of VMAT2 function in disease models of *Drosophila.*

Our results also support the hypothesis that toxicity of cytosolic DA contributes to the initiation and/or acceleration of targeted destruction of DA neurons. In this study, the toxicity of cytosolic DA was unveiled in animals lacking both endogenous d*VMAT* and *parkin*, leading to the manifestation of the phenotypes within a short period of time. It is likely that under normal conditions DA toxicity is largely negligible/undetectable and its detrimental effects become apparent only after long periods of time. However, such toxicity might become unmasked and dominant in sensitized background such as with genetic perturbations (e.g., VMAT or Parkin mutations), natural aging, increased inflammatory stresses, or chronic exposure to toxic contaminants (e.g., paraquat and MPTP-like toxins).

It is also possible that the difference in intracellular handling of DA might also be responsible for the selective vulnerability of PAM cluster neurons in *dVMAT/parkin* double mutant flies. For example, it is noticeable that DA is clearly present in the soma of the DA neurons within the PAL and PPM clusters in both wildtype and *dVMAT* mutant backgrounds, raising a possibility that these neurons normally maintain a more active endogenous protective mechanism against cytosolic DA. This property could render them more immune to DA toxicity in *dVMAT/parkin* double mutant background. In contrast, for DA neurons in the PAM cluster, the near absence of DA immunoreactivity in the soma of these cells raises the likelihood that they normally

employ a less active protective mechanism against cytosolic DA and, thus, are on a low threshold to succumb to the toxic effects of increased cytosolic DA.

Our results in *Drosophila* are consistent with primate data showing significant decrease of VMAT2 activity in the caudate and putamen of subjects with PD (Pifl *et al.*, 1990; Pifl *et al.*, 2015; Pifl *et al.*, 1988). Consistently, administering (METH) to the ventral midbrain DA region of vevet monkey brains induced long-term defects in DA neurons. Such defects are accompanied by a substantial decrease in striatal binding of the DA transporter (DAT)-binding ligand, as well as a significant reduction in the IR signal of VMAT-2, TH, DAT, and the subsequent loss of DA neuron connections (Harvey *et al.*, 2000). The exact mechanism of action by which METH causes degradation of DA terminals is still unknown. Interestingly, co-administration with methylphenidate increases the protein levels of VMAT2 and enhancing vesicular DA uptake, thus preventing the deleterious effects of METH at the terminals. The neuroprotective effect of methylphenidate supports the hypothesis that VMAT2 may prevent METH induced toxicity (Hanson *et al.*, 2004).

Moreover, the age-dependent behavioral decline in mice harboring complete and partial knockouts of Vmat2 and Park, implicates DA neuron toxicity as a common denominator. VMAT2 knockout mice show an aberrant neurotransmission of monoamines resulting early lethality (Wang *et al.*, 1997). Histological analysis of their cerebral cortex show an increased incidence of cell death, a phenotype that is rescued by the inhibition of MAO-A enzyme (Fon *et al.*, 1997). For instance, mice that only express five percent of wild-type Vmat2 level develop to adulthood but show weak

age-dependent motor loss phenotypes. *vmat2* hypomorphs also exhibit a more selective loss of nigrostriatal neurodegeneration, along with the associated motor dysfunction phenotypes (Mooslehner *et al.*, 2001) (Caudle *et al.*, 2007). In contrast, *vmat* mutants in *Drosophila* do not exhibit a loss of DA neurons, suggesting nigrostriatal degeneration in mice and primates involve other complex mechanisms.

Therefore, our findings are consistent with the long-proposed protective effect of VMAT against DA toxicity. They also support a potential causative role of VMAT in PD pathogenesis, as suggested by several recent studies. Taken together, results from this study also raise an interesting possibility that varying dynamics in intracellular DA handling among different groups of DA neurons might contribute to the regional specificity of cell loss in PD brains.

Questions to be addressed

Results from our study raise many questions that should be addressed in future studies and are briefly listed below:

First, why can a combined loss of Parkin and VMAT lead to a more selective destruction of dopamine neurons? One explanation is that in the absence of *parkin,* the majority of cells in the body are in heightened stress and produce an overall weakened organism due to global disruption of Parkin-associated pathways. These pathways include an accumulation of malfunctioned mitochondria and Parkin substrates normally targeted for the UPS and autophagy pathways, increased ROS levels and heightened oxidative stress associated with damaged mitochondria, and defective Parkin-assisted vesicular trafficking.

At the same time, disruption of VMAT leads to additional insults, *specifically* in the DA neurons due to the accumulation of cytosolic dopamine and resulting production of additional ROS and other toxic dopamine metabolites and conjugates, further inflaming the already susceptible system. Such two-fronted assaults may eventually overwhelm the anti-oxidative system and other protective mechanisms in the dopamine neurons, resulting in their gradual degeneration.

Secondly, what are the toxic reagents in the VMAT/Parkin double-mutant animals that kill the DA neurons? Is there a significant increase of ROS species in the double mutant animals? What are the potential toxic DA metabolites in the DA neurons? To address these questions, we will need a more sensitive assay to directly measure the DA metabolites in adult brains of different genotypes, such as only Parkin, d*VMAT* and d*VMAT/Parkin* double mutant animals. It might also be necessary to develop in vivo reporters to evaluate the levels of ROS species and the status of cellular stress in dopamine neurons in adult brains and to determine the cellular pathways that become selectively activated in the double mutant animals.

Additionally, Parkin itself is being associated with increasing number of cellular pathways from the UPS, to mitophagy and mitochondrial integrity, to immune response and vesicular trafficking. Which of these pathways is mostly responsible for the increased vulnerability of dopamine neurons to the accumulated cytosolic dopamine?

Furthermore, in addition to Parkin, about a dozen additional PD-associated genes have been identified and animals models based on these different PD genes have been established. Similar to *parkin* mutants, most of these PD models do not exhibit

selective loss of dopamine neurons. Can cytosolic dopamine play a similar role in potentiating the degeneration of dopamine neurons in these PD models?

Since many of the PD genes are conserved in *Drosophila* and their respective mutant lines are available, they can be tested using similar strategies. For genes that are not conserved in the fly, such as αSynuclein, transgenic fly lines expressing wildtype and mutated genes can be similarly tested.

In light of these questions, I postulate new research directions aimed at addressing: (1) questions pertaining to the physiological role of VMAT2 in the aging fly brain; (2) examine the pathophysiology from mouse models with a concomitant disruption of both VMAT and Parkin; and (3) examine the pathophysiology of post-mortem brain samples of patients with disruption of VMAT or Parkin. I also outlined the significance of pursuing these research directions and discuss their implications to clinical medicine.

Future studies can be established to produce brain-specific *dvmat* mutant clones in DA neurons of adult flies. In collaboration with Dr. Hugo Bellen, we have implemented the MiMIC method to establish a Gal4-trap line in the 5'-UTR region of d*VMAT* gene (Tito *et al.*, under review), which allows targeted expression of studied proteins and RNAi lines specifically in dVMAT-expressing cells. Such studies may implement this line to target knockdown of *parkin* specifically in the VMAT-expressing cells and examine the effects in neighboring neurons. This mosaic technique will allow us to study *parkin* loss-of-function phenotypes at later developmental stages and in adult tissues to circumvent potential involvement of *Parkin* in early

developmental stages. We can also perform targeted knockout of VMAT in adult animals using MIMIC technology, which can be especially important for the study of neurodegeneration as it circumvents any possible lethality.

Validation of Findings in Mammalian System

Results from Drosophila-based studies have their apparent limitations, due to the different physiology between invertebrate flies and mammals. However, similar issues also face the commonly used mouse model. For example, both Parkin and Pink1-knockout mice cannot recapitulate the apparent degeneration of DA neurons as in PD patients.

Additionally, although flies and mammalians share highly conserved pathways for dopamine synthesis and intracellular handling, they utilized different metabolic mechanisms to remove/recycle DA. For example, flies do not have L-Monoamine oxidases (MAO) and catechol-O-methyl transferase (COMT) systems to breakdown dopamine, but instead utilize the beta-alanyl-dopamine synthase Ebony in glial cells to link beta-alanine and DA to form N-β-alanyldopamine (NBAD), and a hydrolase Tan to convert NBAD back to DA to recycle the transmitter.

Thus, it will be important to further validate the findings from the fly system in mammalian models and, if possible, in samples from human patients. Data can be gathered from a proposed mouse model to explore the pathophysiology of VMAT2 deficiency in DA neurons of wild-type and *Parkin* knock-out mice. Various imaging modalities, such as positron emission tomography (PET) and single-photon emission

computed tomography (SPECT), can be used to examine the expression and distribution of DA transporters (VMAT2 and DAT) in live mice brains.

A mechanistic factor to consider is the effect of mutations on VMAT2 density on the membrane surface of SVs since the quantal size of neurotransmitter release positively correlates with the amount of VMAT2 protein at the vesicular lumen (Edwards, 2007). Further research should also clarify the effects of disrupting both *parkin* and d*VMAT* in monoamine neurons of the *Drosophila* brain. Such experiments must discriminate the effects of the mutations on the ability of the transporter to uptake monoamine or in the recycling process mediated by Parkin.

Finally, I also propose a longitudinal study to genotype familial juvenile PD patients and identify those with deficiencies in the regulatory machinery of DA homeostasis. The purpose will be to determine which of the characteristic phenotypes of PD is linked to deficiencies in the DA homeostasis. All patients would be asked for permission to harvest their brains, post-mortem, so as to correlate these findings with DA neuron loss in the SNPc.

PAM cluster as the fly counterpart of the *Substantia nigra* region in human brain?

In Parkinson's disease, the loss of DA neurons is mainly concentrated in the substantia nigra region of the brain, while the DA neurons in the Ventral tegmental area (VTA) are largely spared, though the mechanism behind this regional specificity is still unclear. Similar as those in humans, DA neurons in *Drosophila* brain are distributed in characteristic clustered patterns, raising a question as to whether cells in these clusters are intrinsically different and with differential vulnerability to stresses.

Although the *Drosophila* model has been employed extensively to study Parkinson's Disease-associated gene, most of the studies have been mainly focused on a few dopamine neuron clusters such as PPL and PAL, with few detailed analysis on the PAM clusters that contain the majority of DA neurons in the protocerebral brain. Notably, compared to DA neurons in the PAL and PPL clusters, DA neurons in the PAM clusters have relatively smaller cell sizes and lower levels of TH and VMAT expression in addition to their distinct projection patterns and different brain functions.

In this study, we further showed an apparent difference in intracellular handling of DA in the PAM cluster neurons as compared to neurons in other clusters such as PAL. Moreover, PAM cluster neurons exhibit a higher vulnerability to the simultaneous loss of VMAT and Parkin.

Consistent with this finding, a recent study on αSynuclein toxicity also reported the particular sensitivity of PAM cluster neurons to the ectopically expressed human PD gene products. Together, they raise an intriguing possibility on whether DA neurons in the PAM cluster of the *Drosophila* brain, bear certain similarity to the substantia nigra region of human brain, and whether in human brains, the dynamics of intracellular DA handling is different between neurons in the substantia nigra and those in the VTA system.

Our results also suggest that in future Drosophila based studies on Parkinson's disease, more attention should be paid to the DA neurons in the PAM clusters. Although they have smaller cell sizes and lower level expression of TH and VMAT markers, the larger number of DA neurons in the PAM clusters should allow a more

reliable, accurate, and representative quantification on the degree of potential dopamine neuron loss in the brain.

Moreover, DA neurons in the PAM clusters might be intrinsically more sensitive to different genetic perturbations, thus representing a better and more sensitive system for detecting pathogenic events related to Parkinson's disease.

Perturbed DA package and metabolism as one unifying theme of Parkinson's disease pathogenesis.

From a broad point of view, our study also raises a question on whether dopamine toxicity is a common thread linking most, if not all, of the pathogenic mechanisms associated with different PD genes. Does DA toxicity plays similar effect in potentiating the selective destruction of DA neurons in *parkin* mutants as in other PD-linked genetic alterations and even in the majority idiopathic cases?

In *Parkin* mutant flies, there is a significant loss of dopamine in the brain, though the distribution of DA appears normal and there is no apparent loss of DA neurons in the mutant. Similarly, one early study reported a 50% loss of VMAT and DAT expression in Parkin-knockout mice, despite no overt degeneration of DA neurons. It is possible that other PD-associated genes may directly or indirectly regulate different aspects of DA biology, such as its synthesis, the dynamics of its vesicular sequestration and subcellular delivery, and its metabolism and recycling both in DA neurons and in surround glial cells. Such a scenario will help explain the selective vulnerability of DA neurons in PD.

Finally, one potentially important therapeutic strategy is to minimize the cellular toxicity from cytosolic DA, by boosting the expression level or activity of VMAT and/or stimulate the efficiency of endogenous metabolic pathways involved in the breakdown of cytosolic DA. These questions should be addressed using *Drosophila,* in order to unravel the mystery surrounding the molecular events that lead to the selective destruction of dopamine neurons in PD brains.

6   MATERIALS AND METHODS

Molecular Biology - The EST clones GH22929, GH16917, and GH10249, encoding full-length cDNAs for DAT, dVMAT2 (dVMAT2) and dVMAT-B (dVMAT1) transcripts respectively were obtained from the Berkeley Drosophila Genome Project (BDGP) and further verified by DNA sequencing. The following primers were used to clone the eGFP tag in-frame to the N-terminus of DAT protein and to the C-terminus of dVMAT proteins.

For eGFP-DAT fusion construct, we used the following eGFP primers:

5' primer (V22/pEGFP-N1+586):

      GCTGGTTTAGTGAACCGTCAG

3' primer (sz-V38N):

      tatgcggccgccCTTGTACAGCTCGTCCATGC

DAT primers:

5' primer (DAT-P1-N):

      tgagcggccgcagcTCACCAACCGGACATATATCC

Removed the starting Methione in the encoded DAT protein and also introduced a GGRS linkere sequence in-between eGFP and DAT sequences.

3' primer for amplifying DAT cDNA:

      the SP6 primer from the pOT2a vector in the EST clone GH22929.

The ligated eGFP-DAT chimera construct was cloned into the EcoRI and XhoI restriction enzyme sites in the pUAST transgenic vector, as shown in Appendix 1.

For dVMAT-A-eGFP fusion construct, we used the following EGFP primers:

5' primer (sz-V37NBH):

AAGCTAGCGGATCCAAGCTTGTGAGCAAGGGCGAGGAGCTG

3' primer (V24/pEGFPN1-1424):

CTCTACAAATGTGGTATGGCTG

dVMAT2 (GH16917) primers:

5' primer (dVMAT-A-P5):

CTGCTACAGTTGTTCATGCTG.

3' primer for amplifying C-terminal sequence of dVMAT-A cDNA (dVMAT2-P8NBH):

ccaagcttggatccgctagcTTCGTCTTCCTCGTAGTTTTG.

The ligated dVMAT-A-eGFP chimera construct was cloned into the EcoRI and XbaI restriction enzyme sites in the pUAST transgenic vector.

dVMAT-B (GH10249) primers:

-5' primer (dVMAT-B-P5):

CTGCTACAGTTGTTCATGCTG.

-3' primer for amplifying C-terminal sequence of dVMAT-B cDNA (GH10249, primer dVMAT-P9NBH):

ccaagcttggatccgctagcAAGCCTCTCGCTCTCGTACGC.

The ligated dVMAT-B-eGFP chimera construct was cloned into the EcoRI and XbaI restriction enzyme sites in the pUAST transgenic vector.

The pUAST constructs were injected together with helper DNA encoding $\Delta2$-3 p-element transposase into embryos of w^{1118} flies and transgenic fly lines were selected and established following standard transgenic protocols (Spradling and Rubin, 1982). Standard *Drosophila* husbandry were applied to maintain fly stocks and genetic crosses.

Transmission Electronic Microscope - Salivary glands from early 3rd instar or late wandering 3rd instar were dissected and fixed following by standard fixation (1.25% formaldehyde, 2.5 % glutaraldehyde and 0.03% picric acid in 0.1 M Sodium cacodylate buffer, pH 7.4. Room temperature for 2 hours) and embedding protocol. Thin sectioning of the fixed tissues was performed and imaged using JEOL 1200EX (80kV) scope at the Electron Microscope facility, Cell Biology Department at Harvard Medical School.

Drosophila melanogaster husbandry and stocks - Adult flies were grown and maintained with standard fruit fly food at 25°C. The following Gal4 lines were used in the study: VMAT-Gal4[MI03756], R48B04-Gal4 (BL-50347), R58E02-Gal4 (BL-41347), Ddc-Gal4 (BL-7010), TH-GAL4 (BL- 8848), w^{1118} as wildtype control, VMAT-EGFP[MI07680] tagging and driver lines were derived using MI07680 and MI03756, respectively as described in Venken *et al.* (2011) and Nagarkar-Jaiswal et al (2015).

Over-expression studies - Ddc-Gal4 (BL-7010) was recombined with UAST-VMAT-A-GFP, UAST-VMAT-B-GFP, UAST-mCD8-GFP, and UAST-DAT-GFP on the second chromosome. The recombined lines were observed under the dissecting microscope and crossed in the following combinations:

1. VMAT-A:

    a. DdC-Gal4, UAST-VMAT-A-eGFP x DdC-Gal4, UAST-VMAT6-eGFP

    b. DdC-Gal4, UAST-VMAT-A -eGFP x UAST-VMAT-A -eGFP

2. VMAT-A / TH :

    a. DdC-Gal4, UAST-VMAT-A -eGFP x DdC-Gal4, UAST-TH

    b. DdC-Gal4, UAST-VMAT-A -eGFP x UAST-TH

*UAS-TH was obtained from Bloomington stock center (BL-37539).

3. VMAT-B

    a. DdC-Gal4, UAST-VMAT-B -eGFP x DdC-Gal4, UAST-VMAT-B -eGFP

    b. DdC-Gal4, UAST-VMAT-B -eGFP x UAST-VMAT-B -eGFP

4. VMAT-B / TH

    a. DdC-Gal4, UAST-VMAT-B -eGFP x DdC-Gal4, UAST-TH

    b. DdC-Gal4, UAST-VMAT-B -eGFP x UAST-TH

5. DAT

    a. DdC-Gal4, UAST-eGFP-DAT x DdC-Gal4, UAST-eGFP -DAT

    b. DdC-Gal4, UAST-eGFP -DAT x UAST-eGFP -DAT

6. DAT / TH

    a. DdC-Gal4, UAST-eGFP -DAT x DdC-Gal4, UAST-TH

    b. DdC-Gal4, UAST-eGFP -DAT x UAST-TH

The phenotypes were confirmed to be selective for DA and serotonergic neurons using Ddc-Gal4 since crossing the UAST lines with the following GAL4 lines does not contribute to the pigmentation phenotype. Crosses are indicated by the checkmarks.

	Trident in thorax	**Muscle**	**Neurons**	**Low-ubiquitous**	**High-ubiquitous**
	Pnr- Gal4 (3°) (BL-58788)	MHC-Gal4 (3°)	Elav-Gal4 (3°) (BL-8760)	Da-Gal4 (3°)	Tub-Gal4 (3°)
pUAST-VMAT6-eGFP	✓	✓	✓	✓	✓
pUAST-VMAT9-eGFP	✓	✓	✓	✓	✓
pUAST-eGFP-DAT	✓	✓	✓	✓	✓
pUAST-TH	✓	✓	✓	✓	✓
pUAST-mCD8-eGFP	✓	✓	✓	✓	✓

Genetic interaction studies – The following crosses were performed at 25°C incubator with 3-4 females and 4-5 males on each vial.

	"*vmat ; park*" double mutants
	VMAT^eGFP/ CyO; *parkin* ^f01950/ TM6C
VMAT^p1 / CyO ; *parkin* ^Δ21 / TM6C	✓

"*vmat*" mutant	
	VMAT^eGFP/ CyO
VMAT^p1 / CyO	✓
"*parkin*" mutant	
	parkin ^f01950/ TM6B
parkin ^Δ21 / TM6C	✓

vmat mutant rescue studies – The following crosses were performed at 25°C incubator with 3-4 females and 4-5 males on each vial.	**Complementation of "*vmat*" mutants**
	VMAT^p1 / CyO
VMAT^Gal4 / CyO ; UAS-VMAT6-GFP/ TM6C	✓
VMAT^Gal4 / CyO ; UAS-VMAT9-GFP/ TM6C	✓

VMAT[Gal4] / CyO ; UAS-GFP-DAT / TM6C	✓
VMAT[Gal4] / CyO ; UAS-Ddc / TM6C	✓
	w^{1118} ; +/+
VMAT[Gal4] / CyO ; UAS-VMAT6-GFP / TM6C	✓

"vmat" mutant	
	VMAT[eGFP]/ CyO
VMAT[p1] / CyO	✓

"parkin" mutant	
	parkin [f01950]/ TM6B
parkin [Δ21] / TM6C	✓

Aging - Male and female adult flies were aged in separate vials holding 20 adult flies in each vial along with fresh fly food and transferred every 3-4 days into a new vial.

Solutions for adult brain dissection -   The adult fly brains were dissected in artificial cerebral spinal fluid (aCSF): 119 mM NaCl, 26.2 mM $NaHCO_3$, 2.5 mM KCl, 1 mM NaH_2PO_4, 1.3 mM $MgCl_2$, and 10 mM glucose. Before use, aCSF was gassed with 5% CO_2/95% O_2 for 10-15 min and spiked with 2.5 mM $CaCl_2$. The aCSF solution was sterilized by filtering through a 0.22 µm membrane filter. The aCSF was stored at 4°C. Fly brains can also be dissected in a phosphate-buffered saline (PBS) solution although detailed comparisons of the effects of the two dissection solutions on the final imaging quality of the dissected brains have not been performed.   4% paraformaldehyde (PFA) was used to fix the brains.

Solution for fixation - PFA was prepared in 1XPBS as the fixative solution, which is normally aliquoted and stored at -20°C. 1X phosphate-buffered saline (1xPBS) was used to rinse the formaldehyde from the brains and after the last washing step during the

immunofluorescent staining of the dissected brains.

Solutions for rinses and washes - The 1XPBS was prepared from 10X PBS stock solution (1.37 M NaCl, 27 mM KCl, 100 mM Na_2HPO_4, and 18 mM KH_2PO_4).   0.3% of Tween-20 was prepared in 1XPBS (1XPBT) and used for all the subsequent washing steps during immunofluorescent staining of the dissected brains.

Antibodies -   The primary antibodies in Figures 2 and 3 were rabbit anti-tyrosine hydroxylase antibody (Pel-Freez, catalog # P40101-0) at a 1:200 dilution and rat anti-Elav antibody (7E8A10, Developmental Studies Hybridoma Bank) at a 1:100 dilution, prepared in 1XPBT with 5% normal goat serum (Sigma-G9023) to block nonspecific binding. For secondary antibodies, we used AlexaFluor 488-conjugated goat-anti-rat antibody and AlexaFluor596-conjugated goat anti-rabbit antibody (Invitrogen) at a 1:500 dilution in 1XPBT.

Anesthetization - The adult flies were anesthetized with CO_2. A fly is picked using forceps and its cuticle is briefly de-waxed by dipping it in 70% ethanol for 3-5 s. This ensures that no bubbles adhere to the fly cuticle when immersed in the aCSF or 1XPBS dissection solution.

Fly immobilization - Under a dissecting microscope with a light source at an angle that will not be blocked by hands, the objective lens is set to attain a clear view of the fly (i.e. 1.2X magnification). The fly was then immobilized using forceps with the non-dominant hand, and immersed into the cold dissection solution with its abdomen facing upwards, as shown in Figure 1A.

The forceps were maintained at a $160^{o} - 170^{o}$ angle with respect to the dissection plate, while exerting a small force onto the abdomen of the fly (illustrated as

arrows in Figure 1A). This step immobilizes the fly and forces it to move its head backwards by 15°-25° while extending the proboscis upwards. In the process, a soft and translucent region of the cuticle, underneath the proboscis, becomes apparent. The magnification is increased and the focal plane is adjusted to fix the view onto this region. The forceps are not held too tightly, but rather just firm enough to stabilize the fly. Too much force causes the inside organs to rupture into the solution.

Priming forceps for brain surgery - The dominant hand was then used to press the dissecting forceps so that its tips are closed, generating a mild force on the tips of the forceps. The forceps spring open when pressure from the holding hand is released. The dissecting forceps are positioned perpendicularly to the forceps holding the fly, as shown in Figure 1B. The dissection forceps are then used to pierce through the soft and translucent region of the cuticle underneath the proboscis, as illustrated by the red arrow in Figure 1B. It is important not to penetrate the forceps too deeply to protect the brain. The brain proper should become visible.   A stable grasp of the fly is maintained with the non-dominant hand.

Removing the head case exoskeleton - The tips of the dissecting forceps are quickly but steadily released. The momentum from opening the forceps is used to tear away the exoskeleton surrounding the fly head. An intact brain proper should become visible (the white tissue immediately above the tip of the bottom forceps in Figure 1C). An imaginary line is used to guide the momentum of the released forceps tips (illustrated as the outward red arrows shown in Figure 1C). The natural force from the momentum of the opening forceps, gently removes the exoskeleton and most of the brain-associated eye and trachea, while leaving the exposed brain attached to the rest of the

body.

The proper timing and force applied to open the exoskeleton depends on the investigator's experience, and the removal of remnant accessory tissues, such as the tracheal tissue that appears as white fiber structures attached to the brain. The brain proper is not damaged in the process.

Fixation process - The dissected brain samples are fixed with their associated torsos in approximately 1 mL of 4% paraformaldehyde for 40-60 min. **Note:** For this and subsequent steps, the tubes or plates with samples are kept on a nutator to properly mix the samples in the solution.

Rinsing and washing - The brains are rinsed with 1 mL of 1XPBS by pipetting the solution 3 times (3X). Proper care is maintained to not aspirate the brains into the pipette. The brains are then washed 5 times with 1XPBT for 5 min each. The samples are kept on the nutator during wash incubations at all times.

Antibody incubation - Samples are incubated with primary antibodies at proper dilution overnight at 4°C. DN are visualized using a TH antibody, which recognizes the rate-limiting enzyme for the synthesis of DA (Figure 2) (Kim *et al.*, 2012; Pesah *et al.*, 2004; Trinh *et al.*, 2010; Whitworth *et al.*, 2005; Yang *et al.*, 2006). The following day, primary antibodies are removed, and the brains washed 5 times with 1XPBT. The brains are placed on the nutator and left for 5-10 min in the 1XPBT solution in between each wash. The washed samples are incubated in appropriate secondary antibodies with the suggested dilution and time of incubation.

Washing - The samples are washed six times with 1XPBT with a 10 min incubation between each wash. This step is critical for the removal of non-specifically bound

secondary antibodies from the sample.

Nuclear Staining - The samples are incubated in a 1:10,000 dilution of 1 mg/mL 4',6'-diamidino-2-phenylindole (DAPI) in 1XPBT solution for 30 min. DAPI is a DNA dye that binds to the AT regions of DNA and can be used to reveal the overall brain morphology. The samples are then rinsed three times with 1XPBS and transferred to a dissection dish where the brains are detached from the bodies using forceps.

Mounting - After the staining and washing steps, the brains are mounted in between two cover-slips. The cover-slips are then placed on top of a mounting slides allowing the brain samples to easily flip so both sides of the brain can be imaged with similar signal intensity. The brains are then mounted on an 18 x 18 mm cover-slip which is then placed on top of a mounting slide. The opening of the pipette tip is widened by cutting the tip with a blade. The cut tip is used to transfer the brains in 1xPBS solution onto the 18 x 18 mm cover-slip. The liquid around the brains is removed with a fine pipette tip. 20-40 μL of anti-fade mounting medium (0.2% (w/v) n-propyl gallate in 99.5% ACS grade glycerol) is then added over the brains. The amount of mounting medium added depends on the number of brains examined.

The viscous mounting medium is displaced outwards by using a pipette tip. A second 18 x 18 mm cover slip is placed on top of the brains by first lowering the slide from one side until it makes contact with the surface of the mounting slip, and then slowly lowering the other side to minimize inclusion of air bubbles. **Note:** There is no need to use a spacer in between the two cover slips as the volume of the mounting medium and the brains should provide sufficient space to separate the two cover slips. The slides are allowed to settle. Any excessive liquid that comes from the sides of the

slips is removed with laboratory tissue. To prevent the cover-slips from falling off of the mounting slide, we use a small piece of tape that attaches the cover-slips to the mounting slide. **Note:** Brains mounted in between the slides can be imaged immediately or preserved at 4°C for up to one week without significant loss of fluorescent signal. For long-term preservation of the stained brains, the side of the two slips can be sealed with clear nail polish and stored in a -20°C freezer, although stained brains might lose their signals over time.

Apotome and Image processing - To image the brains, we used an upright compound fluorescent microscope (Zeiss Imager Z.1) equipped with an Apotome function (Apotome 2.1) to acquire Z-stack images of brain slices that cover the whole depth of the region at interest. To obtain a clear visualization and reliable quantification of DN in the PAM cluster region, we used a 40X objective lens. In the Z-series acquisition function from the commercial software, we selected a section thickness of 0.5-1 μm between each imaged slice, which ensured an optimal image quality in a 3-D reconstruction of the PAM cluster region. The thickness of PAM cluster in the brain that covers all the DN is about 8-10 μm in total.

The 40X magnification shows a PAM cluster of about 8-10 μm in thickness, while the 20X magnification shows DN in the anterior and posterior sides of 20-25 μm each. In our experience, the Apotome function can significantly reduce the background signal in imaging the whole PAM cluster or the whole brain.

Head and body tissue homogenization – Flies are first placed under CO2 anesthesia, then weighted in a pre-weighted Eppendorf tube, and homogenized in RIPA

buffer with protease and phosphatase inhibitors. A hand-held homogenizer was utilized to homogenize the tissues in ice six times, for five seconds each. The homogenates are separated into multiple Eppendorf tubes on ice. The aliquots are centrifuged at maximum speed (14,000 rpm) for thirty minutes and supernatants are aliquoted in 10 µl and frozen. Thawing and freezing is minimized to preserve protein structure.

Protein loading, gel electrophoresis, transfer, and protein detection with antibody - The tissue samples (fly brains separately from fly bodies) in RIPA buffer are treated with 1X Loading Buffer (1:1) at RT prior to running them in the gel. The loading buffer (1x) is prepared as a 4X stock and diluted to a 1X solution. 10 µl of each sample, containing 10 µg/µl are diluted in a total volume of 40 µl with RIPA buffer. The samples are homogenized with a hand-held homogenizer with 10 strokes (6-8 seconds per stroke) on ice. The samples were boiled at 95°C for 5 minutes and ran in 8% gels. Protein transfer was performed overnight at 25 Volts and at 4°C. The transferred PVDF membrane is first blocked with a blocking buffer consisting of 0.5 g of powder milk in 10 ml of TBSt (1X 20 mM Tris, pH 7.5. 150 mM NaCl. 0.1% Tween 20) and washed with 1X TBSt five times for two minutes each. Membranes were then incubated with chicken anti-GFP antibody (Sigma G1544) at a dilution of 1:500 in blocking buffer over-night at 4°C and washed five times for two minutes each. The membrane was incubated with an anti-Chicken secondary antibody tagged with a fluorescent conjugate Alexa Fluor® 488 (Thermo Fisher Cat #: A-11039) in blocking buffer for 2 hrs at Room temperature and washed seven times for two minutes each.

7   REFERENCES

Amenta, F., Bronzetti, E., Cantalamessa, F., El-Assouad, D., Felici, L., Ricci, A., and Tayebati, S.K. (2001). Identification of dopamine plasma membrane and vesicular transporters in human peripheral blood lymphocytes. J Neuroimmunol *117*, 133-142.

Aso, Y., Hattori, D., Yu, Y., Johnston, R.M., Iyer, N.A., Ngo, T.T., Dionne, H., Abbott, L.F., Axel, R., Tanimoto, H.*, et al.* (2014). The neuronal architecture of the mushroom body provides a logic for associative learning. Elife *3*, e04577.

Auluck, P.K., Chan, H.Y., Trojanowski, J.Q., Lee, V.M., and Bonini, N.M. (2002). Chaperone suppression of alpha-synuclein toxicity in a Drosophila model for Parkinson's disease. Science *295*, 865-868.

Baez, S., Segura-Aguilar, J., Widersten, M., Johansson, A.S., and Mannervik, B. (1997). Glutathione transferases catalyse the detoxication of oxidized metabolites (o-quinones) of catecholamines and may serve as an antioxidant system preventing degenerative cellular processes. Biochem J *324 (Pt 1)*, 25-28.

Baloh, R.H., Salavaggione, E., Milbrandt, J., and Pestronk, A. (2007). Familial parkinsonism and ophthalmoplegia from a mutation in the mitochondrial DNA helicase twinkle. Arch Neurol *64*, 998-1000.

Banati, R.B., Daniel, S.E., and Blunt, S.B. (1998). Glial pathology but absence of apoptotic nigral neurons in long-standing Parkinson's disease. Mov Disord *13*, 221-227.

Barbeau, A., Gillo-Joffroy, L., Mars, H., and Arsenault, A. (1972). [Treatment of Parkinson's disease with L-dopa alone or combined with Ro 4-4602]. Rev Can Biol *31*, Suppl:169-174.

Bender, A., Krishnan, K.J., Morris, C.M., Taylor, G.A., Reeve, A.K., Perry, R.H., Jaros, E., Hersheson, J.S., Betts, J., Klopstock, T*., et al.* (2006). High levels of mitochondrial DNA deletions in substantia nigra neurons in aging and Parkinson disease. Nat Genet *38*, 515-517.

Berg, J., Roch, M., Altschuler, J., Winter, C., Schwerk, A., Kurtz, A., and Steiner, B. (2015). Human adipose-derived mesenchymal stem cells improve motor functions and are neuroprotective in the 6-hydroxydopamine-rat model for Parkinson's disease when cultured in monolayer cultures but suppress hippocampal neurogenesis and hippocampal memory function when cultured in spheroids. Stem Cell Rev *11*, 133-149.

Betarbet, R., Sherer, T.B., MacKenzie, G., Garcia-Osuna, M., Panov, A.V., and Greenamyre, J.T. (2000). Chronic systemic pesticide exposure reproduces features of Parkinson's disease. Nat Neurosci *3*, 1301-1306.

Bisaglia, M., Mammi, S., and Bubacco, L. (2007). Kinetic and structural analysis of the early oxidation products of dopamine: analysis of the interactions with alpha-synuclein. J Biol Chem *282*, 15597-15605.

Bisaglia, M., Soriano, M.E., Arduini, I., Mammi, S., and Bubacco, L. (2010). Molecular characterization of dopamine-derived quinones reactivity toward NADH and glutathione: implications for mitochondrial dysfunction in Parkinson disease. Biochim Biophys Acta *1802*, 699-706.

Bischof, J., Bjorklund, M., Furger, E., Schertel, C., Taipale, J., and Basler, K. (2013). A versatile platform for creating a comprehensive UAS-ORFeome library in Drosophila. Development *140*, 2434-2442.

Biyasheva, A., Do, T.V., Lu, Y., Vaskova, M., and Andres, A.J. (2001). Glue secretion in the

Drosophila salivary gland: a model for steroid-regulated exocytosis. Dev Biol *231*, 234-251.

Bjorklund, A., and Dunnett, S.B. (2007). Dopamine neuron systems in the brain: an update. Trends Neurosci *30*, 194-202.

Blesa, J., and Przedborski, S. (2014). Parkinson's disease: animal models and dopaminergic cell vulnerability. Front Neuroanat *8*, 155.

Bonifati, V., Rizzu, P., van Baren, M.J., Schaap, O., Breedveld, G.J., Krieger, E., Dekker, M.C., Squitieri, F., Ibanez, P., Joosse, M*., et al.* (2003). Mutations in the DJ-1 gene associated with autosomal recessive early-onset parkinsonism. Science *299*, 256-259.

Brand, A.H., and Perrimon, N. (1993). Targeted gene expression as a means of altering cell fates and generating dominant phenotypes. Development *118*, 401-415.

Brighina, L., Riva, C., Bertola, F., Saracchi, E., Fermi, S., Goldwurm, S., and Ferrarese, C. (2013). Analysis of vesicular monoamine transporter 2 polymorphisms in Parkinson's disease. Neurobiol Aging *34*, 1712 e1719-1713.

Bromberg-Martin, E.S., Matsumoto, M., and Hikosaka, O. (2010). Dopamine in motivational control: rewarding, aversive, and alerting. Neuron *68*, 815-834.

Brooks, D.J., Torjanski, N., and Burn, D.J. (1995). Ropinirole in the symptomatic treatment of Parkinson's disease. J Neural Transm Suppl *45*, 231-238.

Budnik, V., and White, K. (1988). Catecholamine-containing neurons in Drosophila melanogaster: distribution and development. J Comp Neurol *268*, 400-413.

Burke, C.J., Huetteroth, W., Owald, D., Perisse, E., Krashes, M.J., Das, G., Gohl, D., Silies, M., Certel, S., and Waddell, S. (2012). Layered reward signalling through octopamine and dopamine in Drosophila. Nature *492*, 433-437.

Busch, S., Selcho, M., Ito, K., and Tanimoto, H. (2009). A map of octopaminergic neurons in the Drosophila brain. J Comp Neurol *513*, 643-667.

Bush, W.D., Garguilo, J., Zucca, F.A., Albertini, A., Zecca, L., Edwards, G.S., Nemanich, R.J., and Simon, J.D. (2006). The surface oxidation potential of human neuromelanin reveals a spherical architecture with a pheomelanin core and a eumelanin surface. Proc Natl Acad Sci U S A *103*, 14785-14789.

Calleja, M., Herranz, H., Estella, C., Casal, J., Lawrence, P., Simpson, P., and Morata, G. (2000). Generation of medial and lateral dorsal body domains by the pannier gene of Drosophila. Development *127*, 3971-3980.

Carlsson, A. (1972). Biochemical and pharmacological aspects of Parkinsonism. Acta Neurol Scand Suppl *51*, 11-42.

Cartier, E.A., Parra, L.A., Baust, T.B., Quiroz, M., Salazar, G., Faundez, V., Egana, L., and Torres, G.E. (2010). A biochemical and functional protein complex involving dopamine synthesis and transport into synaptic vesicles. J Biol Chem *285*, 1957-1966.

Caudle, W.M., Richardson, J.R., Wang, M.Z., Taylor, T.N., Guillot, T.S., McCormack, A.L., Colebrooke, R.E., Di Monte, D.A., Emson, P.C., and Miller, G.W. (2007). Reduced vesicular storage of dopamine causes progressive nigrostriatal neurodegeneration. J Neurosci *27*, 8138-8148.

Cha, G.H., Kim, S., Park, J., Lee, E., Kim, M., Lee, S.B., Kim, J.M., Chung, J., and Cho, K.S. (2005). Parkin negatively regulates JNK pathway in the dopaminergic neurons of Drosophila. Proc Natl Acad Sci U S A *102*, 10345-10350.

Chang, H.Y., Grygoruk, A., Brooks, E.S., Ackerson, L.C., Maidment, N.T., Bainton, R.J., and Krantz, D.E. (2006). Overexpression of the Drosophila vesicular monoamine transporter

increases motor activity and courtship but decreases the behavioral response to cocaine. Mol Psychiatry *11*, 99-113.

Chege, P.M., and McColl, G. (2014). Caenorhabditis elegans: a model to investigate oxidative stress and metal dyshomeostasis in Parkinson's disease. Front Aging Neurosci *6*, 89.

Chen, A., Ng, F., Lebestky, T., Grygoruk, A., Djapri, C., Lawal, H.O., Zaveri, H.A., Mehanzel, F., Najibi, R., Seidman, G*., et al.* (2013). Dispensable, redundant, complementary, and cooperative roles of dopamine, octopamine, and serotonin in Drosophila melanogaster. Genetics *193*, 159-176.

Clark, I.E., Dodson, M.W., Jiang, C., Cao, J.H., Huh, J.R., Seol, J.H., Yoo, S.J., Hay, B.A., and Guo, M. (2006). Drosophila pink1 is required for mitochondrial function and interacts genetically with parkin. Nature *441*, 1162-1166.

Cole, S.H., Carney, G.E., McClung, C.A., Willard, S.S., Taylor, B.J., and Hirsh, J. (2005). Two functional but noncomplementing Drosophila tyrosine decarboxylase genes: distinct roles for neural tyramine and octopamine in female fertility. J Biol Chem *280*, 14948-14955.

Coon, S., Stark, A., Peterson, E., Gloi, A., Kortsha, G., Pounds, J., Chettle, D., and Gorell, J. (2006). Whole-body lifetime occupational lead exposure and risk of Parkinson's disease. Environ Health Perspect *114*, 1872-1876.

Corti, O., Lesage, S., and Brice, A. (2011). What genetics tells us about the causes and mechanisms of Parkinson's disease. Physiol Rev *91*, 1161-1218.

Creese, I., Burt, D.R., and Snyder, S.H. (1976). Dopamine receptor binding predicts clinical and pharmacological potencies of antischizophrenic drugs. Science *192*, 481-483.

Crocker, A., and Sehgal, A. (2008). Octopamine regulates sleep in drosophila through protein

kinase A-dependent mechanisms. J Neurosci *28*, 9377-9385.

Crocker, A., and Sehgal, A. (2010). Genetic analysis of sleep. Genes Dev *24*, 1220-1235.

Crosby, M.J., Hanson, J.E., Fleckenstein, A.E., and Hanson, G.R. (2002). Phencyclidine increases

vesicular dopamine uptake. Eur J Pharmacol *438*, 75-78.

Damier, P., Hirsch, E.C., Agid, Y., and Graybiel, A.M. (1999). The substantia nigra of the human

brain. I. Nigrosomes and the nigral matrix, a compartmental organization based on

calbindin D(28K) immunohistochemistry. Brain *122 (Pt 8)*, 1421-1436.

Daniels, R.W., Collins, C.A., Gelfand, M.V., Dant, J., Brooks, E.S., Krantz, D.E., and DiAntonio, A.

(2004). Increased expression of the Drosophila vesicular glutamate transporter leads to

excess glutamate release and a compensatory decrease in quantal content. J Neurosci

24, 10466-10474.

Dawson, T.M. (2000). New animal models for Parkinson's disease. Cell *101*, 115-118.

Dayan, P., and Balleine, B.W. (2002). Reward, motivation, and reinforcement learning. Neuron

36, 285-298.

de Freitas, C.M., Busanello, A., Schaffer, L.F., Peroza, L.R., Krum, B.N., Leal, C.Q., Ceretta, A.P., da

Rocha, J.B., and Fachinetto, R. (2016). Behavioral and neurochemical effects induced by

reserpine in mice. Psychopharmacology (Berl) *233*, 457-467.

Dimaline, R., and Struthers, J. (1996). Expression and regulation of a vesicular monoamine

transporter in rat stomach: a putative histamine transporter. J Physiol *490 (Pt 1)*, 249-

256.

Duerr, J.S., Frisby, D.L., Gaskin, J., Duke, A., Asermely, K., Huddleston, D., Eiden, L.E., and Rand,

J.B. (1999). The cat-1 gene of Caenorhabditis elegans encodes a vesicular monoamine

transporter required for specific monoamine-dependent behaviors. J Neurosci *19*, 72-

84.

Edwards, R.H. (2007). The neurotransmitter cycle and quantal size. Neuron *55*, 835-858.

Ehringer, H., and Hornykiewicz, O. (1960). [Distribution of noradrenaline and dopamine (3-hydroxytyramine) in the human brain and their behavior in diseases of the extrapyramidal system]. Klin Wochenschr *38*, 1236-1239.

Eisenberg, J., Asnis, G.M., van Praag, H.M., and Vela, R.M. (1988). Effect of tyrosine on attention deficit disorder with hyperactivity. J Clin Psychiatry *49*, 193-195.

El-Kholy, S., Stephano, F., Li, Y., Bhandari, A., Fink, C., and Roeder, T. (2015). Expression analysis of octopamine and tyramine receptors in Drosophila. Cell Tissue Res *361*, 669-684.

Erickson, J.D., Schafer, M.K., Bonner, T.I., Eiden, L.E., and Weihe, E. (1996). Distinct pharmacological properties and distribution in neurons and endocrine cells of two isoforms of the human vesicular monoamine transporter. Proc Natl Acad Sci U S A *93*, 5166-5171.

Erion, R., DiAngelo, J.R., Crocker, A., and Sehgal, A. (2012). Interaction between sleep and metabolism in Drosophila with altered octopamine signaling. J Biol Chem *287*, 32406-32414.

Evans, G.J., and Cousin, M.A. (2007). Activity-dependent control of slow synaptic vesicle endocytosis by cyclin-dependent kinase 5. J Neurosci *27*, 401-411.

Exner, N., Lutz, A.K., Haass, C., and Winklhofer, K.F. (2012). Mitochondrial dysfunction in Parkinson's disease: molecular mechanisms and pathophysiological consequences. EMBO J *31*, 3038-3062.

Fei, H., Grygoruk, A., Brooks, E.S., Chen, A., and Krantz, D.E. (2008). Trafficking of vesicular neurotransmitter transporters. Traffic *9*, 1425-1436.

Fei, H., Karnezis, T., Reimer, R.J., and Krantz, D.E. (2007). Membrane topology of the Drosophila vesicular glutamate transporter. J Neurochem *101*, 1662-1671.

Fon, E.A., Pothos, E.N., Sun, B.C., Killeen, N., Sulzer, D., and Edwards, R.H. (1997). Vesicular transport regulates monoamine storage and release but is not essential for amphetamine action. Neuron *19*, 1271-1283.

Foppoli, C., Coccia, R., Cini, C., and Rosei, M.A. (1997). Catecholamines oxidation by xanthine oxidase. Biochim Biophys Acta *1334*, 200-206.

Fraenkel, G., and Brookes, V.J. (1953). The process by which the puparia of many species of flies become fixed to a substrate. The Biological Bulletin *105*, 8.

Freis, E.D. (1954). Mental depression in hypertensive patients treated for long periods with large doses of reserpine. N Engl J Med *251*, 1006-1008.

Friggi-Grelin, F., Coulom, H., Meller, M., Gomez, D., Hirsh, J., and Birman, S. (2003). Targeted gene expression in Drosophila dopaminergic cells using regulatory sequences from tyrosine hydroxylase. J Neurobiol *54*, 618-627.

Gibb, W.R., and Lees, A.J. (1991). Anatomy, pigmentation, ventral and dorsal subpopulations of the substantia nigra, and differential cell death in Parkinson's disease. J Neurol Neurosurg Psychiatry *54*, 388-396.

Gilks, W.P., Abou-Sleiman, P.M., Gandhi, S., Jain, S., Singleton, A., Lees, A.J., Shaw, K., Bhatia, K.P., Bonifati, V., Quinn, N.P*., et al.* (2005). A common LRRK2 mutation in idiopathic Parkinson's disease. Lancet *365*, 415-416.

Glatt, C.E., Wahner, A.D., White, D.J., Ruiz-Linares, A., and Ritz, B. (2006). Gain-of-function haplotypes in the vesicular monoamine transporter promoter are protective for Parkinson disease in women. Hum Mol Genet *15*, 299-305.

Gnerer, J.P., Venken, K.J., and Dierick, H.A. (2015). Gene-specific cell labeling using MiMIC transposons. Nucleic Acids Res *43*, e56.

Goetz, C.G. (1986). Charcot on Parkinson's disease. Mov Disord *1*, 27-32.

Goetz, C.G., Tanner, C.M., Gilley, D.W., and Klawans, H.L. (1989). Development and progression of motor fluctuations and side effects in Parkinson's disease: comparison of Sinemet CR versus carbidopa/levodopa. Neurology *39*, 63-66; discussion 72-63.

Goldstein, D.S., Sullivan, P., Holmes, C., Miller, G.W., Alter, S., Strong, R., Mash, D.C., Kopin, I.J., and Sharabi, Y. (2013). Determinants of buildup of the toxic dopamine metabolite DOPAL in Parkinson's disease. J Neurochem *126*, 591-603.

Graham, D.G., Tiffany, S.M., Bell, W.R., Jr., and Gutknecht, W.F. (1978). Autoxidation versus covalent binding of quinones as the mechanism of toxicity of dopamine, 6-hydroxydopamine, and related compounds toward C1300 neuroblastoma cells in vitro. Mol Pharmacol *14*, 644-653.

Greene, J.C., Whitworth, A.J., Andrews, L.A., Parker, T.J., and Pallanck, L.J. (2005). Genetic and genomic studies of Drosophila parkin mutants implicate oxidative stress and innate immune responses in pathogenesis. Hum Mol Genet *14*, 799-811.

Greene, J.C., Whitworth, A.J., Kuo, I., Andrews, L.A., Feany, M.B., and Pallanck, L.J. (2003). Mitochondrial pathology and apoptotic muscle degeneration in Drosophila parkin mutants. Proc Natl Acad Sci U S A *100*, 4078-4083.

Greenfield, J.G., and Bosanquet, F.D. (1953). The brain-stem lesions in Parkinsonism. J Neurol Neurosurg Psychiatry *16*, 213-226.

Greer, C.L., Grygoruk, A., Patton, D.E., Ley, B., Romero-Calderon, R., Chang, H.Y., Houshyar, R., Bainton, R.J., Diantonio, A., and Krantz, D.E. (2005). A splice variant of the Drosophila

vesicular monoamine transporter contains a conserved trafficking domain and functions in the storage of dopamine, serotonin, and octopamine. J Neurobiol *64*, 239-258.

Grygoruk, A., Chen, A., Martin, C.A., Lawal, H.O., Fei, H., Gutierrez, G., Biedermann, T., Najibi, R., Hadi, R., Chouhan, A.K.*, et al.* (2014). The redistribution of Drosophila vesicular monoamine transporter mutants from synaptic vesicles to large dense-core vesicles impairs amine-dependent behaviors. J Neurosci *34*, 6924-6937.

Grygoruk, A., Fei, H., Daniels, R.W., Miller, B.R., Diantonio, A., and Krantz, D.E. (2010). A tyrosine-based motif localizes a Drosophila vesicular transporter to synaptic vesicles in vivo. J Biol Chem *285*, 6867-6878.

Guillot, T.S., and Miller, G.W. (2009). Protective actions of the vesicular monoamine transporter 2 (VMAT2) in monoaminergic neurons. Mol Neurobiol *39*, 149-170.

Guo, M. (2012). Drosophila as a model to study mitochondrial dysfunction in Parkinson's disease. Cold Spring Harb Perspect Med *2*.

Hague, S., Rogaeva, E., Hernandez, D., Gulick, C., Singleton, A., Hanson, M., Johnson, J., Weiser, R., Gallardo, M., Ravina, B.*, et al.* (2003). Early-onset Parkinson's disease caused by a compound heterozygous DJ-1 mutation. Ann Neurol *54*, 271-274.

Han, K.A., Millar, N.S., and Davis, R.L. (1998). A novel octopamine receptor with preferential expression in Drosophila mushroom bodies. J Neurosci *18*, 3650-3658.

Hanna, M.E., Bednarova, A., Rakshit, K., Chaudhuri, A., O'Donnell, J.M., and Krishnan, N. (2015). Perturbations in dopamine synthesis lead to discrete physiological effects and impact oxidative stress response in Drosophila. J Insect Physiol *73*, 11-19.

Hanson, G.R., Sandoval, V., Riddle, E., and Fleckenstein, A.E. (2004). Psychostimulants and

vesicle trafficking: a novel mechanism and therapeutic implications. Ann N Y Acad Sci *1025*, 146-150.

Hansson, S.R., Hoffman, B.J., and Mezey, E. (1998). Ontogeny of vesicular monoamine transporter mRNAs VMAT1 and VMAT2. I. The developing rat central nervous system. Brain Res Dev Brain Res *110*, 135-158.

Hardie, R.C. (1987). Is histamine a neurotransmitter in insect photoreceptors? J Comp Physiol A *161*, 201-213.

Hardy, J. (2010). Genetic analysis of pathways to Parkinson disease. Neuron *68*, 201-206.

Harvey, D.C., Lacan, G., and Melegan, W.P. (2000). Regional heterogeneity of dopaminergic deficits in vervet monkey striatum and substantia nigra after methamphetamine exposure. Exp Brain Res *133*, 349-358.

Hastings, T.G. (1995). Enzymatic oxidation of dopamine: the role of prostaglandin H synthase. J Neurochem *64*, 919-924.

Hastings, T.G., Lewis, D.A., and Zigmond, M.J. (1996). Role of oxidation in the neurotoxic effects of intrastriatal dopamine injections. Proc Natl Acad Sci U S A *93*, 1956-1961.

Hornykiewicz, O. (1998). Biochemical aspects of Parkinson's disease. Neurology *51*, S2-9.

Hostiuc, S., Drima, E., and Buda, O. (2016). Shake the Disease. Georges Marinesco, Paul Blocq and the Pathogenesis of Parkinsonism, 1893. Front Neuroanat *10*, 74.

Huetteroth, W., Perisse, E., Lin, S., Klappenbach, M., Burke, C., and Waddell, S. (2015). Sweet taste and nutrient value subdivide rewarding dopaminergic neurons in Drosophila. Curr Biol *25*, 751-758.

Humphrey, D.M., Parsons, R.B., Ludlow, Z.N., Riemensperger, T., Esposito, G., Verstreken, P., Jacobs, H.T., Birman, S., and Hirth, F. (2012). Alternative oxidase rescues mitochondria-

mediated dopaminergic cell loss in Drosophila. Hum Mol Genet *21*, 2698-2712.

Inamdar, A.A., Hossain, M.M., Bernstein, A.I., Miller, G.W., Richardson, J.R., and Bennett, J.W. (2013). Fungal-derived semiochemical 1-octen-3-ol disrupts dopamine packaging and causes neurodegeneration. Proc Natl Acad Sci U S A *110*, 19561-19566.

Jenett, A., Rubin, G.M., Ngo, T.T., Shepherd, D., Murphy, C., Dionne, H., Pfeiffer, B.D., Cavallaro, A., Hall, D., Jeter, J.*, et al.* (2012). A GAL4-driver line resource for Drosophila neurobiology. Cell reports *2*, 991-1001.

Johri, A., and Beal, M.F. (2012). Mitochondrial dysfunction in neurodegenerative diseases. J Pharmacol Exp Ther *342*, 619-630.

Kidokoro, Y., Kuromi, H., Delgado, R., Maureira, C., Oliva, C., and Labarca, P. (2004). Synaptic vesicle pools and plasticity of synaptic transmission at the Drosophila synapse. Brain Res Brain Res Rev *47*, 18-32.

Kim, K., Kim, S.H., Kim, J., Kim, H., and Yim, J. (2012). Glutathione s-transferase omega 1 activity is sufficient to suppress neurodegeneration in a Drosophila model of Parkinson disease. J Biol Chem *287*, 6628-6641.

Kitada, T., Asakawa, S., Hattori, N., Matsumine, H., Yamamura, Y., Minoshima, S., Yokochi, M., Mizuno, Y., and Shimizu, N. (1998). Mutations in the parkin gene cause autosomal recessive juvenile parkinsonism. Nature *392*, 605-608.

Konrad, K.D., and Marsh, J.L. (1987). Developmental expression and spatial distribution of dopa decarboxylase in Drosophila. Dev Biol *122*, 172-185.

Langston, J.W., and Ballard, P.A., Jr. (1983). Parkinson's disease in a chemist working with 1-methyl-4-phenyl-1,2,5,6-tetrahydropyridine. N Engl J Med *309*, 310.

Lauvrak, S.U., Hollas, H., Doskeland, A.P., Aukrust, I., Flatmark, T., and Vedeler, A. (2005).

Ubiquitinated annexin A2 is enriched in the cytoskeleton fraction. FEBS Lett *579*, 203-206.

Lawal, H.O., Chang, H.Y., Terrell, A.N., Brooks, E.S., Pulido, D., Simon, A.F., and Krantz, D.E. (2010). The Drosophila vesicular monoamine transporter reduces pesticide-induced loss of dopaminergic neurons. Neurobiol Dis *40*, 102-112.

Lee, Y., Paik, D., Bang, S., Kang, J., Chun, B., Lee, S., Bae, E., Chung, J., and Kim, J. (2008). Loss of spastic paraplegia gene atlastin induces age-dependent death of dopaminergic neurons in Drosophila. Neurobiol Aging *29*, 84-94.

Lesage, S., Durr, A., Tazir, M., Lohmann, E., Leutenegger, A.L., Janin, S., Pollak, P., Brice, A., and French Parkinson's Disease Genetics Study, G. (2006). LRRK2 G2019S as a cause of Parkinson's disease in North African Arabs. N Engl J Med *354*, 422-423.

Li, H., Chaney, S., Roberts, I.J., Forte, M., and Hirsh, J. (2000). Ectopic G-protein expression in dopamine and serotonin neurons blocks cocaine sensitization in Drosophila melanogaster. Curr Biol *10*, 211-214.

Lindquist, N.G., Larsson, B.S., and Lyden-Sokolowski, A. (1988). Autoradiography of [14C]paraquat or [14C]diquat in frogs and mice: accumulation in neuromelanin. Neurosci Lett *93*, 1-6.

Linert, W., Herlinger, E., Jameson, R.F., Kienzl, E., Jellinger, K., and Youdim, M.B. (1996). Dopamine, 6-hydroxydopamine, iron, and dioxygen--their mutual interactions and possible implication in the development of Parkinson's disease. Biochim Biophys Acta *1316*, 160-168.

Liu, C., Placais, P.Y., Yamagata, N., Pfeiffer, B.D., Aso, Y., Friedrich, A.B., Siwanowicz, I., Rubin, G.M., Preat, T., and Tanimoto, H. (2012). A subset of dopamine neurons signals reward

for odour memory in Drosophila. Nature *488*, 512-516.

Liu, Y., and Edwards, R.H. (1997). The role of vesicular transport proteins in synaptic transmission and neural degeneration. Annu Rev Neurosci *20*, 125-156.

Lohr, K.M., Bernstein, A.I., Stout, K.A., Dunn, A.R., Lazo, C.R., Alter, S.P., Wang, M., Li, Y., Fan, X., Hess, E.J.*, et al.* (2014). Increased vesicular monoamine transporter enhances dopamine release and opposes Parkinson disease-related neurodegeneration in vivo. Proc Natl Acad Sci U S A *111*, 9977-9982.

Lohr, K.M., and Miller, G.W. (2014). VMAT2 and Parkinson's disease: harnessing the dopamine vesicle. Expert Rev Neurother *14*, 1115-1117.

Lucking, C.B., Durr, A., Bonifati, V., Vaughan, J., De Michele, G., Gasser, T., Harhangi, B.S., Meco, G., Denefle, P., Wood, N.W.*, et al.* (2000). Association between early-onset Parkinson's disease and mutations in the parkin gene. N Engl J Med *342*, 1560-1567.

Lundell, M.J., and Hirsh, J. (1994). Temporal and spatial development of serotonin and dopamine neurons in the Drosophila CNS. Dev Biol *165*, 385-396.

Mao, Z., and Davis, R.L. (2009). Eight different types of dopaminergic neurons innervate the Drosophila mushroom body neuropil: anatomical and physiological heterogeneity. Front Neural Circuits *3*, 5.

Martin, I., Dawson, V.L., and Dawson, T.M. (2011). Recent advances in the genetics of Parkinson's disease. Annu Rev Genomics Hum Genet *12*, 301-325.

Matsui, H., Uemura, N., Yamakado, H., Takeda, S., and Takahashi, R. (2014). Exploring the pathogenetic mechanisms underlying Parkinson's disease in medaka fish. J Parkinsons Dis *4*, 301-310.

McGeer, P.L., Itagaki, S., Boyes, B.E., and McGeer, E.G. (1988). Reactive microglia are positive for

HLA-DR in the substantia nigra of Parkinson's and Alzheimer's disease brains. Neurology *38*, 1285-1291.

Miller, G.W., Gainetdinov, R.R., Levey, A.I., and Caron, M.G. (1999). Dopamine transporters and neuronal injury. Trends Pharmacol Sci *20*, 424-429.

Monastirioti, M., Linn, C.E., Jr., and White, K. (1996). Characterization of Drosophila tyramine beta-hydroxylase gene and isolation of mutant flies lacking octopamine. J Neurosci *16*, 3900-3911.

Mooslehner, K.A., Chan, P.M., Xu, W., Liu, L., Smadja, C., Humby, T., Allen, N.D., Wilkinson, L.S., and Emson, P.C. (2001). Mice with very low expression of the vesicular monoamine transporter 2 gene survive into adulthood: potential mouse model for parkinsonism. Molecular and cellular biology *21*, 5321-5331.

Moriyama, Y., and Futai, M. (1990). H(+)-ATPase, a primary pump for accumulation of neurotransmitters, is a major constituent of brain synaptic vesicles. Biochem Biophys Res Commun *173*, 443-448.

Myohanen, T.T., Schendzielorz, N., and Mannisto, P.T. (2010). Distribution of catechol-O-methyltransferase (COMT) proteins and enzymatic activities in wild-type and soluble COMT deficient mice. J Neurochem *113*, 1632-1643.

Nagarkar-Jaiswal, S., DeLuca, S.Z., Lee, P.T., Lin, W.W., Pan, H., Zuo, Z., Lv, J., Spradling, A.C., and Bellen, H.J. (2015a). A genetic toolkit for tagging intronic MiMIC containing genes. Elife *4*.

Nagarkar-Jaiswal, S., Lee, P.T., Campbell, M.E., Chen, K., Anguiano-Zarate, S., Gutierrez, M.C., Busby, T., Lin, W.W., He, Y., Schulze, K.L.*, et al.* (2015b). A library of MiMICs allows tagging of genes and reversible, spatial and temporal knockdown of proteins in

Drosophila. Elife *4*.

Nall, A.H., Shakhmantsir, I., Cichewicz, K., Birman, S., Hirsh, J., and Sehgal, A. (2016). Caffeine promotes wakefulness via dopamine signaling in Drosophila. Sci Rep *6*, 20938.

Naudon, L., Raisman-Vozari, R., Edwards, R.H., Leroux-Nicollet, I., Peter, D., Liu, Y., and Costentin, J. (1996). Reserpine affects differentially the density of the vesicular monoamine transporter and dihydrotetrabenazine binding sites. Eur J Neurosci *8*, 842-846.

Neckameyer, W.S., and White, K. (1993). Drosophila tyrosine hydroxylase is encoded by the pale locus. J Neurogenet *8*, 189-199.

Nern, A., Pfeiffer, B.D., and Rubin, G.M. (2015). Optimized tools for multicolor stochastic labeling reveal diverse stereotyped cell arrangements in the fly visual system. Proc Natl Acad Sci U S A *112*, E2967-2976.

Neumann, J., Bras, J., Deas, E., O'Sullivan, S.S., Parkkinen, L., Lachmann, R.H., Li, A., Holton, J., Guerreiro, R., Paudel, R.*, et al.* (2009). Glucocerebrosidase mutations in clinical and pathologically proven Parkinson's disease. Brain *132*, 1783-1794.

Ng, C.H., Guan, M.S., Koh, C., Ouyang, X., Yu, F., Tan, E.K., O'Neill, S.P., Zhang, X., Chung, J., and Lim, K.L. (2012). AMP kinase activation mitigates dopaminergic dysfunction and mitochondrial abnormalities in Drosophila models of Parkinson's disease. J Neurosci *32*, 14311-14317.

Nieoullon, A. (2002). Dopamine and the regulation of cognition and attention. Prog Neurobiol *67*, 53-83.

Nirenberg, M.J., Chan, J., Liu, Y., Edwards, R.H., and Pickel, V.M. (1996). Ultrastructural localization of the vesicular monoamine transporter-2 in midbrain dopaminergic neurons: potential sites for somatodendritic storage and release of dopamine. J

Neurosci *16*, 4135-4145.

Nirenberg, M.J., Chan, J., Liu, Y., Edwards, R.H., and Pickel, V.M. (1997). Vesicular monoamine transporter-2: immunogold localization in striatal axons and terminals. Synapse *26*, 194-198.

Nirenberg, M.J., Liu, Y., Peter, D., Edwards, R.H., and Pickel, V.M. (1995). The vesicular monoamine transporter 2 is present in small synaptic vesicles and preferentially localizes to large dense core vesicles in rat solitary tract nuclei. Proc Natl Acad Sci U S A *92*, 8773-8777.

Nunes, E.J., Randall, P.A., Hart, E.E., Freeland, C., Yohn, S.E., Baqi, Y., Muller, C.E., Lopez-Cruz, L., Correa, M., and Salamone, J.D. (2013). Effort-related motivational effects of the VMAT-2 inhibitor tetrabenazine: implications for animal models of the motivational symptoms of depression. J Neurosci *33*, 19120-19130.

Ottone, C., Galasso, A., Gemei, M., Pisa, V., Gigliotti, S., Piccioni, F., Graziani, F., and Verrotti di Pianella, A. (2011). Diminution of eIF4E activity suppresses parkin mutant phenotypes. Gene *470*, 12-19.

Paillart, C., Li, J., Matthews, G., and Sterling, P. (2003). Endocytosis and vesicle recycling at a ribbon synapse. J Neurosci *23*, 4092-4099.

Paisan-Ruiz, C., Jain, S., Evans, E.W., Gilks, W.P., Simon, J., van der Brug, M., Lopez de Munain, A., Aparicio, S., Gil, A.M., Khan, N.*, et al.* (2004). Cloning of the gene containing mutations that cause PARK8-linked Parkinson's disease. Neuron *44*, 595-600.

Pesah, Y., Pham, T., Burgess, H., Middlebrooks, B., Verstreken, P., Zhou, Y., Harding, M., Bellen, H., and Mardon, G. (2004). Drosophila parkin mutants have decreased mass and cell size and increased sensitivity to oxygen radical stress. Development *131*, 2183-2194.

Peter, D., Liu, Y., Sternini, C., de Giorgio, R., Brecha, N., and Edwards, R.H. (1995). Differential expression of two vesicular monoamine transporters. J Neurosci *15*, 6179-6188.

Pfeiffer, B.D., Jenett, A., Hammonds, A.S., Ngo, T.T., Misra, S., Murphy, C., Scully, A., Carlson, J.W., Wan, K.H., Laverty, T.R.*, et al.* (2008). Tools for neuroanatomy and neurogenetics in Drosophila. Proc Natl Acad Sci U S A *105*, 9715-9720.

Pifl, C., Bertel, O., Schingnitz, G., and Hornykiewicz, O. (1990). Extrastriatal dopamine in symptomatic and asymptomatic rhesus monkeys treated with 1-methyl-4-phenyl-1,2,3,6-tetrahydropyridine (MPTP). Neurochem Int *17*, 263-270.

Pifl, C., Rajput, A., Reither, H., Blesa, J., Cavada, C., Obeso, J.A., Rajput, A.H., and Hornykiewicz, O. (2014). Is Parkinson's disease a vesicular dopamine storage disorder? Evidence from a study in isolated synaptic vesicles of human and nonhuman primate striatum. J Neurosci *34*, 8210-8218.

Pifl, C., Reither, H., and Hornykiewicz, O. (2015). The profile of mephedrone on human monoamine transporters differs from 3,4-methylenedioxymethamphetamine primarily by lower potency at the vesicular monoamine transporter. Eur J Pharmacol *755*, 119-126.

Pifl, C., Schingnitz, G., and Hornykiewicz, O. (1988). The neurotoxin MPTP does not reproduce in the rhesus monkey the interregional pattern of striatal dopamine loss typical of human idiopathic Parkinson's disease. Neurosci Lett *92*, 228-233.

Podurgiel, S.J., Nunes, E.J., Yohn, S.E., Barber, J., Thompson, A., Milligan, M., Lee, C.A., Lopez-Cruz, L., Pardo, M., Valverde, O.*, et al.* (2013). The vesicular monoamine transporter (VMAT-2) inhibitor tetrabenazine induces tremulous jaw movements in rodents: implications for pharmacological models of parkinsonian tremor. Neuroscience *250*,

507-519.

Podurgiel, S.J., Spencer, T., Kovner, R., Baqi, Y., Muller, C.E., Correa, M., and Salamone, J.D. (2016). Induction of oral tremor in mice by the acetylcholinesterase inhibitor galantamine: Reversal with adenosine A2A antagonism. Pharmacol Biochem Behav *140*, 62-67.

Polymeropoulos, M.H., Lavedan, C., Leroy, E., Ide, S.E., Dehejia, A., Dutra, A., Pike, B., Root, H., Rubenstein, J., Boyer, R.*, et al.* (1997). Mutation in the alpha-synuclein gene identified in families with Parkinson's disease. Science *276*, 2045-2047.

Pothos, E.N., Larsen, K.E., Krantz, D.E., Liu, Y., Haycock, J.W., Setlik, W., Gershon, M.D., Edwards, R.H., and Sulzer, D. (2000). Synaptic vesicle transporter expression regulates vesicle phenotype and quantal size. J Neurosci *20*, 7297-7306.

Prado, V.F., Martins-Silva, C., de Castro, B.M., Lima, R.F., Barros, D.M., Amaral, E., Ramsey, A.J., Sotnikova, T.D., Ramirez, M.R., Kim, H.G.*, et al.* (2006). Mice deficient for the vesicular acetylcholine transporter are myasthenic and have deficits in object and social recognition. Neuron *51*, 601-612.

Pringsheim, T., Jette, N., Frolkis, A., and Steeves, T.D. (2014). The prevalence of Parkinson's disease: a systematic review and meta-analysis. Mov Disord *29*, 1583-1590.

Rana, A., Rera, M., and Walker, D.W. (2013). Parkin overexpression during aging reduces proteotoxicity, alters mitochondrial dynamics, and extends lifespan. Proc Natl Acad Sci U S A *110*, 8638-8643.

Rehavi, M., Roz, N., and Weizman, A. (2002). Chronic clozapine, but not haloperidol, treatment affects rat brain vesicular monoamine transporter 2. Eur Neuropsychopharmacol *12*, 261-268.

Reiter, L.T., Potocki, L., Chien, S., Gribskov, M., and Bier, E. (2001). A systematic analysis of human disease-associated gene sequences in Drosophila melanogaster. Genome Res *11*, 1114-1125.

Richards, D.A., Guatimosim, C., and Betz, W.J. (2000). Two endocytic recycling routes selectively fill two vesicle pools in frog motor nerve terminals. Neuron *27*, 551-559.

Riddle, E.L., Topham, M.K., Haycock, J.W., Hanson, G.R., and Fleckenstein, A.E. (2002). Differential trafficking of the vesicular monoamine transporter-2 by methamphetamine and cocaine. Eur J Pharmacol *449*, 71-74.

Riemensperger, T., Issa, A.R., Pech, U., Coulom, H., Nguyen, M.V., Cassar, M., Jacquet, M., Fiala, A., and Birman, S. (2013). A single dopamine pathway underlies progressive locomotor deficits in a Drosophila model of Parkinson disease. Cell Rep *5*, 952-960.

Rilstone, J.J., Alkhater, R.A., and Minassian, B.A. (2013). Brain dopamine-serotonin vesicular transport disease and its treatment. N Engl J Med *368*, 543-550.

Rinne, U.K., Bracco, F., Chouza, C., Dupont, E., Gershanik, O., Marti Masso, J.F., Montastruc, J.L., Marsden, C.D., Dubini, A., Orlando, N.*, et al.* (1997). Cabergoline in the treatment of early Parkinson's disease: results of the first year of treatment in a double-blind comparison of cabergoline and levodopa. The PKDS009 Collaborative Study Group. Neurology *48*, 363-368.

Ritz, M.C., Lamb, R.J., Goldberg, S.R., and Kuhar, M.J. (1988). Cocaine self-administration appears to be mediated by dopamine uptake inhibition. Prog Neuropsychopharmacol Biol Psychiatry *12*, 233-239.

Rizzoli, S.O., and Betz, W.J. (2005). Synaptic vesicle pools. Nat Rev Neurosci *6*, 57-69.

Rodriguez-Boulan, E., and Powell, S.K. (1992). Polarity of epithelial and neuronal cells. Annu Rev

Cell Biol *8*, 395-427.

Rodriguez-Oroz, M.C., Jahanshahi, M., Krack, P., Litvan, I., Macias, R., Bezard, E., and Obeso, J.A. (2009). Initial clinical manifestations of Parkinson's disease: features and pathophysiological mechanisms. Lancet Neurol *8*, 1128-1139.

Romero-Calderon, R., Uhlenbrock, G., Borycz, J., Simon, A.F., Grygoruk, A., Yee, S.K., Shyer, A., Ackerson, L.C., Maidment, N.T., Meinertzhagen, I.A.*, et al.* (2008). A glial variant of the vesicular monoamine transporter is required to store histamine in the Drosophila visual system. PLoS Genet *4*, e1000245.

Saini, N., Georgiev, O., and Schaffner, W. (2011). The parkin mutant phenotype in the fly is largely rescued by metal-responsive transcription factor (MTF-1). Mol Cell Biol *31*, 2151-2161.

Sang, T.K., Chang, H.Y., Lawless, G.M., Ratnaparkhi, A., Mee, L., Ackerson, L.C., Maidment, N.T., Krantz, D.E., and Jackson, G.R. (2007). A Drosophila model of mutant human parkin-induced toxicity demonstrates selective loss of dopaminergic neurons and dependence on cellular dopamine. J Neurosci *27*, 981-992.

Sarthy, P.V. (1991). Histamine: a neurotransmitter candidate for Drosophila photoreceptors. J Neurochem *57*, 1757-1768.

Scarffe, L.A., Stevens, D.A., Dawson, V.L., and Dawson, T.M. (2014). Parkin and PINK1: much more than mitophagy. Trends Neurosci *37*, 315-324.

Schwab, R.S., Amador, L.V., and Lettvin, J.Y. (1951). Apomorphine in Parkinson's disease. Trans Am Neurol Assoc *56*, 251-253.

Segura-Aguilar, J., and Lind, C. (1989). On the mechanism of the Mn3(+)-induced neurotoxicity of dopamine:prevention of quinone-derived oxygen toxicity by DT diaphorase and

superoxide dismutase. Chem Biol Interact *72*, 309-324.

Sejourne, J., Placais, P.Y., Aso, Y., Siwanowicz, I., Trannoy, S., Thoma, V., Tedjakumala, S.R., Rubin, G.M., Tchenio, P., Ito, K.*, et al.* (2011). Mushroom body efferent neurons responsible for aversive olfactory memory retrieval in Drosophila. Nat Neurosci *14*, 903-910.

Shulman, J.M., De Jager, P.L., and Feany, M.B. (2011). Parkinson's disease: genetics and pathogenesis. Annu Rev Pathol *6*, 193-222.

Simon, A.F., Daniels, R., Romero-Calderon, R., Grygoruk, A., Chang, H.Y., Najibi, R., Shamouelian, D., Salazar, E., Solomon, M., Ackerson, L.C.*, et al.* (2009). Drosophila vesicular monoamine transporter mutants can adapt to reduced or eliminated vesicular stores of dopamine and serotonin. Genetics *181*, 525-541.

Singleton, A.B., Farrer, M., Johnson, J., Singleton, A., Hague, S., Kachergus, J., Hulihan, M., Peuralinna, T., Dutra, A., Nussbaum, R.*, et al.* (2003). alpha-Synuclein locus triplication causes Parkinson's disease. Science *302*, 841.

Sitaraman, D., Zars, M., Laferriere, H., Chen, Y.C., Sable-Smith, A., Kitamoto, T., Rottinghaus, G.E., and Zars, T. (2008). Serotonin is necessary for place memory in Drosophila. Proc Natl Acad Sci U S A *105*, 5579-5584.

Song, C.H., Fan, X., Exeter, C.J., Hess, E.J., and Jinnah, H.A. (2012). Functional analysis of dopaminergic systems in a DYT1 knock-in mouse model of dystonia. Neurobiol Dis *48*, 66-78.

Song, H., Ming, G., Fon, E., Bellocchio, E., Edwards, R.H., and Poo, M. (1997). Expression of a putative vesicular acetylcholine transporter facilitates quantal transmitter packaging. Neuron *18*, 815-826.

Spencer, J.P., Jenner, P., Daniel, S.E., Lees, A.J., Marsden, D.C., and Halliwell, B. (1998).

Conjugates of catecholamines with cysteine and GSH in Parkinson's disease: possible mechanisms of formation involving reactive oxygen species. J Neurochem *71*, 2112-2122.

Spradling, A.C., and Rubin, G.M. (1982). Transposition of cloned P elements into Drosophila germ line chromosomes. Science *218*, 341-347.

Steiner-Mordoch, S., Shirvan, A., and Schuldiner, S. (1996). Modification of the pH profile and tetrabenazine sensitivity of rat VMAT1 by replacement of aspartate 404 with glutamate. J Biol Chem *271*, 13048-13054.

Stokes, A.H., Hastings, T.G., and Vrana, K.E. (1999). Cytotoxic and genotoxic potential of dopamine. J Neurosci Res *55*, 659-665.

Sulzer, D., Bogulavsky, J., Larsen, K.E., Behr, G., Karatekin, E., Kleinman, M.H., Turro, N., Krantz, D., Edwards, R.H., Greene, L.A.*, et al.* (2000). Neuromelanin biosynthesis is driven by excess cytosolic catecholamines not accumulated by synaptic vesicles. Proc Natl Acad Sci U S A *97*, 11869-11874.

Sulzer, D., and Zecca, L. (2000). Intraneuronal dopamine-quinone synthesis: a review. Neurotox Res *1*, 181-195.

Sweeney, S.T., Hidalgo, A., de Belle, J.S., and Keshishian, H. (2011). Dissection of adult Drosophila brains. Cold Spring Harb Protoc *2011*, 1472-1474.

Tain, L.S., Mortiboys, H., Tao, R.N., Ziviani, E., Bandmann, O., and Whitworth, A.J. (2009). Rapamycin activation of 4E-BP prevents parkinsonian dopaminergic neuron loss. Nat Neurosci *12*, 1129-1135.

Takahashi, N., Miner, L.L., Sora, I., Ujike, H., Revay, R.S., Kostic, V., Jackson-Lewis, V., Przedborski, S., and Uhl, G.R. (1997). VMAT2 knockout mice: heterozygotes display reduced

amphetamine-conditioned reward, enhanced amphetamine locomotion, and enhanced MPTP toxicity. Proc Natl Acad Sci U S A *94*, 9938-9943.

Taylor, T.N., Alter, S.P., Wang, M., Goldstein, D.S., and Miller, G.W. (2014). Reduced vesicular storage of catecholamines causes progressive degeneration in the locus ceruleus. Neuropharmacology *76 Pt A*, 97-105.

Taylor, T.N., Caudle, W.M., and Miller, G.W. (2011). VMAT2-Deficient Mice Display Nigral and Extranigral Pathology and Motor and Nonmotor Symptoms of Parkinson's Disease. Parkinsons Dis *2011*, 124165.

Thompson, C.M., Capdevila, J.H., and Strobel, H.W. (2000). Recombinant cytochrome P450 2D18 metabolism of dopamine and arachidonic acid. J Pharmacol Exp Ther *294*, 1120-1130.

Tomassoni, D., Traini, E., Mancini, M., Bramanti, V., Mahdi, S.S., and Amenta, F. (2015). Dopamine, vesicular transporters, and dopamine receptor expression in rat major salivary glands. Am J Physiol Regul Integr Comp Physiol *309*, R585-593.

Tordera, R.M., Totterdell, S., Wojcik, S.M., Brose, N., Elizalde, N., Lasheras, B., and Del Rio, J. (2007). Enhanced anxiety, depressive-like behaviour and impaired recognition memory in mice with reduced expression of the vesicular glutamate transporter 1 (VGLUT1). Eur J Neurosci *25*, 281-290.

Torres, G.E., Gainetdinov, R.R., and Caron, M.G. (2003). Plasma membrane monoamine transporters: structure, regulation and function. Nat Rev Neurosci *4*, 13-25.

Trempe, J.F., and Fon, E.A. (2013). Structure and Function of Parkin, PINK1, and DJ-1, the Three Musketeers of Neuroprotection. Front Neurol *4*, 38.

Trinh, K., Andrews, L., Krause, J., Hanak, T., Lee, D., Gelb, M., and Pallanck, L. (2010). Decaffeinated coffee and nicotine-free tobacco provide neuroprotection in Drosophila

models of Parkinson's disease through an NRF2-dependent mechanism. J Neurosci *30*, 5525-5532.

Tse, D.C., McCreery, R.L., and Adams, R.N. (1976). Potential oxidative pathways of brain catecholamines. J Med Chem *19*, 37-40.

Valente, E.M., Abou-Sleiman, P.M., Caputo, V., Muqit, M.M., Harvey, K., Gispert, S., Ali, Z., Del Turco, D., Bentivoglio, A.R., Healy, D.G.*, et al.* (2004). Hereditary early-onset Parkinson's disease caused by mutations in PINK1. Science *304*, 1158-1160.

Valles, A.M., and White, K. (1988). Serotonin-containing neurons in Drosophila melanogaster: development and distribution. J Comp Neurol *268*, 414-428.

Venken, K.J., Schulze, K.L., Haelterman, N.A., Pan, H., He, Y., Evans-Holm, M., Carlson, J.W., Levis, R.W., Spradling, A.C., Hoskins, R.A.*, et al.* (2011). MiMIC: a highly versatile transposon insertion resource for engineering Drosophila melanogaster genes. Nat Methods *8*, 737-743.

Waddell, S. (2010). Dopamine reveals neural circuit mechanisms of fly memory. Trends Neurosci *33*, 457-464.

Waddell, S. (2016). Neural Plasticity: Dopamine Tunes the Mushroom Body Output Network. Curr Biol *26*, R109-112.

Wakamatsu, K., Murase, T., Zucca, F.A., Zecca, L., and Ito, S. (2012). Biosynthetic pathway to neuromelanin and its aging process. Pigment Cell Melanoma Res *25*, 792-803.

Wang, Y., Li, S., Liu, W., Wang, F., Hu, L.F., Zhong, Z.M., Wang, H., and Liu, C.F. (2016). Vesicular monoamine transporter 2 (Vmat2) knockdown elicits anxiety-like behavior in zebrafish. Biochem Biophys Res Commun *470*, 792-797.

Wang, Y.M., Gainetdinov, R.R., Fumagalli, F., Xu, F., Jones, S.R., Bock, C.B., Miller, G.W.,

Wightman, R.M., and Caron, M.G. (1997). Knockout of the vesicular monoamine transporter 2 gene results in neonatal death and supersensitivity to cocaine and amphetamine. Neuron *19*, 1285-1296.

Wangler, M.F., Yamamoto, S., and Bellen, H.J. (2015). Fruit flies in biomedical research. Genetics *199*, 639-653.

Wanrooij, S., Luoma, P., van Goethem, G., van Broeckhoven, C., Suomalainen, A., and Spelbrink, J.N. (2004). Twinkle and POLG defects enhance age-dependent accumulation of mutations in the control region of mtDNA. Nucleic Acids Res *32*, 3053-3064.

Whitehead, R.E., Ferrer, J.V., Javitch, J.A., and Justice, J.B. (2001). Reaction of oxidized dopamine with endogenous cysteine residues in the human dopamine transporter. J Neurochem *76*, 1242-1251.

Whitley, J., Parsons, J., Freeman, J., Liu, Y., Edwards, R.H., and Near, J.A. (2004). Electrochemical monitoring of transport by a vesicular monoamine transporter expressed in Xenopus oocytes. J Neurosci Methods *133*, 191-199.

Whitworth, A.J., Theodore, D.A., Greene, J.C., Benes, H., Wes, P.D., and Pallanck, L.J. (2005). Increased glutathione S-transferase activity rescues dopaminergic neuron loss in a Drosophila model of Parkinson's disease. Proc Natl Acad Sci U S A *102*, 8024-8029.

Wilson, N.R., Kang, J., Hueske, E.V., Leung, T., Varoqui, H., Murnick, J.G., Erickson, J.D., and Liu, G. (2005). Presynaptic regulation of quantal size by the vesicular glutamate transporter VGLUT1. J Neurosci *25*, 6221-6234.

Winklhofer, K.F. (2014). Parkin and mitochondrial quality control: toward assembling the puzzle. Trends Cell Biol *24*, 332-341.

Wise, R.A. (2004). Dopamine, learning and motivation. Nat Rev Neurosci *5*, 483-494.

Wittkopp, P.J., Carroll, S.B., and Kopp, A. (2003). Evolution in black and white: genetic control of pigment patterns in Drosophila. Trends Genet *19*, 495-504.

Wojcik, S.M., Katsurabayashi, S., Guillemin, I., Friauf, E., Rosenmund, C., Brose, N., and Rhee, J.S. (2006). A shared vesicular carrier allows synaptic corelease of GABA and glycine. Neuron *50*, 575-587.

Wojcik, S.M., Rhee, J.S., Herzog, E., Sigler, A., Jahn, R., Takamori, S., Brose, N., and Rosenmund, C. (2004). An essential role for vesicular glutamate transporter 1 (VGLUT1) in postnatal development and control of quantal size. Proc Natl Acad Sci U S A *101*, 7158-7163.

Wolff, T., Iyer, N.A., and Rubin, G.M. (2015). Neuroarchitecture and neuroanatomy of the Drosophila central complex: A GAL4-based dissection of protocerebral bridge neurons and circuits. J Comp Neurol *523*, 997-1037.

Wright, T.R. (1987). The genetics of biogenic amine metabolism, sclerotization, and melanization in Drosophila melanogaster. Adv Genet *24*, 127-222.

Wu, J.S., and Luo, L. (2006). A protocol for dissecting Drosophila melanogaster brains for live imaging or immunostaining. Nat Protoc *1*, 2110-2115.

Xu, Y., An, F., Borycz, J.A., Borycz, J., Meinertzhagen, I.A., and Wang, T. (2015). Histamine Recycling Is Mediated by CarT, a Carcinine Transporter in Drosophila Photoreceptors. PLoS Genet *11*, e1005764.

Yahr, M.D. (1978). Overview of present day treatment of Parkinson's disease. J Neural Transm *43*, 227-238.

Yamagata, N., Ichinose, T., Aso, Y., Placais, P.Y., Friedrich, A.B., Sima, R.J., Preat, T., Rubin, G.M., and Tanimoto, H. (2015). Distinct dopamine neurons mediate reward signals for short- and long-term memories. Proc Natl Acad Sci U S A *112*, 578-583.

Yamamoto, S., and Seto, E.S. (2014). Dopamine dynamics and signaling in Drosophila: an overview of genes, drugs and behavioral paradigms. Exp Anim *63*, 107-119.

Yang, Y., Gehrke, S., Imai, Y., Huang, Z., Ouyang, Y., Wang, J.W., Yang, L., Beal, M.F., Vogel, H., and Lu, B. (2006). Mitochondrial pathology and muscle and dopaminergic neuron degeneration caused by inactivation of Drosophila Pink1 is rescued by Parkin. Proc Natl Acad Sci U S A *103*, 10793-10798.

Yao, J., Erickson, J.D., and Hersh, L.B. (2004). Protein kinase A affects trafficking of the vesicular monoamine transporters in PC12 cells. Traffic *5*, 1006-1016.

Yelin, R., and Schuldiner, S. (1995). The pharmacological profile of the vesicular monoamine transporter resembles that of multidrug transporters. FEBS Lett *377*, 201-207.

Zhang, W., Phillips, K., Wielgus, A.R., Liu, J., Albertini, A., Zucca, F.A., Faust, R., Qian, S.Y., Miller, D.S., Chignell, C.F.*, et al.* (2011). Neuromelanin activates microglia and induces degeneration of dopaminergic neurons: implications for progression of Parkinson's disease. Neurotox Res *19*, 63-72.

Zhao, C.M., Chen, D., Lintunen, M., Panula, P., and Hakanson, R. (1999). Effects of reserpine on ECL-cell ultrastructure and histamine compartmentalization in the rat stomach. Cell Tissue Res *295*, 131-140.

Zhu, M., Li, X., Tian, X., and Wu, C. (2015). Mask loss-of-function rescues mitochondrial impairment and muscle degeneration of Drosophila pink1 and parkin mutants. Hum Mol Genet *24*, 3272-3285.

8   APPENDIX
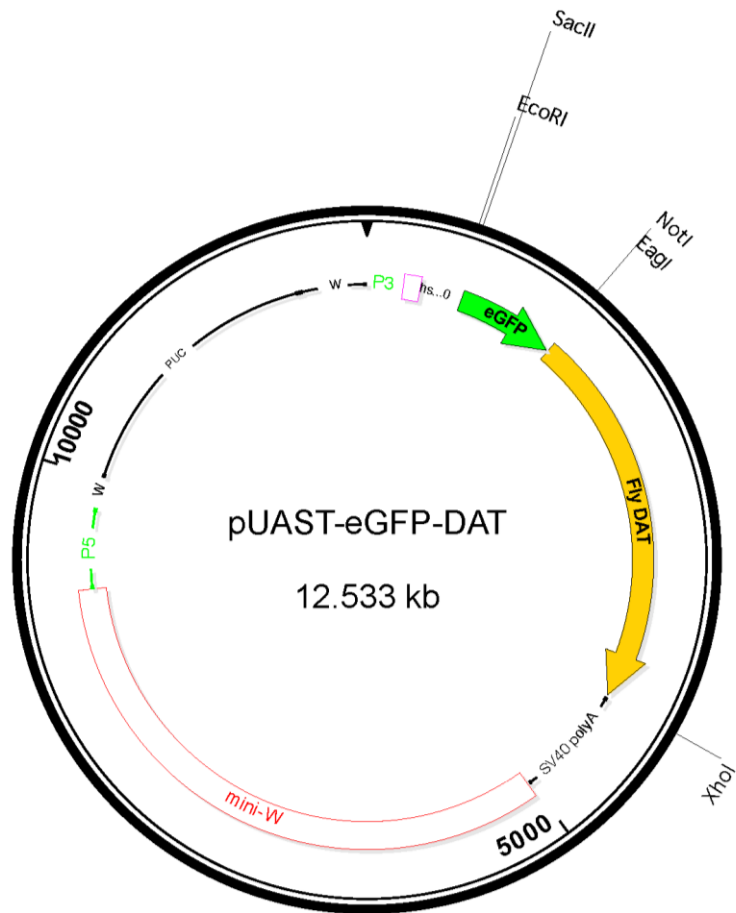
Appendix 1: Map for pUAST-eGFP-dDAT
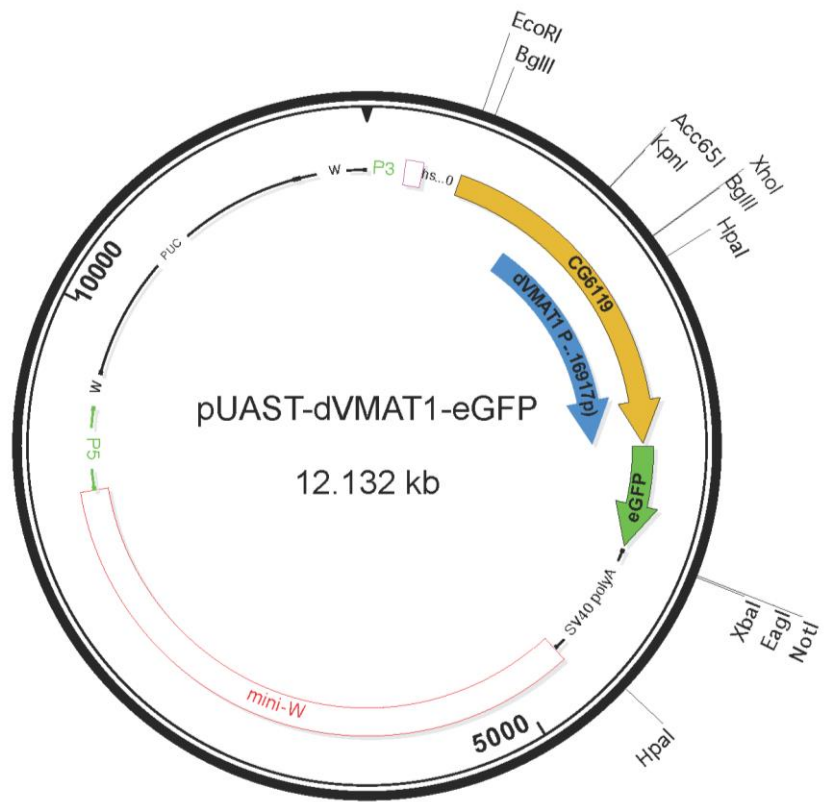
Appendix 2: Map for pUAST-dVMAT1-eGFP
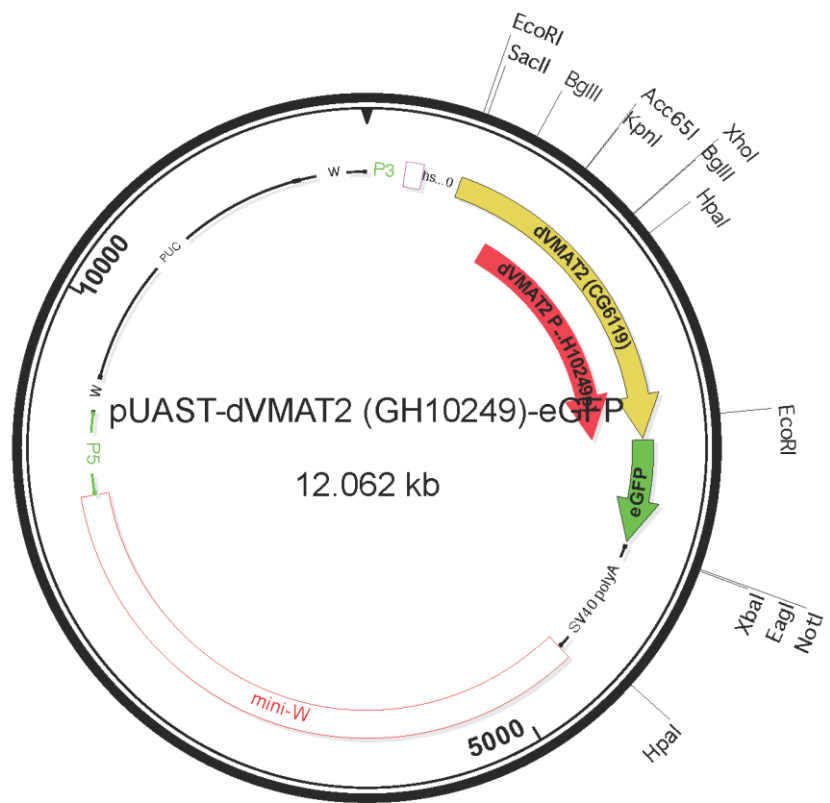
Appendix 3: Map for pUAST-dVMAT2-eGFP

```
                                    10
1   M L R T - - - - - - - - - - - I L D A P Q R L L K E G - - - - - - - - - - - - - - - - - - - - - - - -   VMAT1 (h NP_001129163.1).pro
1   M Q S S T D A G N G G P R K H T Q S T A P Q K Q - S E I S E T T S F T V N A N T T T N S Q Q Q Q I P   dVMAT1-GH10249-AAN71163.1.pro
1   M Q S S T D A G N G G P R K H T Q S T A P Q K Q - S E I S E T T S F T V N A N T T T N S Q Q Q Q I P   dVMAT2-GH16917-AA039614.1.pro
1   M A L S - - - - - - - - - - - E L A L V R W L - Q E S - - - - - - - - - - - - - - - - - - - - - - - -   VMAT2 (h NP_003045.2).pro

17  - - - - - - - - - - - - - - - - - - - - - - - - - - - - - - - - - - - - - - - - - - - - - - - - - - - -   VMAT1 (h NP_001129163.1).pro
50  G G P A S N T P S K N P F K Q Q L D S N Q Q N G N M E P D C G I M G V G K E P P V P P P P T Y Q S Q   dVMAT1-GH10249-AAN71163.1.pro
50  G G P A S N T P S K N P F K Q Q L D S N Q Q N G N M E P D C G I M G V G K E P P V P P P P T Y Q S Q   dVMAT2-GH16917-AA039614.1.pro
16  - - - - - - - - - - - - - - - - - - - - - - - - - - - - - - - - - - - - - - - - - - - - - - - - - - - -   VMAT2 (h NP_003045.2).pro

                                                                                        20          30
17  - - - - - - - - - - - - - - - - - - - - - - - - - - - - - - - - - - - R A S R Q L V L V V F V A L   VMAT1 (h NP_001129163.1).pro
100 T Y A G R Q A P P P A D Q Y R E E D P R A A G S W A A A K S W M V S W R G S N R L V L V I V A I A L   dVMAT1-GH10249-AAN71163.1.pro
100 T Y A G R Q A P P P A D Q Y R E E D P R A A G S W A A A K S W M V S W R G S N R L V L V I V A I A L   dVMAT2-GH16917-AA039614.1.pro
16  - - - - - - - - - - - - - - - - - - - - - - - - - - - - - - - - - - - R R S R K L I L F I V F L A L   VMAT2 (h NP_003045.2).pro

            40              50                      60                  70
32  L L D N M L F T V V V P I V P T F L Y D M E F K E V N S S L H L G H A G S S P H A L A S P A F S T I   VMAT1 (h NP_001129163.1).pro
150 L L D N M L L T T V V P I I P E F L Y D I - - R H P D A P L D S F P R T P L T S N V P P P P - - - -   dVMAT1-GH10249-AAN71163.1.pro
150 L L D N M L L T T V V P I I P E F L Y D I - - R H P D A P L D S F P R T P L T S N V P P P P - - - -   dVMAT2-GH16917-AA039614.1.pro
31  L L D N M L L T V V V P I I P S Y L Y S I - - K H E K N A T E I Q T A R P V H T A S I S D S F Q S I   VMAT2 (h NP_003045.2).pro

            80              90              100             110                 120
82  F S F F N N N T V A V E E S V P S G I A W M N D T A S T I P P P A T E A I S A H K N N C L Q G T G F   VMAT1 (h NP_001129163.1).pro
194 - - - - - T P C P C N K D G S E A A P L E - I - - - - - S T I S P E E N E T Y Y R E L E E - - R H N E L   dVMAT1-GH10249-AAN71163.1.pro
194 - - - - - T P C P C N K D G S E A A P L E - I - - - - - S T I S P E E N E T Y Y R E L E E - - R H N E L   dVMAT2-GH16917-AA039614.1.pro
79  F S Y Y D N S T M - V T G N A T R D L T - L H Q T A T Q H M V T N A S A V P S D C P S - - E D K D L   VMAT2 (h NP_003045.2).pro

                130             140             150             160             170
132 L E E E I T R V G V L F A S K A V M Q L L V N P F V G P L T N R I G Y H I P M F A G F V I M F L S T   VMAT1 (h NP_001129163.1).pro
233 V G E T V - E V G L L F A S K A F V Q L L V N P I V G P L T H R I G Y S I P M F A G F V I M F L S T   dVMAT1-GH10249-AAN71163.1.pro
233 V G E T V - E V G L L F A S K A F V Q L L V N P I V G P L T H R I G Y S I P M F A G F V I M F L S T   dVMAT2-GH16917-AA039614.1.pro
125 L N E N V - Q V G L L F A S K A T V Q L I T N P F I G L L T N R I G Y P I P I F A G F C I M F V S T   VMAT2 (h NP_003045.2).pro
```

```
                180             190             200             210             220
182 V M F A F S G T Y T L L F V A R T L Q G I G S S F S S V A G L G M L A S V Y T D D H E R G R A M G T   VMAT1 (h NP_001129163.1).pro
282 I I I F A F G R S Y L V L F V A R A L Q G I G S S C S S V S G M G M L A D R F T D D K E R G N A M G I   dVMAT1-GH10249-AAN71163.1.pro
282 I I I F A F G R S Y L V L F V A R A L Q G I G S S C S S V S G M G M L A D R F T D D K E R G N A M G I   dVMAT2-GH16917-AA039614.1.pro
174 I M F A F S S S Y A F L L I A R S L Q G I G S S C S S V A G M G M L A S V Y T D D E E R G N V M G I   VMAT2 (h NP_003045.2).pro

                230             240             250             260             270
232 A L G G L A L G L L V G A P F G S V M Y E F V G K S A P F L I L A F L A L L D G A L Q L C I L Q P S   VMAT1 (h NP_001129163.1).pro
332 A L G G L A L G V L I G P P F G G V M Y E F V G K S A P F L I L A A L A L G D G L L Q L F M L Q P S   dVMAT1-GH10249-AAN71163.1.pro
332 A L G G L A L G V L I G P P F G G V M Y E F V G K S A P F L I L A A L A L G D G L L Q L F M L Q P S   dVMAT2-GH16917-AA039614.1.pro
224 A L G G L A M G V L V G P P F G S V L Y E F V G K T A P F L V L A A L V L L D G A I Q L F V L Q P S   VMAT2 (h NP_003045.2).pro

                280             290             300             310             320
282 K V S P E S A K G T P L F M L L K D P Y I L V A A G S I C F A N M G V A I L E P T L P I W M M Q T M   VMAT1 (h NP_001129163.1).pro
382 - I Q K A E T E P P S L K S L I S D P Y I L I A A G A I T F A N M G I A M L E P S L P L W M V D N M   dVMAT1-GH10249-AAN71163.1.pro
382 - I Q K A E T E P P S L K S L I S D P Y I L I A A G A I T F A N M G I A M L E P S L P L W M V D N M   dVMAT2-GH16917-AA039614.1.pro
274 R V Q P E S Q K G T P L T T L L K D P Y I L I A A G S I C F A N M G I A M L E P A L P I W M M E T M   VMAT2 (h NP_003045.2).pro

                330             340             350             360             370
332 C S P K W Q L G L A F L P A S V S Y L I G T N L F G V L A N K M G R W L C S L I G M L V V G T S L L   VMAT1 (h NP_001129163.1).pro
431 G A T R W E Q G V A F L P A S I S Y L I G T N L F G P L G H K I G R W F A A C L G L I I I G G C L I   dVMAT1-GH10249-AAN71163.1.pro
431 G A T R W E Q G V A F L P A S I S Y L I G T N L F G P L G H K I G R W F A A C L G L I I I G G C L I   dVMAT2-GH16917-AA039614.1.pro
324 C S R K W Q L G V A F L P A S I S Y L I G T N I F G I L A H K M G R W L C A L L G M I I V G V S I L   VMAT2 (h NP_003045.2).pro

                380             390             400             410             420
382 C V P L A H N I F G L I G P N A G L G L A I G M V D S S M M P I M G H L V D L R H T S V Y G S V Y A   VMAT1 (h NP_001129163.1).pro
481 F I P M A T S I T H L I I P N A G L G F A I G M V D S S M M P E L G Y L V D I R H S A V Y G S V Y A   dVMAT1-GH10249-AAN71163.1.pro
481 F I P M A T S I T H L I I P N A G L G F A I G M V D S S M M P E L G Y L V D I R H S A V Y G S V Y A   dVMAT2-GH16917-AA039614.1.pro
374 C I P F A K N I Y G L I A P N F G V G F A I G M V D S S M M P I M G Y L V D L R H V S V Y G S V Y A   VMAT2 (h NP_003045.2).pro

                430             440             450             460             470
432 I A D V A F C M G F A I G P S T G G A I V K A I G F P W L M V I T G V I N I V Y A P L C Y Y L R S P   VMAT1 (h NP_001129163.1).pro
531 L G D V A F C V G F A V G P A L S G S L V K S I G F E W M L F G I A I L C F M Y A P L L T L L L K N P   dVMAT1-GH10249-AAN71163.1.pro
531 L G D V A F C V G F A V G P A L S G S L V K S I G F E W M L F G I A I L C F M Y A P L L T L L L K N P   dVMAT2-GH16917-AA039614.1.pro
424 I A D V A F C M G Y A I G P S A G G A I A K A I G F P W L M T I I G I I D I L F A P L C F F L R S P   VMAT2 (h NP_003045.2).pro
```

```
        480            490           500
482 P A K E E K L A I L - S Q D C P M E T R M Y A T Q K P T K E F P L - - - - - - - - - - - - - - - -          VMAT1 (h NP_001129163.1).pro
581 P T S D E K - - - - - - - - - - K V R M - - A R E A A E A A A A A A A S G E F S G I P Q M T A S          dVMAT1-GH10249-AAN71163.1.pro
581 P T S D E K - - - - - - - - - - K S L I Y - G R D R A Q V R Y V - - - - - - - - - - - - - - - -          dVMAT2-GH16917-AA039614.1.pro
474 P A K E E K M A I L M D H N C P I K T K M Y - T Q N N I Q S Y P I - - - - - - - - - - - - - - - -          VMAT2 (h NP_003045.2).pro

                         510
514 - - - - - - - - - - - - - - - - - - - - - - G E D S D E E P D H E E                                      VMAT1 (h NP_001129163.1).pro
618 C P A I M H G A S V P D S D A E A G R T N E A Y E S E R L                                                dVMAT1-GH10249-AAN71163.1.pro
602 - - - - - - - - - - - - - - - - - - T Y Q N Y E E D E                                                    dVMAT2-GH16917-AA039614.1.pro
506 - - - - - - - - - - - - - - - - - - - - - - G E D E E S E S D                                            VMAT2 (h NP_003045.2).pro
```

Decoration 'Decoration #1': Shade (with solid dark green) residues that match VMAT2 (h NP_003045.2).pro within 1 distance units.

Decoration 'Decoration #2': Shade (with solid bright cobalt) residues that match VMAT2 (h NP_003045.2).pro within 2 distance units.

Decoration 'Decoration #3': Shade (with solid deep red) residues that match VMAT2 (h NP_003045.2).pro exactly.

Decoration 'Decoration #4': Shade (with solid black) residues that match the Consensus exactly.

Appendix 4: Amino Acid sequence alignments for VMATs

VITA

Antonio Joel Tito Jr. was born in Pucallpa, Peru on February 5, 1987, the son of Elizabeth Tito and Jorge Antonio Tito-Izquierdo. After completing his work at Westchester Academy for International Studies, Houston, Texas in 2005, he entered University of Houston-Downtown (UHD) in Houston, Texas. He received the degree of Bachelors of Science with a major in biotechnology and minors in microbiology and chemistry from UHD in December, 2008. For the next three years, he worked as a Research Assistant while pursuing his Master's degree in the Lab of Dr. Myriam Fornage in the department of Neurobiology and Anatomy at the Institute of Molecular Medicine (IMM) at the UT-Health Graduate School of Biomedical Sciences (GSBS) at Houston. In January 2012 he continued at the UT-Health Graduate School of Biomedical Sciences at Houston to pursue his doctoral degree in Biomedical Sciences with concentrations in Human Molecular Genetics and Neuroscience, in the lab of Dr. Sheng Zhang at the department of Metabolic and Degenerative Diseases at the IMM.

Permanent address:

12926 Westhorpe Dr.
Houston, Texas 77077
United States